



NAVAL POSTGRADUATE SCHOOL

MONTEREY, CALIFORNIA

THESIS

**DEVELOPMENT OF CODE FOR A PHYSICAL OPTICS
RADAR CROSS SECTION PREDICTION AND ANALYSIS
APPLICATION**

by

Filippos Chatzigeorgiadis

September 2004

Thesis Co-Advisors:

David C. Jenn

D. Curtis Schleher

Approved for public release; distribution is unlimited

THIS PAGE INTENTIONALLY LEFT BLANK

REPORT DOCUMENTATION PAGE			<i>Form Approved OMB No. 0704-0188</i>	
Public reporting burden for this collection of information is estimated to average 1 hour per response, including the time for reviewing instruction, searching existing data sources, gathering and maintaining the data needed, and completing and reviewing the collection of information. Send comments regarding this burden estimate or any other aspect of this collection of information, including suggestions for reducing this burden, to Washington headquarters Services, Directorate for Information Operations and Reports, 1215 Jefferson Davis Highway, Suite 1204, Arlington, VA 22202-4302, and to the Office of Management and Budget, Paperwork Reduction Project (0704-0188) Washington DC 20503.				
1. AGENCY USE ONLY (Leave blank)		2. REPORT DATE September 2004	3. REPORT TYPE AND DATES COVERED Master's Thesis	
4. TITLE AND SUBTITLE: Development of Code for a Physical Optics Radar Cross Section Prediction and Analysis Application			5. FUNDING NUMBERS	
6. AUTHOR(S) Filippou Chatzigeorgiadis				
7. PERFORMING ORGANIZATION NAME(S) AND ADDRESS(ES) Naval Postgraduate School Monterey, CA 93943-5000			8. PERFORMING ORGANIZATION REPORT NUMBER	
9. SPONSORING / MONITORING AGENCY NAME(S) AND ADDRESS(ES) N/A			10. SPONSORING/MONITORING AGENCY REPORT NUMBER	
11. SUPPLEMENTARY NOTES The views expressed in this thesis are those of the author and do not reflect the official policy or position of the Department of Defense or the U.S. Government.				
12a. DISTRIBUTION / AVAILABILITY STATEMENT Approved for public release; distribution is unlimited			12b. DISTRIBUTION CODE	
13. ABSTRACT (maximum 200 words) <p>The significance of the Radar Cross Section (RCS) in the outcome of military engagements makes its prediction an important problem in modern Electronic Warfare. The POFACETS program, previously developed at the Naval Postgraduate School (NPS), uses the Physical Optics method to predict the RCS of complex targets, which are modeled with the use of triangular facets. The program has minimum computer resource requirements and provides convenient run-times. This thesis upgraded, enhanced and expanded the functionalities and capabilities of the POFACETS program. The new functionalities were implemented by upgrading the Graphical User Interface and model database, allowing the creation of models with an unlimited number of facets, providing capabilities for the automatic creation of models with standard geometric shapes, allowing the combination of existing target models, providing capabilities for sharing target models with commercial CAD programs, and creating new display formats for RCS results. The new computational capabilities include the development of a user-updatable database of materials and coatings that can be applied to models in one or multiple layers, and the computation of their effects on the models' RCS. Also implemented are the computations of the ground's effect on the RCS, and the exploitation of symmetry planes in models, in order to decrease run-time for RCS prediction.</p>				
14. SUBJECT TERMS Physical Optics, Radar Cross Section, Monostatic, Bistatic, Electromagnetic Scattering, Graphical User Interface, Faceted Models			15. NUMBER OF PAGES 149	
			16. PRICE CODE	
17. SECURITY CLASSIFICATION OF REPORT Unclassified	18. SECURITY CLASSIFICATION OF THIS PAGE Unclassified	19. SECURITY CLASSIFICATION OF ABSTRACT Unclassified	20. LIMITATION OF ABSTRACT UL	

THIS PAGE INTENTIONALLY LEFT BLANK

Approved for public release; distribution is unlimited

**DEVELOPMENT OF CODE FOR A PHYSICAL OPTICS RADAR CROSS
SECTION PREDICTION AND ANALYSIS APPLICATION**

Filippos Chatzigeorgiadis
Major, Hellenic Air Force
B.S., Hellenic Air Force Academy, 1990

Submitted in partial fulfillment of the
requirements for the degree of

**MASTER OF SCIENCE IN SYSTEMS ENGINEERING
and
MASTER OF SCIENCE IN ELECTRICAL ENGINEERING**

from the

**NAVAL POSTGRADUATE SCHOOL
September 2004**

Author: Filippos Chatzigeorgiadis

Approved by: David C. Jenn
Thesis Co-Advisor

D. Curtis Schleher
Thesis Co-Advisor

John P. Powers
Chairman, Department of Electrical and Computer Engineering

Dan C. Boger
Chairman, Department of Information Sciences

THIS PAGE INTENTIONALLY LEFT BLANK

ABSTRACT

The significance of the Radar Cross Section (RCS) in the outcome of military engagements makes its prediction an important problem in modern Electronic Warfare. The POFACETS program, previously developed at the Naval Postgraduate School (NPS), uses the Physical Optics method to predict the RCS of complex targets, which are modeled with the use of triangular facets. The program has minimum computer resource requirements and provides convenient run-times. This thesis upgraded, enhanced and expanded the functionalities and capabilities of the POFACETS program. The new functionalities were implemented by upgrading the Graphical User Interface and model database, allowing the creation of models with an unlimited number of facets, providing capabilities for the automatic creation of models with standard geometric shapes, allowing the combination of existing target models, providing capabilities for sharing target models with commercial CAD programs, and creating new display formats for RCS results. The new computational capabilities include the development of a user-updateable database of materials and coatings that can be applied to models in one or multiple layers, and the computation of their effects on the models' RCS. Also implemented are the computations of the ground's effect on the RCS, and the exploitation of symmetry planes in models, in order to decrease run-time for RCS prediction.

THIS PAGE INTENTIONALLY LEFT BLANK

TABLE OF CONTENTS

I.	INTRODUCTION.....	1
A.	MOTIVATION	1
B.	BACKGROUND	2
C.	STATEMENT OF PURPOSE	3
D.	DELIMITATIONS OF THE PROJECT	5
E.	THESIS OVERVIEW	5
II.	RADAR CROSS SECTION THEORY	7
A.	RADAR CROSS SECTION AND THE RADAR EQUATION	7
B.	SIGNIFICANCE OF THE RADAR CROSS-SECTION	8
C.	RADAR CROSS SECTION DEFINED	11
D.	SCATTERING REGIONS	14
1.	Low Frequency Region or Rayleigh Region $\left(\frac{2\pi}{\lambda} L \ll 1\right)$	14
2.	Resonance Region or Mie Region $\left(\frac{2\pi}{\lambda} L \approx 1\right)$	14
3.	High Frequency Region or Optical Region $\left(\frac{2\pi}{\lambda} L \gg 1\right)$	14
E.	RADAR CROSS SECTION PREDICTION METHODS	15
1.	Method of Moments	15
2.	Finite Difference Methods	16
3.	Microwave Optics	16
4.	Physical Optics	17
F.	SUMMARY	17
III.	PHYSICAL OPTICS APPLIED TO TRIANGULAR FACET MODELS	19
A.	RADIATION INTEGRALS FOR FAR ZONE SCATTERED FIELDS	19
B.	RADIATION INTEGRALS FOR A TRIANGULAR FACET	20
C.	RADIATION INTEGRALS FOR A TRIANGULAR FACET	22
D.	COORDINATE TRANSFORMATIONS	24
E.	PHYSICAL OPTICS SURFACE CURRENT COMPUTATION	26
F.	SCATTERED FIELD COMPUTATION	27
G.	DIFFUSE FIELD COMPUTATION	29
H.	TOTAL FIELD FROM A TARGET	31
I.	SUMMARY	33
IV.	NEW FUNCTIONALITIES ADDED TO THE POFACETS PROGRAM.....	35
A.	GRAPHICAL USER INTERFACE (GUI) UPGRADE TO CURRENT MATLAB VERSION	35
1.	Rationale	35
2.	Procedure	36

	3.	Results	36
B.		MODEL DATABASE UPGRADE	38
	1.	Rationale	38
	2.	Procedure	39
	3.	Results	39
C.		MANUAL MODEL DESIGN	40
	1.	Rationale	40
	2.	Procedure	41
	3.	Results	44
D.		GRAPHICAL MODEL DESIGN	45
	1.	Rationale	45
	2.	Procedure	46
	3.	Results	50
E.		IMPORT/EXPORT OF MODELS	51
	1.	Rationale	51
	2.	Procedure	52
	3.	Results	53
F.		COMBINATION OF MODELS	56
	1.	Rationale	56
	2.	Procedure	56
	3.	Results	58
G.		RCS COMPUTATION OPTIONS	60
	1.	Rationale	60
	2.	Procedure and Results	61
		a. <i>RCS versus Observation Angles</i>	61
		b. <i>RCS versus Frequency</i>	68
H.		RCS RESULTS DISPLAY OPTIONS	70
	1.	Rationale	70
	2.	Procedure and Results	70
		a. <i>User-Selectable Dynamic Range</i>	70
		b. <i>Polar Plots</i>	71
		c. <i>Combination Plots</i>	72
I.		SUMMARY	76
V.		NEW COMPUTATIONAL CAPABILITIES ADDED TO THE POFACETS PROGRAM	77
A.		EXPLOITATION OF SYMMETRY PLANES	77
	1.	Rationale	77
	2.	Background	77
	3.	Procedure	81
	4.	Results	84
B.		EFFECTS OF MATERIALS AND COATINGS ON RCS	85
	1.	Rationale	85
	2.	Background	86
		a. <i>Case 1: Multiple Composite Layers</i>	87
		b. <i>Case 2: Composite Layer on PEC</i>	89

c.	<i>Case 3: Composite Layer</i>	90
d.	<i>Case 4: Multiple Layers on PEC</i>	90
3.	Procedure	91
4.	Results	94
C.	EFFECTS OF GROUND	98
1.	Rationale	98
2.	Background	99
3.	Procedure	104
4.	Results	105
D.	SUMMARY	107
VI.	SUMMARY AND RECOMMENDATIONS	109
A.	SUMMARY	109
B.	RECOMMENDATIONS	110
APPENDIX.	POFACETS FILES AND MODEL DATABASE STRUCTURE	111
A.	POFACETS FILE FRAMEWORK	111
B.	POFACETS FILE DESCRIPTION	119
C.	POFACETS DATA STRUCTURES DESCRIPTION	122
1.	Model File Structure	122
a.	<i>Coord</i>	122
b.	<i>Facet</i>	122
c.	<i>Scale</i>	122
d.	<i>Symplanes</i>	122
e.	<i>Comments</i>	122
f.	<i>Matrl</i>	123
2.	Material Database File Structure	123
a.	<i>Name</i>	123
b.	<i>er</i>	123
c.	<i>tande</i>	123
d.	<i>mpr</i>	123
e.	<i>m2pr</i>	123
	LIST OF REFERENCES	125
	INITIAL DISTRIBUTION LIST	127

THIS PAGE INTENTIONALLY LEFT BLANK

LIST OF FIGURES

Figure 1.	Typical Radar–Target Scenario (From Ref. 5.)	7
Figure 2.	Advantage of Stealth Fighter over Conventional Fighter (After Ref. 1.)	10
Figure 3.	Coordinate System (After Ref. 5.)	12
Figure 4.	Radar Cross Section of a Sphere (From Ref. 5.)	15
Figure 5.	Far Field Scattering from an Arbitrary Body (After Ref. 2.)	19
Figure 6.	Arbitrary Oriented Facet (After Ref. 3.)	21
Figure 7.	Arbitrary Oriented Facet (a) Geometry (b) Facet Sub–Areas (From Ref. 3.)	22
Figure 8.	Global and Local Coordinate Systems (From Ref. 3.)	24
Figure 9.	Rotation Angles (From Ref. 3.)	25
Figure 10.	Gaussian Approximation of a Rough Surface (From Ref. 3.)	30
Figure 11.	(a) Large Correlation Distance, (b) Small Correlation Distance (From Ref. 3.)	31
Figure 12.	Flow Chart for the RCS Calculation of a Collection of Facets	33
Figure 13.	POFACETS Main Screen	37
Figure 14.	POFACETS Contributors	38
Figure 15.	File Conversion Options (circled)	40
Figure 16.	Manual Model Design GUI Form	41
Figure 17.	Vertex Coordinate Input	42
Figure 18.	Facet Definition	43
Figure 19.	Plate Model Display	44
Figure 20.	Dart Model Display	45
Figure 21.	Graphical Model Design GUI Form	46
Figure 22.	Sphere Parameters	47
Figure 23.	Sphere Model (20 Points per Circle)	47
Figure 24.	Sphere Model (40 Points per Circle)	48
Figure 25.	Model Rotation Dialog Box	49
Figure 26.	(a) Cone Model, (b) Rotation of 60 Degrees Around X Axis	49
Figure 27.	Graphically Designed Models (a) Ellipsoid, (b) Fuselage, (c) Ogive, (d) Box	51
Figure 28.	Import/Export Options (circled)	53
Figure 29.	Cylinder Model Imported from Stereo–Lithographic Format	54
Figure 30.	T–62 AFV Model Imported from ACADS Format	54
Figure 31.	X–29 Aircraft Model Imported from DEMACO Format	55
Figure 32.	Star–Shaped Model Imported from <i>Pdetool</i>	55
Figure 33.	Model Combination (circled)	56
Figure 34.	UAV Model	57
Figure 35.	Facet Descriptions	58
Figure 36.	Various Models (a) X–29, (b) AIM–9, (c) AGM–84	59
Figure 37.	Armed X–29 Aircraft Model	60
Figure 38.	Monostatic RCS Calculation GUI	63

Figure 39.	RCS of a 1 m by 1 m PEC Plate at 1 GHz, TM wave, for $\phi = 0$	64
Figure 40.	RCS of a 1 m by 1 m PEC Plate for at 1 GHz, TM Wave	65
Figure 41.	Bistatic RCS Calculation GUI	66
Figure 42.	Bistatic RCS Example	67
Figure 43.	Specular Reflection and Forward Scatter from a Plate	67
Figure 44.	Monostatic RCS versus Frequency GUI	68
Figure 45.	RCS of a 1 m by 1 m PEC Plate versus Frequency (Vertical Incidence)	69
Figure 46.	Bistatic RCS versus Frequency GUI	69
Figure 47.	Dynamic Range Effects	71
Figure 48.	Polar Plot	72
Figure 49.	Combination Plot	73
Figure 50.	Combination Graph of the UAV Model	74
Figure 51.	Annotated UAV RCS Plot	75
Figure 52.	Symmetry Plane Scenario – Global Coordinates	78
Figure 53.	Symmetry Plane Scenario – Local Coordinates	79
Figure 54.	Cases of Incidence Angle in Local Coordinates	80
Figure 55.	Symmetry Controls in the Graphical Model Design GUI (circled)	81
Figure 56.	Symmetry Plane Definition	82
Figure 57.	Symmetry Planes for a Sphere Model	83
Figure 58.	Symmetry Selection for Monostatic RCS Calculations (circled)	84
Figure 59.	Monostatic RCS of a Sphere with Radius of 3 m at 18 GHz	85
Figure 60.	Wave Incident on Multiple Layers (After Ref. 8.)	87
Figure 61.	Incidence and Transmission Angles at the Boundary Between Two Layers ..	89
Figure 62.	Composite Layer on PEC	90
Figure 63.	Materials Database Management GUI	91
Figure 64.	New Material Data Input GUI	91
Figure 65.	Material Application GUI	92
Figure 66.	Material View GUI	93
Figure 67.	Material Type Selection Dialog Box	93
Figure 68.	RCS vs. Frequency of a 1 m by 1 m PEC Plate (normal incidence)	94
Figure 69.	RCS vs. Frequency of a 1 m by 1 m Plate with One Composite Layer (normal incidence)	95
Figure 70.	RCS vs. Frequency of a 1 m by 1 m Plate with Two Composite Layers (normal incidence)	96
Figure 71.	RCS vs. Frequency of a 1 m by 1 m Plate with One Composite Layer on PEC (normal incidence)	97
Figure 72.	RCS vs. Frequency of a 1 m by 1 m Plate with Two Composite Layers on PEC (normal incidence)	98
Figure 73.	Target Over Infinite Ground Plane	99
Figure 74.	Direct Incident – Direct Scattered	100
Figure 75.	Direct Incident – Reflected Scattered	101
Figure 76.	Reflected Incident – Direct Scattered	102
Figure 77.	Reflected Incident – Direct Scattered Equivalent Scenario	102
Figure 78.	Reflected Incident – Reflected Scattered	103
Figure 79.	Reflected Incident – Reflected Scattered Equivalent Scenario	103

Figure 80.	Ground Plane Controls (circled)	105
Figure 81.	RCS vs. Frequency of a 1 m by 1 m PEC Plate (normal incidence).....	106
Figure 82.	RCS vs. Frequency of a 1 m by 1 m PEC Plate (normal incidence) with PEC Ground Plane 9.25 m Below the Plate	106
Figure 83.	POFACETS Main Screen File Framework.....	112
Figure 84.	Manual Model Design File Framework	113
Figure 85.	Graphical Model Design File Framework	114
Figure 86.	Monostatic RCS Calculation File Framework	115
Figure 87.	Bistatic RCS Calculation File Framework.....	116
Figure 88.	Utilities File Framework	117
Figure 89.	RCS Computation and Display File Framework	118

THIS PAGE INTENTIONALLY LEFT BLANK

ACKNOWLEDGMENTS

The author is grateful to his country, Greece, and the Hellenic Air Force for providing him with the opportunity to study at the Naval Postgraduate School.

The author would also like to acknowledge with sincere gratitude the advice, help, guidance and encouragement he received from Professor David C. Jenn during the nine months that led to the conclusion of this thesis.

Many thanks are also due to Professors D. Curtis Schleher, Phillip E. Pace, A. W. Cooper, and Roberto Cristi for making his studies at NPS a truly worthwhile learning experience.

The author would like to also thank his wife, Effrosyni, and his daughter, Niki, for their tireless patience, enduring understanding and unfailing support.

He is also thankful of his parents for encouraging him to improve himself constantly through education and personal study.

THIS PAGE INTENTIONALLY LEFT BLANK

EXECUTIVE SUMMARY

Signature control, one of the most significant aspects of Electronic Warfare, places great emphasis on the reduction of RF signatures emitted from military platforms. One important aspect in RF signature reduction involves the Radar Cross Section (RCS) of the platforms. The goal of the RCS reduction is to decrease the range at which an enemy radar can detect the platform, in order to minimize the reaction time available to the threat or to deny detection altogether, by allowing the platform to remain “hidden” in the ground or sea clutter.

Thus, the prediction of the Radar Cross Section of operational platforms and the evaluation of the effects of potential RCS reduction techniques, such as shaping and use of radar absorbing materials (RAM), for the full spectrum of usable radar frequencies provides a challenging problem in modern electronic warfare. The POFACETS 2.3 program, a MATLAB application, developed at the Naval Postgraduate School, is an inexpensive, user-friendly, easy to use, RCS prediction software tool that has minimum requirements on computer resources and is capable of producing RCS predictions within small amounts of time for standard three-dimensional geometric shapes.

The program models any arbitrary target by utilizing triangular facets. The scattered field from each facet is computed using the radiation integrals. The Physical Optics method is used to calculate the currents on each facet. This method is a high frequency approximation that provides the best results for electrically large targets as well as in the specular direction.

The need to improve the program was dictated by certain inherent limitations in the target modeling, the structure of the file models, and some compatibility issues with the current MATLAB version. Hence, the objective of this thesis was to improve the existing POFACETS RCS prediction software tool. This objective was achieved by providing new functionalities and adding new computational capabilities to the POFACETS 2.3 version.

The new functionalities included the Graphical User Interface (GUI) and model database upgrade, the improvement of the manual model design options, the creation of a graphical model design GUI, the inclusion of capabilities for importing and exporting models compatible with commercial Computer Aided Design (CAD) programs, the inclusion of capabilities for a combination of existing models, the computation of RCS versus frequency, and the creation of new options for the display of RCS results.

The new computational capabilities included the exploitation of symmetry planes in target models to decrease run-time for RCS prediction, the development of a user-updateable database of materials, which can be applied to models in one or multiple layers, the computation of the effects of materials and coatings in the model RCS, and the computation of the effects of the ground on the RCS of a model.

Overall, the program is now user-friendlier, by providing easy-to-use GUIs and familiar controls, while minimizing the possibility for erroneous input. Moreover, the creation of complex models was facilitated through the use of automated standard model design and the new capabilities, which allow the program to combine existing models and share models with CAD software. Despite the new improvements and computational capabilities, minimal effect occurred to the required program execution time, while the option for the exploitation of symmetry planes, when these exist, can drastically decrease execution time.

The versatility of the program was enhanced by allowing the capability for RCS computation versus frequency and providing a broader range of options for RCS display. Indeed, these capabilities allow for the use of the program not only for RCS prediction, but for RCS analysis as well.

Finally, the capability to use very complex models, the materials database, the capability to apply different types of materials and coatings to the models' surfaces and the inclusion of the effects of the ground on RCS, have made the POFACETS 3.0 a much more useful tool regarding real-world RCS prediction and analysis problems.

The POFACETS 3.0 program was implemented in the current version of the MATLAB software, and thus, it can be easily modified and upgraded through the wide variety of tools provided by this software package. Two areas of potential improvements involve including additional scattering mechanisms, such as second reflections, diffraction, and traveling waves in the RCS calculations and providing capabilities for importing a wider variety of model file types from commercial CAD software.

THIS PAGE INTENTIONALLY LEFT BLANK

I. INTRODUCTION

A. MOTIVATION

Signature control is recognized today as one of the most significant aspects of Electronic Warfare. In the past decades, signature control technology, commonly known as stealth, has become a critical technology area, as it directly affects the survivability of both the military weapon platforms and the weapons themselves. The goal of signature control is to reduce the various signatures of a platform to a level that allows the platform to remain undetected from the threat sensors.

In the effort to produce such low-observable platforms, various signatures can be considered, such as RF (Radio Frequency), IR (Infrared), visible, laser, acoustic and magnetic. However, in general, the RF signatures are considered to be of prime importance in military applications, because radar is the premier military sensor today and is capable of providing reliable target detection at long ranges and under a wide variety of environmental conditions (Ref. 1).

Consequently, the reduction of the RF signature has received high priority in the design of many new military platforms (e.g., F-117 and B-2 aircraft, the Swedish Navy's Visby Class Stealth Corvette, etc.). One aspect of the reduction of the RF signatures involves the reduction of emissions. Indeed, if a high-power radar is operating aboard a platform, its emissions will probably be detected by the enemy's passive sensors, such as the electronic support measures (Ref. 2). The other aspect of the reduction of the RF signatures involves the Radar Cross Section (RCS) of the platforms. The goal of the RCS reduction is to decrease the range at which an enemy radar can detect the platform, in order to minimize the reaction time available to the threat or to deny detection altogether, by allowing the platform to remain "hidden" in the ground or sea clutter.

Thus, the prediction of the Radar Cross Section of operational platforms and the evaluation of the effects of potential RCS reduction techniques, such as shaping and use of radar absorbing materials (RAM) for the full spectrum of usable radar frequencies provides a challenging problem in modern electronic warfare. One approach to high fre-

quency RCS prediction calculations is to describe a complex model with an array of simple shapes, such as triangles or flat plates. The contribution of each simple shape is calculated in order to obtain the RCS of the whole target.

Although several RCS prediction methods exist for arbitrary three-dimensional targets, most of them require a considerable amount of computer resources and processing time. In addition, the procurement of the software, which implements these methods, usually represents a significant amount of investment in capital and training time. Hence, there is a need for an inexpensive, user-friendly, easy to use, RCS prediction software tool that will run on a standard computer and will be able to produce RCS predictions within small amounts of time (in the order of seconds or minutes) for standard three-dimensional geometric shapes. This software tool should also provide the user the capability to model any three-dimensional object with simple component shapes, display the geometry of the model in order to allow inspection by the user and, of course, allow the user to enter the necessary parameters for the calculation of the Radar Cross Section of the model.

B. BACKGROUND

Such a software code was developed by Professor David C. Jenn and Commander Elmo E. Garrido Jr. The code was implemented in MATLAB and utilizes the Physical Optics (PO) approximation technique for the RCS calculation. This technique, as explained in Chapter II, is not overly computationally demanding and provides relatively accurate results for most large target models, while requiring minimal amounts of run-time. The initial RCS prediction code was developed by Professor David C. Jenn. Commander Elmo J. Garrido Jr. upgraded the code by adding Graphical User Interface (GUI) capabilities (Ref. 3). The end-product is the POFACETS program, whose current version is 2.3.

The POFACETS program provides the user an easy-to-use GUI that allows the input of all necessary parameters, while preventing erroneous data input and other user errors. The program enables the user to create a model comprised of triangular facets, with options for specifying various surface characteristics of the facets, such as surface resistivity, surface roughness and whether a facet side is external (hence potentially illuminated).

nated by the threat radar) or internal (hence not illuminated). The program allows the user to display and inspect the model and it provides additional options for enhancing the visualization of its geometry.

Once a model is defined, the user can calculate its RCS, defined in the next chapter, based on the radar frequency and other parameters of interest. Once the RCS is computed, an appropriate plot is generated to display the calculated data.

The main disadvantages of the existing POFACETS version are related to its model design features. Specifically, the GUI allows the user to enter a limited number of facets (40 maximum) making it impossible to model more complex objects. At the same time, since the program requires the coordinates of each vertex of a facet to be entered manually, the whole process can become time consuming and counter-productive for larger models. In addition, there is no capability to combine existing models to create ones that are more complex or to import models created in other commercially available Computer Aided Design (CAD) programs.

Finally, since the POFACETS 2.3 version was developed in 2000, in a previous version of MATLAB, this creates maintenance and compatibility problems with the current MATLAB versions, especially in the area of the GUI figure definition.

C. STATEMENT OF PURPOSE

The purpose of this thesis was to enhance the existing POFACETS RCS prediction software tool. It exploits the existing RCS calculation code and aims to achieve the following two goals.

The first is to improve the existing functionalities of the POFACETS 2.3 version by:

- Upgrading the GUI to the current MATLAB version
- Upgrading the POFACETS models database
- Providing capabilities for the creation of models with an arbitrary number of facets (limited only by the computer capabilities)
- Providing capabilities for the automatic creation of models with standard geometric shapes
- Allowing the combination/merging of existing target models

- Providing capabilities for importing models created in commercially available CAD programs
- Providing capabilities for exporting models, so that they can be used by commercially available CAD programs
- Providing new options for computing RCS versus frequency
- Providing new display options of RCS results, such as polar plots, and RCS plots superimposed on the model geometry

The second is to add new computational capabilities to the program. These include:

- Exploitation of symmetry planes in target models to decrease run-time for RCS prediction
- Computation of the RCS of a model over infinite ground plane
- Development of a user-updateable database of materials which can be applied to models in one or multiple layers
- Computation of effects of materials and coatings in the model RCS

The existing POFACETS version is already in use by NPS students, students of other universities and RCS professionals. This thesis is expected to provide new capabilities regarding the prediction of RCS and to make the application even more versatile and easy to use. Specifically:

- The added capabilities (e.g., RCS of targets over ground planes, effects of materials and coatings) will make the existing application a serious candidate for use not only by universities for educational purposes but by other services and institutions.
- The versatility of the application will be greatly enhanced by adding the capability to import target models designs implemented in other CAD software. Similarly, the capability to combine and merge existing target models will provide the option to create very complex target models by combining simpler models of subcomponents designed by different individuals or students.
- The application will become even more user-friendly by upgrading the existing Graphical User Interface, adding a database of materials and coatings that the user can choose from and providing the capability to use certain standard model shapes (e.g., spheres, plates, boxes, cylinders, ellipsoids, trapezoids, cones, radomes, fuselages, etc.).

D. DELIMITATIONS OF THE PROJECT

This thesis will aim to expand, enhance and upgrade the current POFACETS software version. The existing core software code of this program, which produced the calculation of the scattered field from a triangular facet for a given set of parameters, also formed the basis of the new POFACETS version, which resulted from this thesis. All the new features, options, functionalities, and capabilities that this thesis added to the POFACETS program utilized this code at some point in the program.

This delimitation makes also clear that the program is based exclusively on the Physical Optics approximation method for the calculation of the RCS of a model. Chapter II discusses the limitations and weaknesses of this method.

Furthermore, during the design, development and implementation of the code, which implements the new functionalities and capabilities of the new POFACETS version, certain assumptions or approximations will have to be made, in order to limit the program complexity and to produce acceptable run-times. When these assumption or approximations occur, the appropriate section in the following chapters of this thesis explains their rationale.

E. THESIS OVERVIEW

This chapter provides a brief background regarding the need for an inexpensive and easy-to-use software tool for the prediction of the Radar Cross Section of complex models, along with the features that such a tool should incorporate. The statement of purpose and the detailed goals of this project have been specified and its delimitations described.

Chapter II describes the importance of the radar cross-section, as this appears in the radar equation and provides a practical example of its significance in a military engagement. The RCS is then formally defined, followed by a brief discussion regarding electromagnetic scattering fundamentals. The chapter concludes with a comparative discussion of some common methods of RCS prediction.

Chapter III contains the theoretical framework of the Physical Optics approximation method and the mathematical formulations used in the POFACETS program to implement this method. All the auxiliary tools and formulas utilized in the program are de-

defined and explained. The prediction of the scattered field from a single facet is first explained and then it is used as the basis for the calculation of the scattered field from a collection of facets (i.e., an arbitrary model). Essentially, this chapter contains the fundamental theory utilized in the existing POFACETS version.

Chapter IV contains the description of the new functionalities of the POFACETS version resulting from this thesis work. It provides the details of the available options for the manual or graphical design of a model, the capabilities for importing models from, or exporting models to, other commercially available CAD software, the description of available RCS computation options and the available RCS results display options.

Chapter V presents the new RCS computation capabilities added to the POFACETS program as a result of this thesis. These include the calculation of the effects of infinite ground planes on target RCS, the calculation of the effects of various materials and coatings, and the exploitation of symmetry planes. For each case, the theoretical framework upon which the software is based is presented, followed by the implemented program features and the RCS results obtained.

Chapter VI summarizes the outcomes of the thesis work and suggests further improvements to the program.

Finally, since the end result of this thesis work is quite a complex program, consisting of more than 30 MATLAB script files and 15 MATLAB figure files, the Appendix at the end of the thesis provides the framework that shows the interconnection and functionality of each script or figure file. The main goal of this framework is to help the reader understand how the program operates, rather than providing a user manual, since the program itself incorporates detailed user instructions either through dialog boxes or help screens.

II. RADAR CROSS SECTION THEORY

This chapter discusses the importance of the Radar Cross Section and its role in the radar equation and provides examples of its significance in Electronic Warfare. The RCS is then formally defined, followed by a brief discussion regarding scattering regions. The chapter concludes with a comparative discussion of some common methods of RCS prediction.

A. RADAR CROSS SECTION AND THE RADAR EQUATION

The radar equation relates the range of a radar to the characteristics of the transmitter, the receiver, the antennas, the target, and the environment. It is useful for determining the maximum range at which a given radar can detect a target and it can serve as a means for understanding the factors that affect radar performance (Ref. 4).

A typical scenario is depicted in Figure 1. The TX box represents the radar transmitter, the RX box the radar receiver, while the grey object to the right represents the target. The transmit and receive antennas are located close to each other; hence it is assumed that their range to the target is equal to R .

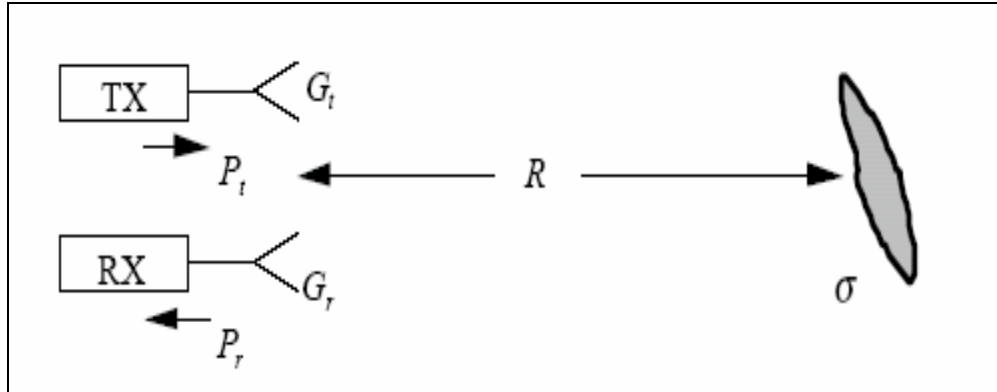


Figure 1. Typical Radar–Target Scenario (From Ref. 5.)

The simplest form of the radar equation is given by

$$P_r = \left(\frac{P_t G_t}{4\pi R^2} \right) \left(\frac{\sigma}{4\pi R^2} \right) \left(\frac{G_r \lambda^2}{4\pi} \right) \quad (2.1)$$

where, P_r is the power received by the radar (in watts), P_t the output power of the transmitter (in watts), G_t the gain of the transmitter antenna, G_r the gain of the receiver antenna, σ the Radar Cross Section of the target (in m^2), λ the wavelength of the radar's operating frequency (in meters) and R the range between the radar and the target (in meters).

Notice that the first term in parenthesis represents the radar power density at the target (in watts/m^2). The product of the first and second terms in parenthesis represents the power density at the radar receiver due to the reflection or scattering that occurs on the target. The third term in parenthesis represents the amount of the reflected power captured by the receiving antenna aperture.

For the monostatic radar case, in which the radar uses the same antenna for transmitting and receiving, G_t is equal to G_r and by setting $G_t = G_r = G$, Equation (2.1) can be written as:

$$P_r = \frac{P_t G^2 \sigma \lambda^2}{(4\pi)^3 R^4}. \quad (2.2)$$

The maximum range of a radar, R_{\max} , is the distance beyond which the target cannot be detected. It occurs when the received signal power P_r just equals the minimum detectable signal S_{\min} (Ref. 4). Substituting $P_r = S_{\min}$ in Equation (2.2) and rearranging terms gives:

$$R_{\max} = \left[\frac{P_t G^2 \sigma \lambda^2}{(4\pi)^3 S_{\min}} \right]^{1/4}. \quad (2.3)$$

Although this form of the radar equation excludes many important factors and usually predicts high values for maximum range, it depicts the relationship between the maximum radar range and the target's RCS.

B. SIGNIFICANCE OF THE RADAR CROSS-SECTION

Equation (2.3) indicates that the free-space detection range of a radar is proportional to the RCS of the target, raised to the one-quarter power ($\sigma^{1/4}$). Thus, decreasing the RCS by a factor of 10 translates to a 56% decrease in the free-space detection range. Consequently, the reaction time of the weapon system that utilizes this radar will be de-

creased to approximately half. In addition, if the target is an aircraft flying at low altitude in heavy clutter, the MTI improvement factor required for detection will be increased by 10 dB, rendering many radars designed to detect conventional aircraft inoperable (Ref. 1).

An illustration of the effectiveness of RCS in military engagements is depicted in Figure 2. In this scenario, a “stealth” fighter with RCS that varies from 0.01 m^2 to 10 m^2 is engaged head on with a conventional fighter aircraft, whose RCS is 5 m^2 . The engagement occurs at 30,000 feet and both aircraft fly at Mach 0.9. Three different curves are shown. One curve corresponds to an engagement scenario in which both aircraft have long-range radars capable of detecting a target with RCS of 5 m^2 at 125 km. The second curve corresponds to an engagement scenario in which both aircraft have short-range radars capable of detecting a target with RCS of 5 m^2 at 50 km. The third curve corresponds to an engagement scenario in which the “stealth” fighter has a radar with a 90-km detection range against a target with RCS of 5 m^2 , while the conventional fighter has a long-range radar capable of detecting the same target at 125-km range (Ref. 1).

The shaded area in the middle of the graph represents a region in which either fighter can fire the first missile shot. It is easy to see that as the RCS of the “stealth” aircraft is reduced and that the margin for the first missile launch by this aircraft against the conventional fighter is increased. For example, if the “stealth” aircraft has a RCS of 0.1 m^2 , then it could target the conventional fighter for approximately 60 seconds, before the conventional fighter can fire its missiles (for the equal short-range radar scenario). This time margin exceeds 70 seconds in the scenario in which the conventional fighter is equipped with a superior range radar and reaches approximately 110 seconds in the scenario in which both aircraft have equal long-range radars.

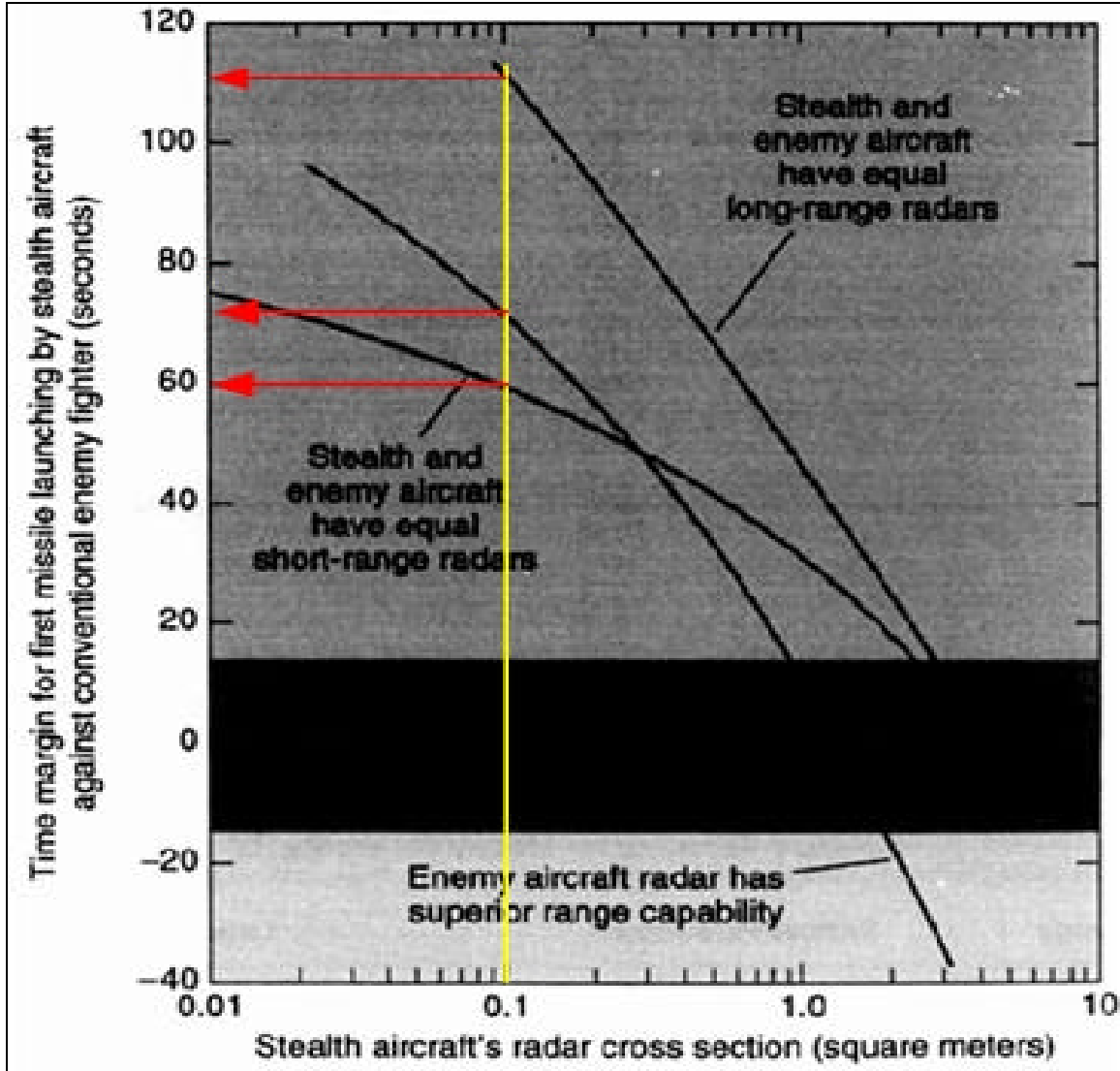


Figure 2. Advantage of Stealth Fighter over Conventional Fighter (After Ref. 1.)

In addition, the RCS of a platform plays an important role in defining the jammer capability requirements of this platform. Indeed, the “burn-through range,” which is the range at which a threat radar overcomes the jamming effects of a platform, is found to be proportional to the square root of the ratio of the platform’s RCS and the platform’s jamming effective radiated power, shown in the following equation (Ref. 1):

$$R_{BT} \propto \left[\frac{\sigma}{ERP_j} \right]^{1/2} \quad (2.4)$$

where R_{BT} is the burn-through range and ERP_j is the jammer's effective radiated power. It is clear that, for the same jamming effect (i.e., the same burn-through range), if the target RCS (σ) is decreased then the self-protection jammer effective radiated power can be decreased in the same proportion. Eventually, as the Radar Cross Section becomes small enough, no jammer is required. Thus, the term (σ / ERP_j) can be considered a figure of merit for the jammer (Ref. 1).

C. RADAR CROSS SECTION DEFINED

As demonstrated in the radar equation, the Radar Cross Section (σ) is a property of a scattering object (target) representing the magnitude of the echo signal returned to the radar by this object. The definition of RCS can be stated as:

$$\sigma \equiv \frac{\text{Power reflected to receiver per unit solid angle}}{\text{Incident power density}/4\pi}.$$

It is evident that the RCS of a target is the measure of the power scattered in a given direction, when the target is illuminated by an incident wave, normalized to the power density of the incident field. The purpose of the normalization is to remove the effect of the range and, hence, to arrive at a RCS value that is independent of the distance between the target and the illumination source (Ref. 3).

In terms of the incident and scattered fields, it is more suitable to write the RCS as:

$$\sigma = \lim_{R \rightarrow \infty} 4\pi R^2 \frac{|\vec{E}_s|^2}{|\vec{E}_i|^2} \quad (2.5)$$

where R is the range between the target and the illumination source (radar), and $|\vec{E}_i|$ and $|\vec{E}_s|$ the electric field amplitudes of the incident and scattered field, respectively. It is assumed that the target is far enough from the radar that the incident wave can be considered to be planar, rather than spherical. Moreover, in the far zone of the target, the scattered field dependence on range will approach $1/R$ and, therefore, σ will be independent of range (Refs. 1 and 4).

The Radar Cross Section can be characterized as monostatic when the transmitter and receiver are collocated, or bistatic when the transmitter and receiver are placed in different locations. The Radar Cross Section has units of square meters. However, it is usually expressed in decibels relative to a square meter (dBsm):

$$\sigma \text{ [dBsm]} = 10\log(\sigma \text{ [m}^2\text{]}). \quad (2.6)$$

The Radar Cross Section is a scalar number that is a function of the target configuration and its material composition, frequency and polarization of the incident wave, and target aspect (i.e., its orientation relative to the radar). Consequently, in general, the Radar Cross Section could be specified as $\sigma_{pq}(\theta, \phi)$, where p and q pertain to the scattered and incident polarizations, respectively, while θ and ϕ are the polar spherical angles, as shown in Figure 3.

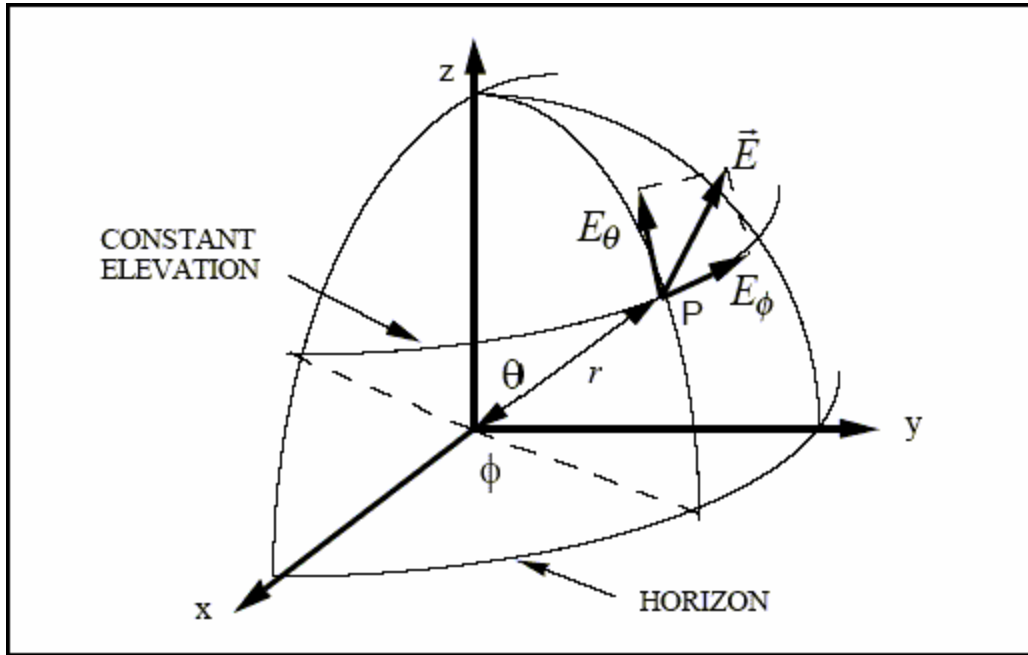


Figure 3. Coordinate System (After Ref. 5.)

In the general case, the polarization of the incident wave from the radar will not be in the same orientation as the polarization of the target coordinate system. Therefore, it is necessary to decompose the polarization of the incident wave into components in the target coordinate system. Since the wave vector components at large distances are tangent

to a sphere, two orthogonal components in terms of the variables θ and ϕ are sufficient to represent the incident field in a spherical system centered at the target. Thus, in general, it is possible to write the incident field as:

$$\vec{E}_i = E_{i\theta}\hat{\theta} + E_{i\phi}\hat{\phi} \quad (2.7)$$

where $\hat{\theta}$ and $\hat{\phi}$ are the unit vectors in the target coordinate system and the index i signifies incident field (Ref. 2).

In addition, the polarization of the scattered field will not necessarily be the same as the incident field, since most complex targets generate a cross-polarized scattering component due to multiple diffractions and reflections. The scattering matrix reflects this, and it can be used to specify the relationship between the polarization of the incident and the scattered field:

$$\begin{bmatrix} E_{s\theta} \\ E_{s\phi} \end{bmatrix} = \begin{bmatrix} S_{\theta\theta} & S_{\theta\phi} \\ S_{\phi\theta} & S_{\phi\phi} \end{bmatrix} \begin{bmatrix} E_{i\theta} \\ E_{i\phi} \end{bmatrix} \quad (2.8)$$

where the index s denotes the scattered field.

The S_{pq} symbols represent the scattering parameters, with the index p specifying the scattered field polarization and the index q specifying the incident field polarization. The elements of the scattering matrix are complex quantities related to the RCS with the following equation (Ref. 2):

$$S_{pq} = \frac{\sqrt{\sigma_{pq}}}{\sqrt{4\pi R^2}}. \quad (2.9)$$

It is possible to write this in terms of amplitude and phase as:

$$S_{pq} = \frac{|\sigma_{pq}|^{1/2} e^{j\psi_{pq}}}{\sqrt{4\pi R^2}} \quad (2.10)$$

where

$$\psi_{pq} = \arctan \left[\frac{\text{Im}(\sigma_{pq})}{\text{Re}(\sigma_{pq})} \right] \quad (2.11)$$

and $\text{Re}(\cdot)$ and $\text{Im}(\cdot)$ are the real and imaginary operators.

D. SCATTERING REGIONS

As mentioned in the previous paragraphs, the Radar Cross Section depends on the frequency of the incident wave. There are three frequency regions in which the RCS of a target is distinctly different. The regions are defined based on the size of the target in terms of the incident wavelength. For a smooth target of length L , the definitions of the three frequency regimes follow.

1. Low Frequency Region or Rayleigh Region $\left(\frac{2\pi}{\lambda} L \ll 1 \right)$

At these frequencies, the phase variation of the incident plane wave across the extent of the target is small. Thus, the induced current on the body of the target is approximately constant in amplitude and phase. The particular shape of the body is not important. Generally, σ versus $\frac{2\pi}{\lambda} L$ is smooth and varies as $1/\lambda^4$ (Ref. 2).

2. Resonance Region or Mie Region $\left(\frac{2\pi}{\lambda} L \approx 1 \right)$

For these frequencies, the phase variation of the current across the body of the target is significant and all parts contribute to the scattering. Generally, σ versus $\frac{2\pi}{\lambda} L$ and will oscillate (Ref. 2).

3. High Frequency Region or Optical Region $\left(\frac{2\pi}{\lambda} L \gg 1 \right)$

For these frequencies, there are many cycles in the phase variation of the current across the target body and, consequently, the scattered field will be very angle-dependent. In this region, σ versus $\frac{2\pi}{\lambda} L$ is smooth and may be independent of λ (Ref. 2).

Figure 4 depicts the Radar Cross Section of a sphere with radius a , where β is defined as $\beta = 2\pi/\lambda$. The three scattering regions are clearly illustrated. When $\beta a < 0.5$, the curve in the Rayleigh region is almost linear. However, above 0.5, in the resonance region, the RCS oscillates. The oscillations die out as βa takes higher values. Eventually, for $\beta a > 10$, the value of the RCS is essentially constant and equal to πa^2 .

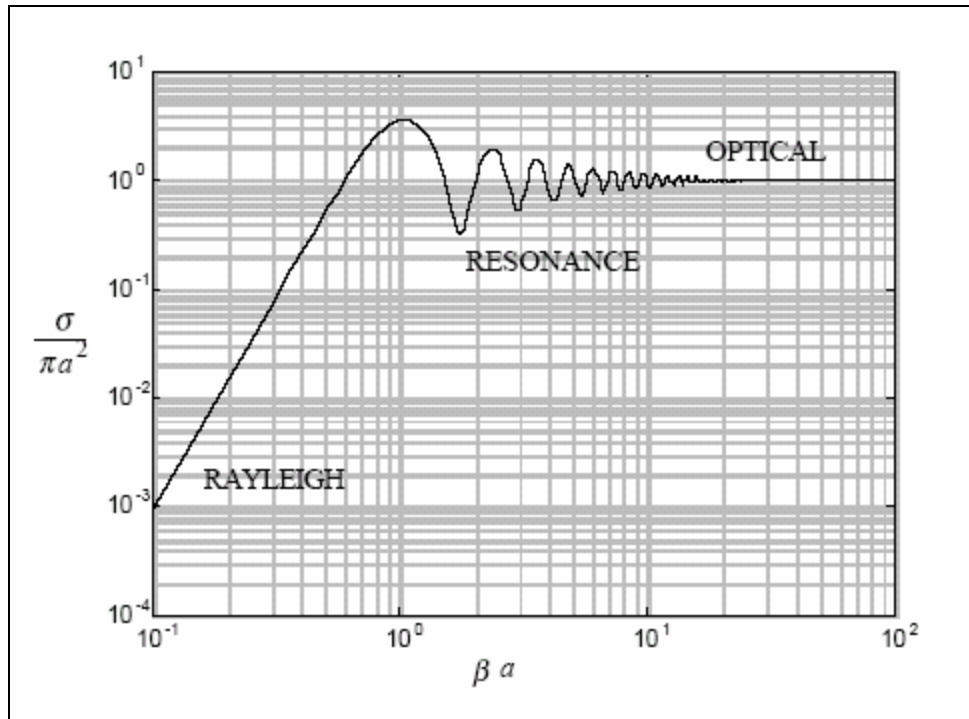


Figure 4. Radar Cross Section of a Sphere (From Ref. 5.)

E. RADAR CROSS SECTION PREDICTION METHODS

Some of the most common numerical RCS prediction methods for any arbitrary three-dimensional target are the Method of Moments, the Finite Difference Method, Microwave Optics and Physical Optics. For each method, its advantages and limitations will be discussed.

1. Method of Moments

The most common technique used to solve an integral equation is the Method of Moments (MM). In the RCS prediction case, integral equations are derived from Maxwell's equations and the boundary conditions, with the unknown quantity being an electric or magnetic current (either volume or surface). The Method of Moments reduces the integral equations to a set of simultaneous linear equations that can be solved using standard matrix algebra. Most Method of Moments formulations require a discretization (segmentation) of the target body and, therefore, are compatible with finite element methods used in structural engineering. In fact, the two are frequently used in tandem during the design of a platform (Ref. 2).

Another advantage of the Method of Moments is that it provides a rigorous solution to the RCS prediction problem, yielding very accurate results. However, this method tends to produce large matrices, resulting in high computational requirements and increased run time. In addition, since current computer capabilities allow the modeling of targets on the order of 10 to 20 wavelengths, the method is not practical for large targets at high frequencies due to computer limitations (Refs. 1 and 3).

2. Finite Difference Methods

Finite Difference methods are used to approximate the differential operators in Maxwell's equations in either the time or frequency domain. Similar to the Method of Moments, the target must be discretized. Maxwell's equations and the boundary conditions are enforced on the surface of the target and at the boundaries of the discretization cells. In the time domain, this method is used extensively in computing transient responses of targets to various waveforms. Since the solution is stepped in time throughout the scattering body, the finite difference method does not require large matrices as does the Method of Moments. Frequency domain data is obtained by Fourier-transforming the time data.

This method also provides a rigorous solution to the RCS prediction problem. However, since it calculates the fields in a computational grid around the target, the calculation of the RCS of a target with a characteristic dimension of several orders of magnitude of the wavelength would entail considerable amount of time to execute (Refs. 1 and 3).

3. Microwave Optics

Ray tracing methods that can be used to analyze electrically large targets of arbitrary shape are referred to as Microwave Optics. This term actually refers to a collection of ray tracing techniques that can be used individually or in concert. The two most used are the Geometrical Optics (GO) method and the Geometrical Theory of Diffraction (GTD) method. The rules for ray tracing in a simple medium (i.e., linear, homogenous and isotropic) are similar to reflection and refraction in optics. In addition, this method takes into account diffracted rays, which originate from the scattering of the incident wave at edges, corners and vertices. The formulae are derived on the basis of infinite fre-

quency ($\lambda \rightarrow 0$), which implies an electrically large target. The major disadvantage of this method is the bookkeeping required when tracking a large number of reflections and diffractions for complex targets.

4. Physical Optics

The Physical Optics (PO) method estimates the surface current induced on an arbitrary body by the incident radiation. On the portions of the body that are directly illuminated by the incident field, the induced current is simply proportional to the incident magnetic field intensity. On the shadowed portion of the target, the current is set to zero. The current is then used in the radiation integrals to compute the scattered field far from the target (Ref. 2).

This method is a high frequency approximation that provides the best results for electrically large targets as well as in the specular direction. Since it abruptly sets the current to zero at the shadow boundary, the computed field values at wide angles and in the shadow regions are inaccurate. Furthermore, surface waves, multiple reflections and edge diffractions are not included (Refs. 1 and 3). However, the simplicity of the approach ensures low demands on computing resources and convenient run-times.

The POFACETS program utilizes the Physical Optics method to compute the surface currents on the triangular facets that comprise the building blocks of a target model. Then, the radiation integrals are used to compute the scattered field.

F. SUMMARY

This chapter discussed the importance of RCS, its role in the radar equation, and its significance in the outcome of military engagements. It provides the formal definition of RCS and discusses its behavior in the three scattering regions. Finally, the most common methods for RCS prediction are described. The next chapter discusses the mathematical equations and the theory that pertains to these computations.

THIS PAGE INTENTIONALLY LEFT BLANK

III. PHYSICAL OPTICS APPLIED TO TRIANGULAR FACET MODELS

This chapter contains the theoretical framework of the Physical Optics approximation method and the mathematical formulations used in the POFACETS program to implement this method. Starting from the radiation integrals for an arbitrary object, the scattered field formulas are derived for the case of a triangular facet. The Physical Optics approximation is used to provide values for the surface currents on a facet and Taylor series are utilized to calculate the scattered field. In the process, all tools and formulas used in the calculations are defined and explained. Finally, the computational model is expanded to implement the calculation of the scattered field from a collection of facets (i.e., an arbitrary target model).

A. RADIATION INTEGRALS FOR FAR ZONE SCATTERED FIELDS

The scattering from a triangular facet is a special case of the scattering from an arbitrary body. Hence, the formula for the scattered field for a triangular facet will be derived from the one obtained for an arbitrary body. Consider the situation depicted in Figure 5. An arbitrary scattering body is placed at the origin, with the observation point being at coordinates (x, y, z) .

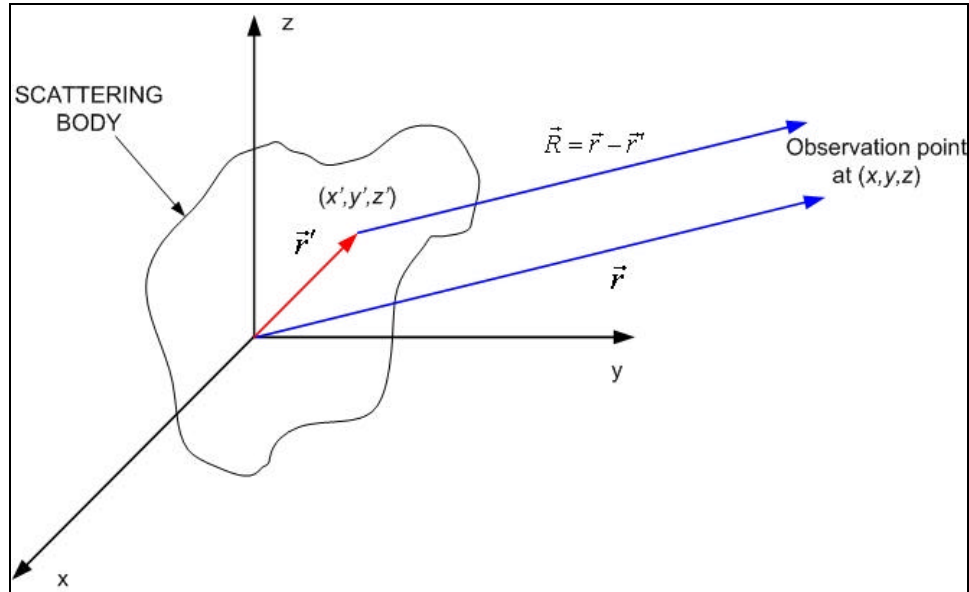


Figure 5. Far Field Scattering from an Arbitrary Body (After Ref. 2.).

For Radar Cross Section calculations, the observation point is considered to be in the far zone of the target. Thus, the vectors \vec{R} and \vec{r} are approximately parallel.

The body is segmented into infinitely small source points of volume v' located at coordinates (x', y', z') . The position vector to a source point is:

$$\vec{r}' = \hat{x}x' + \hat{y}y' + \hat{z}z' \quad (3.1)$$

with \hat{x} , \hat{y} , \hat{z} being the coordinate-axes unit vectors.

The unit vector in the direction of the observation point is:

$$\hat{r} = \hat{x}u + \hat{y}v + \hat{z}w \quad (3.2)$$

where

$$\begin{aligned} u &= \sin\theta \cos\phi \\ v &= \sin\theta \sin\phi \\ w &= \cos\theta \end{aligned} \quad (3.3)$$

with θ and ϕ being the spherical coordinates of the observation point.

Assuming that the magnetic volume current in the body is $\vec{J}_m = 0$, the scattered field from the body is given by the following equation:

$$\vec{E}_s(r, \theta, \phi) = E_\theta(r, \theta, \phi)\hat{\theta} + E_\phi(r, \theta, \phi)\hat{\phi} = \frac{-jkZ_o}{4\pi r} e^{-jkr} \iiint_V \vec{J} e^{jkg} dv' \quad (3.4)$$

where \vec{J} is the electric volume current, Z_o is the intrinsic impedance of the space surrounding the body, $k = 2\pi/\lambda$ (with λ being the wavelength) and g is defined as:

$$g = \vec{r}' \cdot \hat{r} = x'u + y'v + z'w. \quad (3.5)$$

Notice that in Equation (3.4), the electric field has components only in the θ and ϕ direction, so that the E_r component in (3.4) is ignored (Ref. 2).

B. RADIATION INTEGRALS FOR A TRIANGULAR FACET

Consider a triangular facet with arbitrary orientation defined by the vertices 1, 2 and 3, as shown in Figure 6.

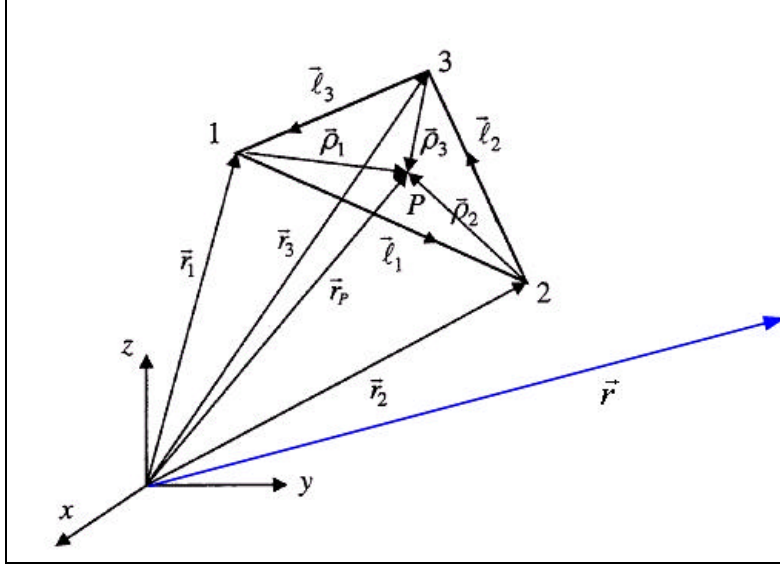


Figure 6. Arbitrary Oriented Facet (After Ref. 3.).

The integration point now is P , which is located at coordinates (x_p, y_p, z_p) corresponding to the (x', y', z') coordinates of the integration point for the arbitrary body examined in the previous section. Its position vector is

$$\vec{r}_p = x_p \hat{x} + y_p \hat{y} + z_p \hat{z} . \quad (3.6)$$

Since the triangular facet is a two-dimensional object, the volume integration in Equation (3.4) becomes a surface integration. Similarly, there is only surface current flowing on the triangular facet. Hence, Equation (3.4) becomes:

$$\vec{E}_s(r, \theta, \phi) = \frac{-jkZ_o}{4\pi r} e^{-jkr} \iint_A \vec{J}_s e^{jkg} ds_p \quad (3.7)$$

where \vec{J}_s is the surface current, A the area of the triangular facet, ds_p the differential surface area and g is defined as:

$$g = \vec{r}_p \cdot \hat{r} = x_p u + y_p v + z_p w . \quad (3.8)$$

Hence, the problem of evaluating the scattered field from a single facet has been narrowed to two simpler problems: (1) the computation of the surface current \vec{J}_s flowing on the facet by using the Physical Optics method, and (2) the computation of the integral in Equation (3.7).

It is necessary to describe some of the tools to be used in the calculations before addressing these two problems.

C. RADIATION INTEGRALS FOR A TRIANGULAR FACET

Figure 7 depicts the detailed geometry of a single facet with arbitrary orientation. The facet vertices are known in terms of their Cartesian coordinates (x_n, y_n, z_n) for $n=1,2,3$. It is assumed that the vertices are labeled in a right-hand sense (i.e., counter-clockwise), so that the thumb of the right hand gives the outward normal direction. For a closed body that surrounds the origin of the axes, the outward normal will, in general, point away from the origin.

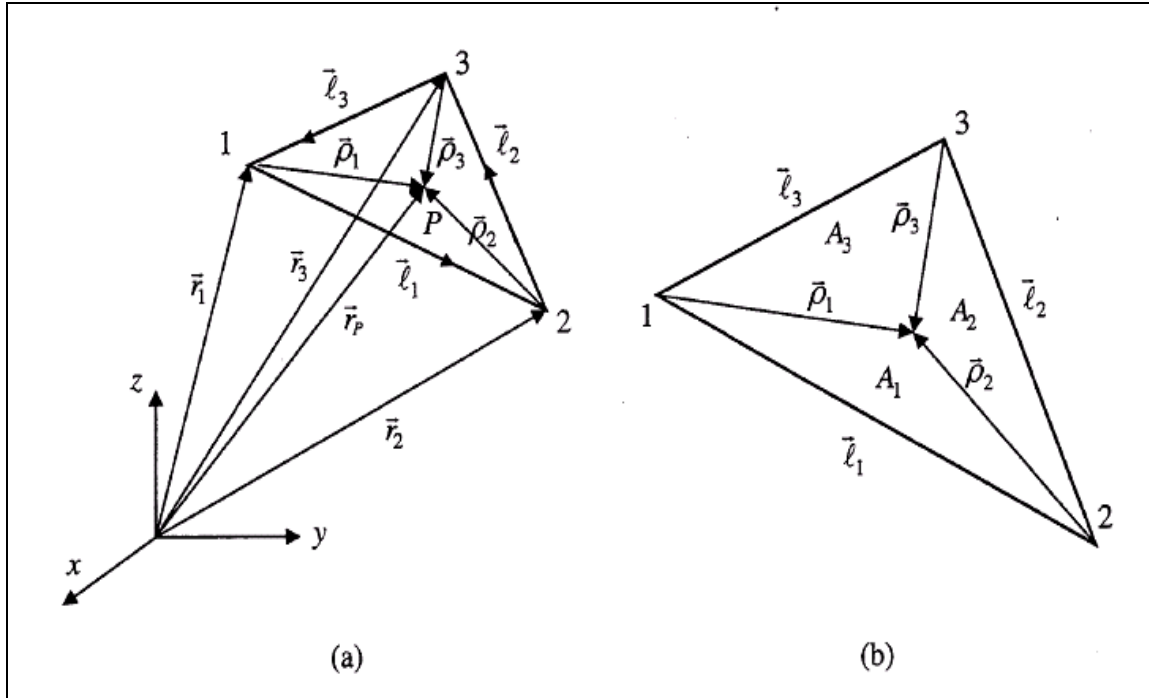


Figure 7. Arbitrary Oriented Facet (a) Geometry (b) Facet Sub-Areas (From Ref. 3.).

The position vectors to the vertices are given by:

$$\vec{r}_n = x_n \hat{x} + y_n \hat{y} + z_n \hat{z} . \quad (3.9)$$

Then, the edge-vectors can be determined from the node coordinates as follows:

$$\vec{l}_1 = \vec{r}_2 - \vec{r}_1, \quad \vec{l}_2 = \vec{r}_3 - \vec{r}_2, \quad \vec{l}_3 = \vec{r}_1 - \vec{r}_3 . \quad (3.10)$$

The outward normal of the facets can then be obtained by taking the cross product of any two edge-vectors in a right-hand sense. For example:

$$\hat{n} = \frac{\vec{\ell}_1 \times \vec{\ell}_3}{|\vec{\ell}_1| |\vec{\ell}_3|} \equiv n_x \hat{x} + n_y \hat{y} + n_z \hat{z}. \quad (3.11)$$

With this ordering of the vertices, the outward side of the facet is denoted as the front face with the opposite side being the back face. If a plane wave is incident from an angle (θ_i, ϕ_i) , propagating towards the origin, then its propagation vector is:

$$\hat{k}_i = -\hat{r} = -(\hat{x}u_i + \hat{y}v_i + \hat{z}w_i) \quad (3.12)$$

where (u_i, v_i, w_i) are the direction cosines and \hat{r} is the radial unit vector from the origin to the source at (θ_i, ϕ_i) . A front facet is illuminated when the following condition is satisfied:

$$-\hat{k}_i \cdot \hat{n} \geq 0 \quad (3.13)$$

It is possible to compute the total area of the facet A from the cross product of the two edge vectors:

$$A = \frac{1}{2} |\vec{\ell}_1 \times \vec{\ell}_3|. \quad (3.14)$$

In order to simplify integration over the surface of the facets, normalized areas are used. Specifically, sub-areas A_1, A_2, A_3 are defined, from which normalized area coordinates are computed:

$$\zeta = \frac{A_1}{A}, \xi = \frac{A_2}{A}, \eta = \frac{A_3}{A}. \quad (3.15)$$

Since $A_1 + A_2 + A_3 = A$, it is possible to write $\zeta + \xi + \eta = 1$, and hence, $\zeta = 1 - \xi - \eta$.

Then, the integration over the area of the facet can be written as (Ref. 3):

$$\iint_A ds_p = 2A \int_0^1 \int_0^{1-\eta} d\xi d\eta. \quad (3.16)$$

D. COORDINATE TRANSFORMATIONS

In the general case, the local facet coordinate system will not be aligned with the global coordinate system. In the local facet coordinate system (x'', y'', z'') , the facet lies on the $x''y''$ plane, with \hat{z}'' being the normal to the facet surface, hence $\hat{n} = \hat{z}''$, as depicted in Figure 8.

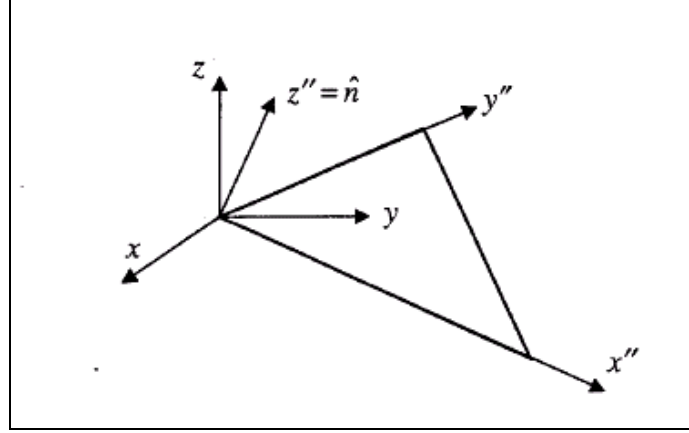


Figure 8. Global and Local Coordinate Systems (From Ref. 3.).

For any arbitrary oriented facet with known global coordinates, its local coordinates can be obtained by a series of two rotations. First, the angles α and β , shown in Figure 9, are calculated from

$$\alpha = \tan^{-1} \left(\frac{n_y}{n_x} \right) \quad \text{and} \quad \beta = \cos^{-1}(\hat{z} \cdot \hat{n}) \quad (3.17)$$

with n_y, n_x , as defined in Equation (3.11).

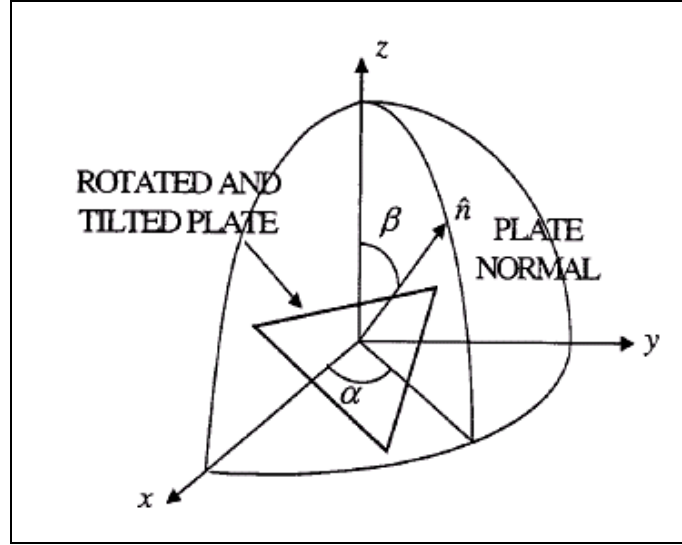


Figure 9. Rotation Angles (From Ref. 3.).

Then, the transformation matrices are computed:

$$\underline{T}' = \begin{bmatrix} \cos \alpha & \sin \alpha & 0 \\ -\sin \alpha & \cos \alpha & 0 \\ 0 & 0 & 1 \end{bmatrix} \quad (3.18)$$

$$\underline{T}'' = \begin{bmatrix} \cos \beta & 0 & -\sin \beta \\ 0 & 1 & 0 \\ \sin \beta & 0 & \cos \beta \end{bmatrix}. \quad (3.19)$$

Using these matrices, the global coordinates can be transformed to local coordinates:

$$\begin{bmatrix} x'' \\ y'' \\ z'' \end{bmatrix} = \underline{T}'' \underline{T}' \begin{bmatrix} x \\ y \\ z \end{bmatrix}. \quad (3.20)$$

The inverse transformation (i.e., from local to global coordinates) is simply

$$\begin{bmatrix} x \\ y \\ z \end{bmatrix} = (\underline{T}'' \underline{T}')^{-1} \begin{bmatrix} x'' \\ y'' \\ z'' \end{bmatrix}. \quad (3.21)$$

The transformations described in Equations (3.20) and (3.21) are also valid for the unit vectors and the direction cosines (Ref. 3).

E. PHYSICAL OPTICS SURFACE CURRENT COMPUTATION

According to the Physical Optics method, on the portions of the body that are directly illuminated by the incident field, the induced current is simply proportional to the incident magnetic field intensity. On the shadowed portion of the target, the current is set to zero. Hence:

$$\vec{J}_s = \begin{cases} 2\hat{n} \times \vec{H}_i & \text{for the illuminated facets} \\ 0 & \text{for the shadowed facets} \end{cases} \quad (3.22)$$

where \vec{H}_i is the incident magnetic field intensity at the surface.

In general, the incident field is of the form

$$\vec{E}_i = (E_{\theta}\hat{\theta} + E_{\phi}\hat{\phi})e^{-jk_i \cdot \vec{r}} \quad (3.23)$$

where $\vec{k}_i = k\hat{k}_i = -k\hat{r}_i$, with $k = 2\pi/\lambda$. Since $\hat{r}_p = \hat{r}$ for a point (x_p, y_p, z_p) on the surface:

$$\vec{E}_i = (E_{\theta}\hat{\theta} + E_{\phi}\hat{\phi})e^{jk\hat{r}_i \cdot \vec{r}_p} . \quad (3.24)$$

Then, the magnetic field intensity is:

$$\vec{H}_i = \frac{\vec{k}_i \times \vec{E}_i}{Z_o} = \frac{1}{Z_o} (E_{\phi}\hat{\theta} - E_{\theta}\hat{\phi})e^{jk\hat{r}_i \cdot \vec{r}_p} . \quad (3.25)$$

The physical optics approximation for the surface current flowing on the facet is:

$$\vec{J}_s = 2\hat{n} \times \vec{H}_i = \frac{2}{Z_o} (E_{\phi}\hat{\theta} - E_{\theta}\hat{\phi})e^{jkh} \quad (3.26)$$

where h is defined as:

$$h = \vec{r}_p \cdot \hat{r}_i = x_p u_i + y_p v_i + z_p w_i . \quad (3.27)$$

It is now possible to write Equation (3.26) as:

$$\vec{J}_s = (J_x \hat{x} + J_y \hat{y} + J_z \hat{z})e^{jkh} . \quad (3.28)$$

However, in facet local coordinates, the surface current does not have a \hat{z}'' component, since the facet lies on the $x''y''$ plane. Hence:

$$\vec{J}_s = (J_x'' \hat{x}'' + J_y'' \hat{y}'')e^{jkh} . \quad (3.29)$$

The values of the surface current components are (Ref. 3):

$$J_x'' = \left[-\frac{E_{i\theta}'' \cos \phi''}{Z_o} \Gamma_{\parallel} + \frac{E_{i\phi}'' \sin \phi''}{Z_o} \Gamma_{\perp} \right] \cos \theta'' \quad (3.30)$$

$$J_y'' = \left[-\frac{E_{i\theta}'' \sin \phi''}{Z_o} \Gamma_{\parallel} - \frac{E_{i\phi}'' \cos \phi''}{Z_o} \Gamma_{\perp} \right] \cos \theta'' \quad (3.31)$$

where $E_{i\theta}'', E_{i\phi}''$ are the components of the incident field in the local facet coordinates and θ'', ϕ'' are the spherical polar angles of the local coordinates.

Various materials can be handled by the inclusion of Γ_{\parallel} and Γ_{\perp} , the transverse magnetic (TM) and the transverse electric (TE) reflection coefficients, respectively.

These are defined as:

$$\Gamma_{\parallel} = \Gamma_{TM} = \frac{-Z_o \cos \theta''}{2R_s + Z_o \cos \theta''} \quad (3.32)$$

$$\Gamma_{\perp} = \Gamma_{TE} = \frac{-Z_o}{2R_s \cos \theta'' + Z_o} \quad (3.33)$$

with R_s being the surface resistivity of the facet material. When $R_s = 0$, the surface is a perfect electric conductor. As $R_s \rightarrow \infty$, the surface becomes transparent ($|\Gamma| \rightarrow 0$).

F. SCATTERED FIELD COMPUTATION

To obtain the scattered field, simply replace Equation (3.29) in the radiation integral for the triangular facet, which was determined in Equation (3.7), so

$$\vec{E}_s(r, \theta, \phi) = \frac{-jkZ_o}{4\pi r} e^{-jkr} (J_x'' \hat{x}'' + J_y'' \hat{y}'') \iint_A e^{jk(g+h)} ds_p. \quad (3.34)$$

In order to compute the scattered field, it is only necessary to evaluate the integral:

$$I_c = \iint_A e^{jk(g+h)} ds_p. \quad (3.35)$$

However, it is not possible to obtain an exact closed form solution for this integral. Given that the incident wavefront is assumed plane and that the incident field is known at the facet vertices, the amplitude and phase at the interior integration points can

be found by interpolation. Then, the integrand can be expanded using Taylor series, and each term integrated to give a closed form result. Usually, a small number of terms in the Taylor series (on the order of 5) will give a sufficiently accurate approximation (Ref. 3).

Thus, using the notation of Ref. 6, the following equation is defined as:

$$I_c = \iint_A C_c(\eta, \xi) e^{jD_c(\eta, \xi)} d\eta d\xi \quad (3.36)$$

where

$$C_c(\eta, \xi) = C_p\eta + C_q\xi + C_o \equiv |\vec{E}_i|. \quad (3.37)$$

For a unit amplitude plane wave:

$$|\vec{E}_i| = 1 \Rightarrow C_p = C_q = 0, C_o = 1. \quad (3.38)$$

Similarly,

$$D_c(\eta, \xi) = D_p\eta + D_q\xi + D_o \quad (3.39)$$

with

$$\begin{aligned} D_p &= k[(x_1 - x_3)u + (y_1 - y_3)v + (z_1 - z_3)w] \\ D_q &= k[(x_2 - x_3)u + (y_2 - y_3)v + (z_2 - z_3)w] \\ D_o &= k[x_3u + y_3v + z_3w] \end{aligned} \quad (3.40)$$

Now the integral of Equation (3.35) is given by:

$$I_c = 2Ae^{jD_o} \left\{ e^{jD_p} \left[\frac{C_o}{D_p(D_q - D_p)} \right] - e^{jD_q} \left[\frac{C_o}{D_q(D_q - D_p)} \right] - \frac{C_o}{D_p D_q} \right\}. \quad (3.41)$$

In order to avoid numerical errors that occur near the singularities (i.e., denominators near zero), the following special cases are considered separately:

Case 1: $|D_p| < L_t$ and $|D_q| \geq L_t$

$$I_c = \frac{2Ae^{jD_o}}{jD_q} \sum_{n=0}^{\infty} \frac{(jD_p)^n}{n!} \left\{ -\frac{C_o}{n+1} + e^{jD_q} C_o G(n, -D_q) \right\} \quad (3.42)$$

Case 2: $|D_p| < L_t$ and $|D_q| < L_t$

$$I_c = 2Ae^{jD_o} \sum_{n=0}^{\infty} \sum_{m=0}^{\infty} \frac{C_o (jD_p)^n (jD_q)^m}{(m+n+2)!} \quad (3.43)$$

Case 3: $|D_p| \geq L_t$ and $|D_q| < L_t$

$$I_c = 2Ae^{jD_o}e^{jD_p} \sum_{n=0}^{\infty} \frac{(jD_q)^n}{n!} \frac{C_o}{n+1} G(n+1, -D_p) \quad (3.44)$$

Case 4: $|D_p| \geq L_t$ and $|D_q| \geq L_t$

$$I_c = \frac{2Ae^{jD_o}}{jD_q} \sum_{n=0}^{\infty} \frac{(jD_p - jD_q)^n}{n!} \left\{ -C_o G(n, D_q) + \frac{e^{jD_p} C_o}{n+1} \right\} \quad (3.45)$$

where L_t is the length of the Taylor series region. The function G is defined by

$$G(n, \gamma) = \int_0^1 s^n e^{j\gamma s} ds \quad (3.46)$$

and is evaluated with the use of the following recursive relationship:

$$G(n, \gamma) = \frac{e^{j\gamma} - nG(n-1, \gamma)}{j\gamma}, \quad n \geq 1 \quad (3.47)$$

with

$$G(0, \gamma) = \frac{e^{j\gamma} - 1}{e^{j\gamma}}. \quad (3.48)$$

G. DIFFUSE FIELD COMPUTATION

Thus far, the discussion assumes that the facets are completely smooth. In reality, of course, targets rarely have perfectly smooth surfaces, due to irregularities or material and manufacturing imperfections. Surface roughness introduces path differences relative to the smooth surface. Consequently, it is essential to consider a scattering component due to these imperfections in the RCS computations.

Since the various imperfections in manufacturing and assembly processes of a target tend to behave in a random fashion, the quantities chosen to represent these parameters can be modeled as random variables. The scattered field and the RCS are functions of these random variables. The effect of the random errors on the resulting RCS pattern is to subtract energy from the specular reflection, converting it to random scattering, that is nearly equally distributed in all directions, which is called diffuse scattering (Ref. 2).

In order to model a rough surface, the thesis takes into account that the deviation of points in the same area is usually correlated. For instance, in most cases, a dent in a plate will have an approximately hemispherical shape. In this case, if the dent has a diameter of 1 cm, the deviation of points whose distance is less than 0.5 cm from the center of the dent will be correlated to the deviation at the center (Ref. 2).

Thus, the modeling of the rough surface begins by assuming that the surface deviations resemble Gaussian dents, as shown in Figure 10.

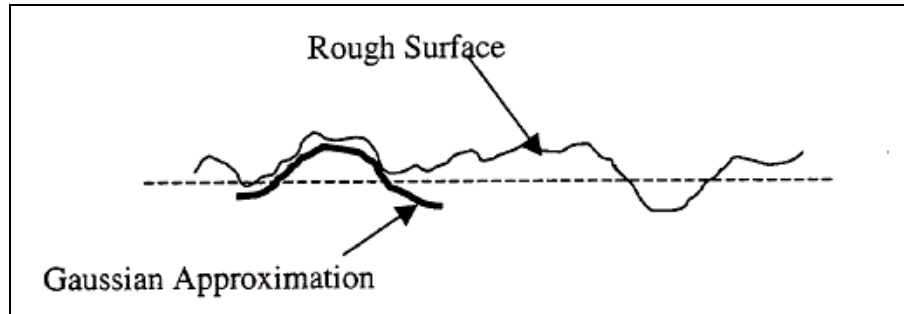


Figure 10. Gaussian Approximation of a Rough Surface (From Ref. 3.)

Next, it is necessary to define two parameters. The correlation interval C (in meters) is the average distance at which the deviations become uncorrelated. As Figure 11 indicates, a large correlation distance suggests a slowly varying surface error, while a small correlation distance characterizes a rapidly varying error. The variance itself of the irregularities is defined as δ^2 , with δ being the standard deviation of the irregularities (Ref. 2).

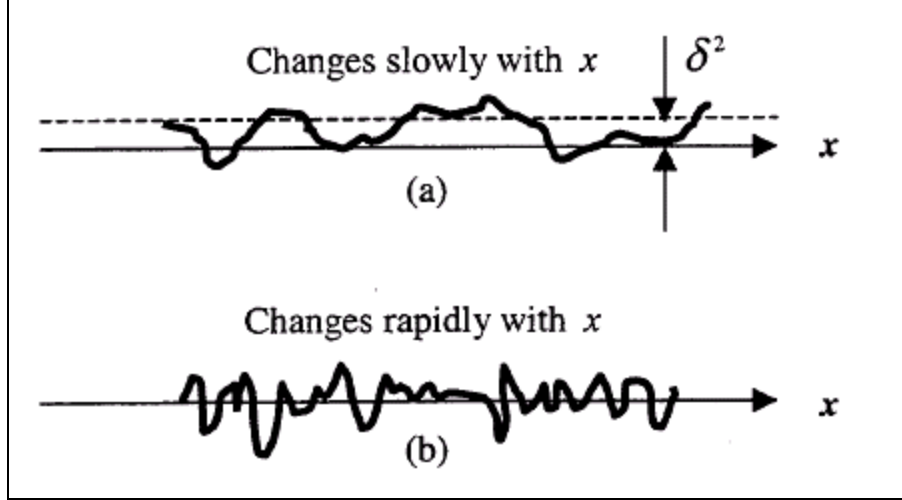


Figure 11. (a) Large Correlation Distance, (b) Small Correlation Distance (From Ref. 3.)

The POFACETS program allows the user to select the correlation distance and standard deviation. The average value of the RCS of a facet is approximately (Ref. 7):

$$\sigma_{ave} \approx \frac{4\pi A^2}{\lambda^2} e^{-4k^2\delta^2} \cos^2\theta'' \left[\frac{4\pi k^2\delta^2 C^2}{A} \exp\left(-\frac{\pi^2 C^2 \sin^2\theta''}{\lambda^2}\right) \right] \quad (3.49)$$

with A being the area of the facet and θ'' the same as previously defined.

This value is simply added to the specular term, which is calculated using Equation (3.34).

H. TOTAL FIELD FROM A TARGET

Thus far, the discussion has involved the calculation of the scattered field from a single facet. A large target is approximated by a model consisting of many triangular facets. Superposition is used to calculate the scattered field from the target. First, the scattered field is computed for each facet. Then, the scattered field from each facet is vector-summed to produce the total field in the observation direction. Once the scattered field is known, the RCS in that direction is computed. This is repeated for all the observation directions selected by the user. The entire process, including model generation and data presentation has been programmed in the software package POFACETS.

Specifically, the following steps, diagramed in Figure 12, take place in the RCS computation process:

1. The parameters of the RCS computation, including frequency, Taylor series parameters, surface roughness parameters, angle of incidence (for bistatic RCS case), angles of observation, incident field polarization and model name are selected by the user.
2. The program reads the model characteristics (coordinates of facets, facet description and surface resistivity).
3. Initial computations are executed to obtain certain facet characteristics, including facet area, normal vector and rotation angles, using Equations (3.11), (3.14) and (3.17), respectively.
4. For each facet, its illumination condition is assessed, using Equation (3.13). If the facet is not illuminated, all scattered and diffuse components are set to zero and the program proceeds to the next facet. If the facet is illuminated, the following steps are performed.
 - The incident field, the angle of incidence (for the bistatic RCS case) and the observation angle are transformed to the local coordinate system of the facet, using the transformation described in Equation (3.20).
 - The Physical Optics Current is computed from the incident magnetic field, using Equations (3.30) and (3.31).
 - The scattered field is computed in local facet coordinates using the radiation integral, via Equations (3.34) and (3.41) to (3.45).
 - The diffuse component is computed using Equation (3.49).
 - The scattered field is transformed back to global coordinates, using Equation (3.21).
 - The scattered field components from each facet are superimposed (vector added) to obtain the total scattered field in the observation direction.
5. The diffuse and scattered RCS are computed from the total fields.
6. Steps 4 to 5 are repeated for each observation angle.
7. Selected graphical plots of RCS versus observation angle are displayed.

Notice that in the bistatic RCS calculation, the incidence angle is fixed. As a result, it is not necessary to compute the surface currents for each observation angle, contrary to what happens in the monostatic case, where the incidence angle is the same as the observation angle.

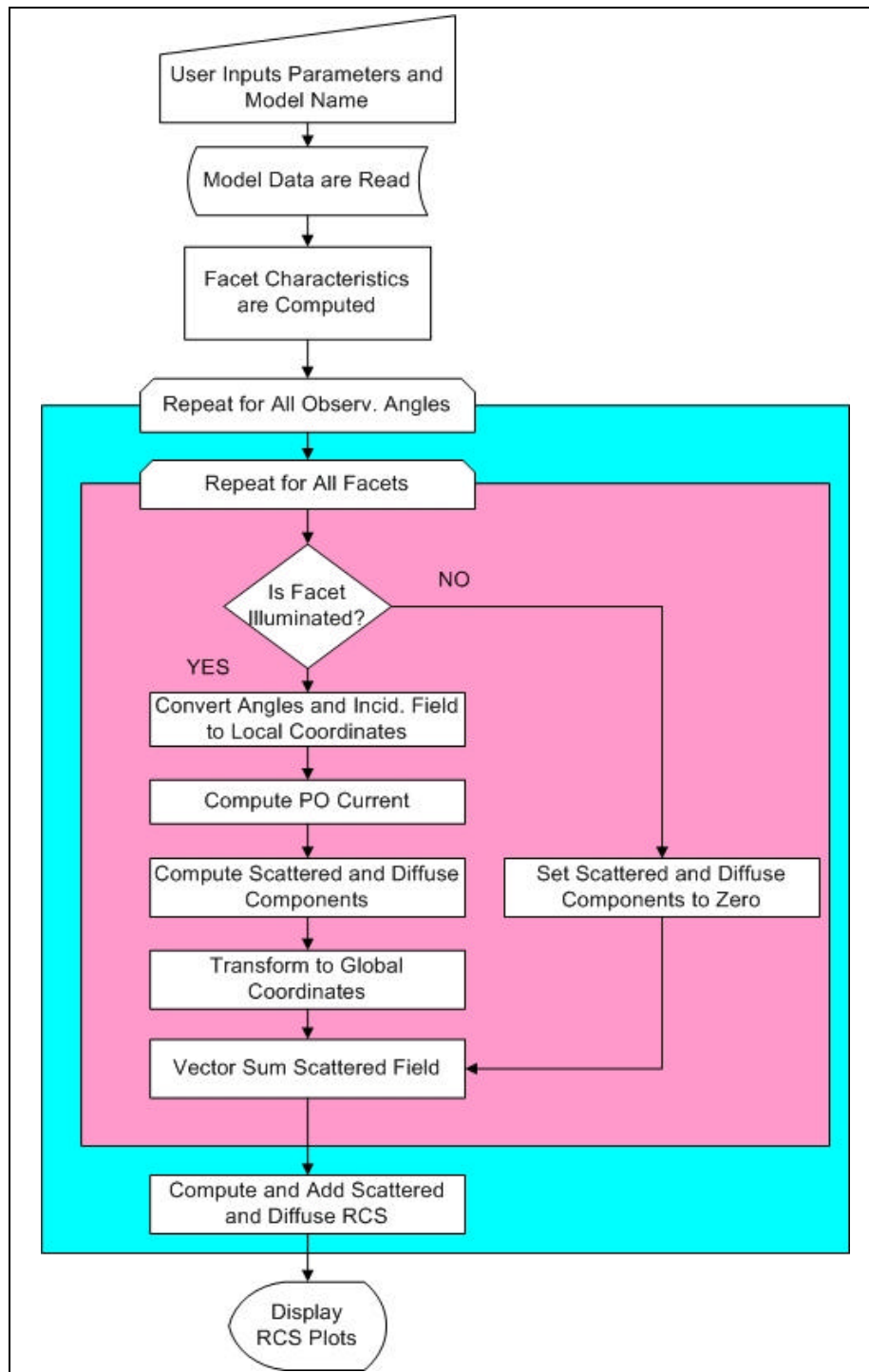


Figure 12. Flow Chart for the RCS Calculation of a Collection of Facets

I. SUMMARY

This chapter described the fundamental theory utilized in the original POFACETS version. The scattered field from a triangular facet is computed using the radiation inte-

grals. The Physical Optics method is used to calculate the surface currents on each facet and the scattered field from all facets of a model is vector summed to produce the RCS value for given angles of incidence and observation. The next chapter presents the new functionalities and improvements incorporated in the POFACETS program as a result of this thesis.

IV. NEW FUNCTIONALITIES ADDED TO THE POFACETS PROGRAM

This chapter contains the description of the improvements and the new functionalities added in the POFACETS program as a result of this thesis work. Specifically, it discusses the details of the Graphical User Interface and model database upgrades, the new options for manual or graphical design of a model, the capabilities for importing models from or exporting models to other commercially available CAD software, the RCS computation options for the monostatic and bistatic case, and the available display options for the RCS results.

For each of these improvements or new functionalities, a brief rationale is provided regarding the necessity for their implementation, followed by a brief description of the method by which this implementation was accomplished. Although all upgrades to the program are discussed, greater emphasis is given to issues pertaining to program features directly related to model creation and manipulation, and RCS computation. When applicable, screenshots of the program, including menus, dialogs, forms and graphical plots are provided to explain or illustrate concepts and familiarize the reader with the POFACETS program.

A. GRAPHICAL USER INTERFACE (GUI) UPGRADE TO CURRENT MATLAB VERSION

1. Rationale

The POFACETS 2.3 program was developed in 2000 in a previous version of MATLAB. Although the code could still be executed and produce results in the current MATLAB version (MATLAB 6.5, Release 13, June 2002), there were some important maintenance and compatibility concerns. The previous MATLAB version stored all the features of the GUI in script files (*.m), resulting in long, complex, and difficult to maintain files. The current MATLAB version creates a pair of files, which includes a script file (*.m), where the callback procedures of the various screen controls are stored, and one figure file (*.fig), which stores the properties of the screen controls. The resulting

script file is usually easy to understand and maintain. Although these maintenance reasons alone could justify the GUI upgrade effort, the compatibility issues made it even more necessary.

Specifically, MATLAB uses the GUIDE tool to create and modify Graphical User Interfaces. This tool would have to be used both for the creation of new GUIs to support the new computational capabilities and options added to the POFACETS, and for the necessary changes to the existing previous version POFACET GUIs. This meant that the previous version GUIs, stored in script files, would have to be upgraded to the current MATLAB version. Essentially, this was the necessary first step to complete prior to any other modification to the POFACETS program.

2. Procedure

Each GUI script file created in the previous MATLAB version was imported in the GUIDE tool. After the script was executed, the resulting figure (containing a dialog box, menu, form, etc.) was used to create the pair of files (script file and figure file) required in the current MATLAB version. Subsequently, the new script files were manually updated with the necessary callbacks, taken from the old script files.

3. Results

The conclusion of this step resulted in all GUI components of the POFACETS being converted to the current version and, hence, being available for improvements and upgrades. Taking advantage of the fact that the GUIDE program allows easy graphical components manipulation, new features, such as color coding of components by function, information frames, help screens and standard MATLAB figure menus were added, as applicable, to all the existing GUI forms to make them easier to comprehend and use. This approach to GUI form design was subsequently followed for all the new GUI components, which were developed to implement the new POFACETS functionalities or computational capabilities.

Figure 13, which shows the first screen that appears after the POFACETS execution, provides an example of this approach to GUI form design. There are three main function areas, coded in different colors: the blue area pertains to the manual or graphical design of a model using the triangular facets approach, the green area pertains to the cal-

calculation of the monostatic or bistatic RCS of an existing model and the violet area pertains to the program utilities. Each area contains information that further explains the functions performed in each case to the user.

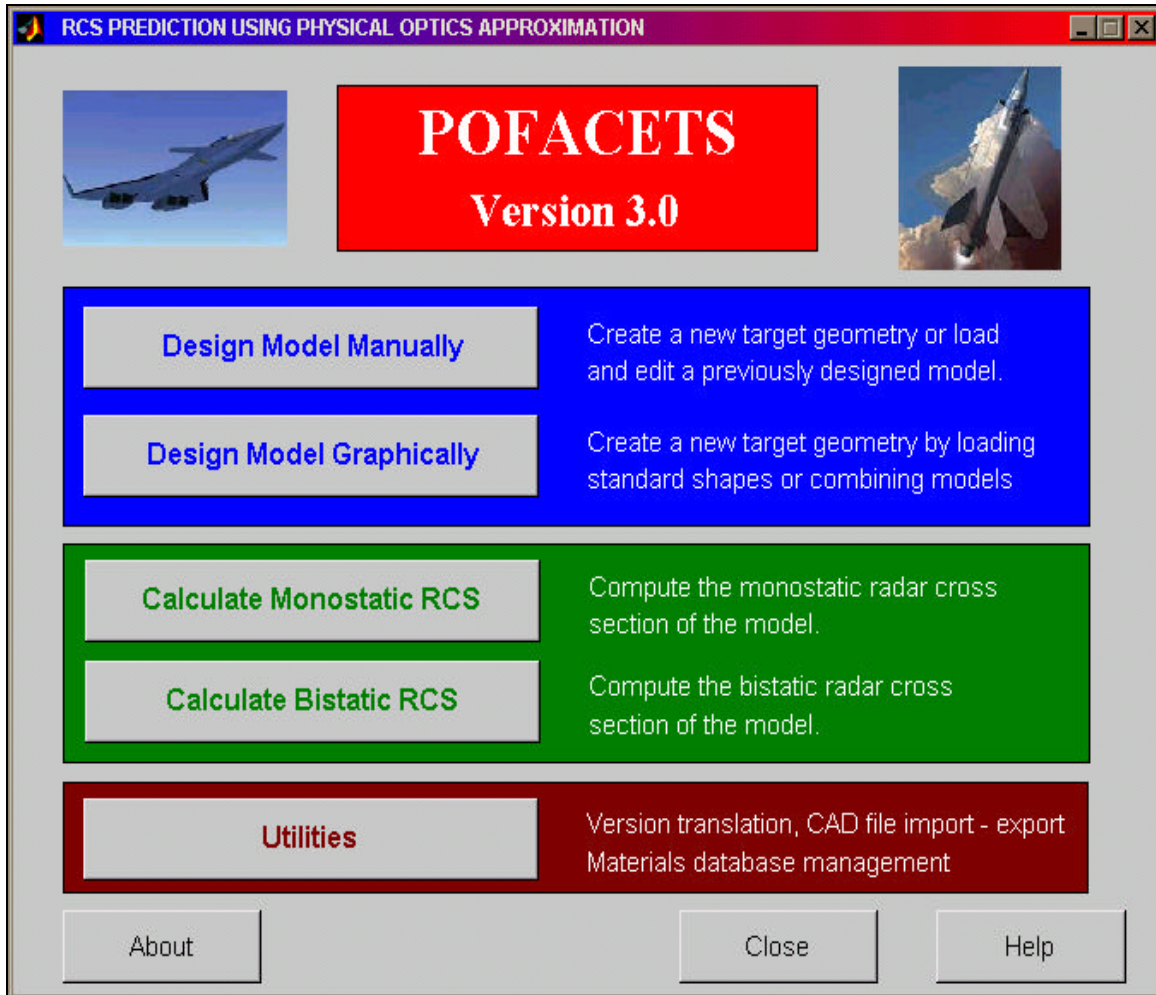


Figure 13. POFACETS Main Screen

In order to keep all GUI forms as user-friendly as possible, only simple GUI components were used. Thus, the majority of the functions are executed by buttons or pull-down menus, decisions between two alternatives are made with check boxes, information is entered in an edit box or selected in list boxes, and sliders are used to allow selection from a large space of numbered alternatives. Overall, the main effort in the GUI design was to provide the user a familiar environment, which would be similar to other Windows programs. Following standard Windows program conventions, an “About “

form was also added invoked by clicking the About button in the form depicted in Figure 13. The “About” form, shown in Figure 14, acknowledges the work of all the contributors to the last version (3.0) of the POFACETS program.

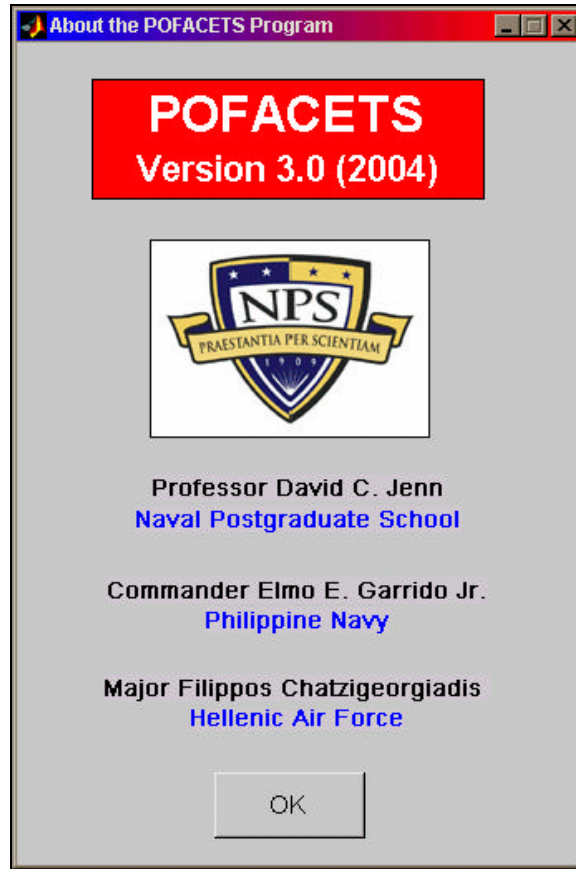


Figure 14. POFACETS Contributors

B. MODEL DATABASE UPGRADE

1. Rationale

The POFACETS 2.3 version allowed the user to design models of targets by manually entering the coordinates of the vertices of the model, numbering these vertices and then describing each facet with three vertices. When the process was completed, the target model was stored in two standard MATLAB data files (*.mat). One file, called *coordinates.mat*, contained the coordinates of the vertices, while the other file, called *facets.mat*, contained the vertices' numbers of each facet. As the names of these files were the same for all models, the files for each model had to be stored in different directories, with the name of each directory containing the description of the model to which the files

were related. Thus, the models called *plate* and *box* were saved in two different directories, called *plate* and *box*, respectively, with both directories containing two files, called *coordinates.mat* and *facets.mat*.

Although this approach did not create any functional problems within the POFACETS program, it could lead to file maintenance problems, since it created large numbers of files with the same names. Moreover, the new functionalities and capabilities added to the POFACETS program required new data to be stored for each model, such as symmetry planes, material data and parts descriptions. If the previously described approach was followed, each model would have to be saved in a different directory using five files (one file for each type of data stored). This, of course, would probably create serious file maintenance problems in the future.

2. Procedure

Taking into consideration that other commercial model design software packages (e.g., AUTOCAD) save the data of each design into a single file, it was decided to follow a similar approach in the new POFACETS version. Thus, each model is saved in a single standard MATLAB data file (*.mat), which bears the name of the model whose data it contains. For example, the *plate* model is stored in file *plate.mat*, while the *box* model is stored in file *box.mat*. Each file contains all the data structures (i.e., MATLAB data arrays or cell arrays) that are necessary to store the coordinates of the vertices, the vertices of the facets, the model's symmetry planes (if any), the material of each facet and the description of the various parts of complex models. The Appendix describes details of these data structures.

3. Results

All the existing model files from POFACETS version 2.3 were successfully converted to the new model file version. In addition, all new models created subsequently by POFACETS version 3.0 model design tools were also saved in the new model file version.

However, taking into consideration that previous versions of the POFACETS program, namely the 2.3 version and the original, non-GUI version developed by Professor D. C. Jenn, were already in use by students and RCS professionals worldwide, it was decided to provide the new POFACETS program with the tools that would allow these

users to convert those models created in previous versions of POFACETS to the current model file version. Moreover, in order to keep full backward compatibility with previous POFACETS versions, it was decided to provide tools that would allow users to convert the new model file version to the older model file versions. Thus, users selecting to continue using their older version of POFACETS could still have access to models designed in the 3.0 version.

These tools were incorporated in the Utilities part of the POFACETS program. Figure 15 depicts the GUI form that provides access to the Utilities functions. The model file conversion tools are listed in the circled left column of buttons (blue-colored). As described above, conversion of files can occur between version 3.0 and version 2.3, and version 3.0 and the non-GUI version.

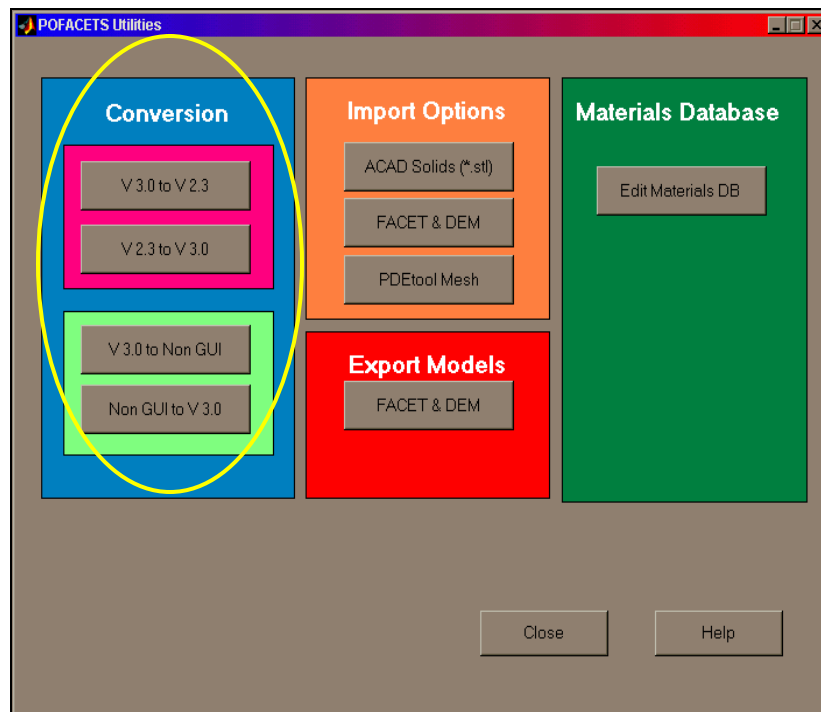


Figure 15. File Conversion Options (circled)

C. MANUAL MODEL DESIGN

1. Rationale

As previously discussed in Section B, the POFACETS 2.3 version provided the user a GUI for manual model design using triangular facets. However, several important limitations exist on the number of vertices and facets that could be stored in a model.

Specifically, the maximum number for both cases was 40. Memory or storage constraints did not impose this limitation, but the amount of edit boxes available on a single GUI form.

Although the new version of POFACETS would also provide a graphical way for easy and automated design of models, it was decided to maintain the manual way of designing models, since it offers additional versatility and allows for direct, “low-level” modifications in the coordinates of the vertices and the description of the facets. In other words, the graphical model design can be used to create a rough model of a target, while the manual model design can be subsequently used for making specific modifications and adding details or features not covered in the graphical design. Of course, the manual model design tool was upgraded in order to be able to handle any number of vertices and facets.

2. Procedure

Figure 16 depicts the Manual Model Design GUI form.

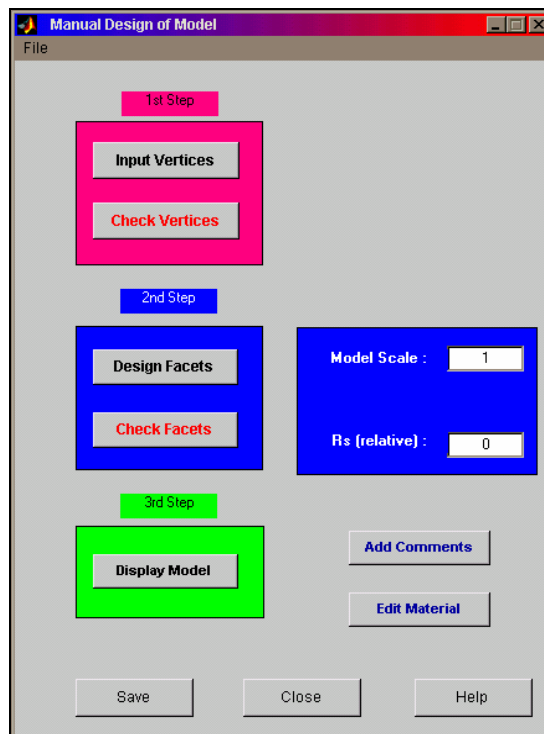
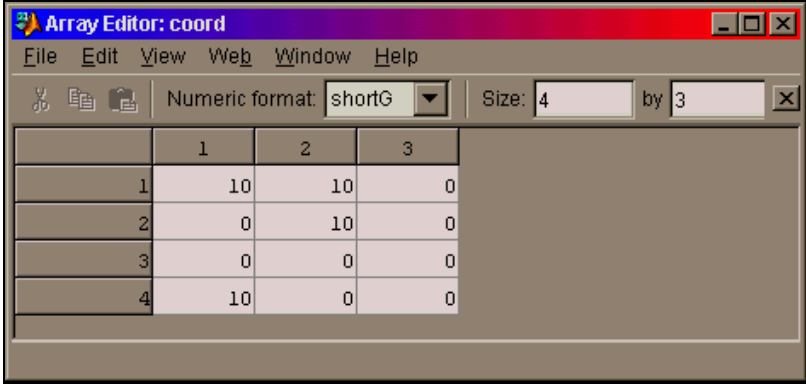


Figure 16. Manual Model Design GUI Form

This form can be used to create a new model or to make changes to an existing model. A model can even be saved at any point in the design process and loaded at a later time for further design and completion. As shown in Figure 16, the full model design process is completed in three steps.

The first step in the design process involves the definition of the coordinates of the vertices. The standard MATLAB array editor is used to allow the user to enter coordinates for the desired number of vertices. Figure 17 depicts the array editor contents for the coordinates of the vertices of a 10 m by 10 m plate model, located on the (x,y) plane. Each row corresponds to a vertex of the plate for a total of 4 vertices, with each column containing the x , y and z coordinates of each plate.



	1	2	3
1	10	10	0
2	0	10	0
3	0	0	0
4	10	0	0

Figure 17. Vertex Coordinate Input

Upon completion of the input of the coordinates, the user performs an automated check on the validity of coordinates, in order to eliminate multiple vertices with the same coordinates.

The second step in the manual model design process involves the definition of the facets, using the vertex numbers. Again, as shown in Figure 18 for the plate model, the MATLAB array editor is used.

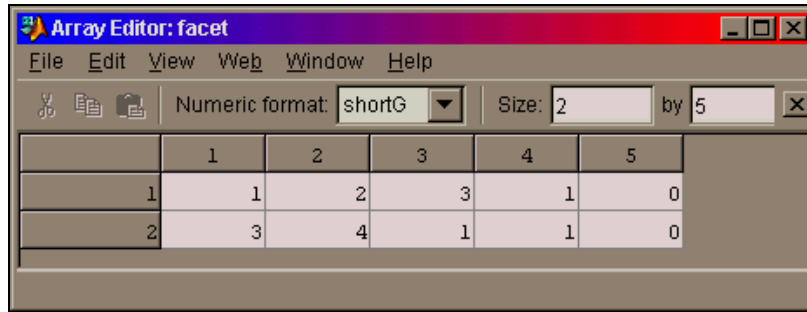


Figure 18. Facet Definition

Each row now corresponds to a facet. The first three columns indicate the vertices of the facet. For example, in the plate model described in Figure 18, the second facet is defined by vertices 3, 4 and 1. The sequence of the vertices defines the outward normal to the facet in a right-hand sense. Column 4 indicates whether a facet can be illuminated on its front side only (when its value is 1) or on both its front and back side (when its value is 0). Column 5 contains the surface resistivity value of the facet, normalized to the impedance of free space (377 ohms). In the example in Figure 18, the 0 values in Column 5 indicate that the facets are a Perfect Electric Conductor (PEC).

After the completion of the facet definition, the user performs an automated check to detect multiple facets with same vertices (i.e., identical facets) and facets that are not properly defined (e.g., not defined by three different vertices).

The third step involves the display of the designed model. The plate example described in the previous steps, created the model depicted in Figure 19.

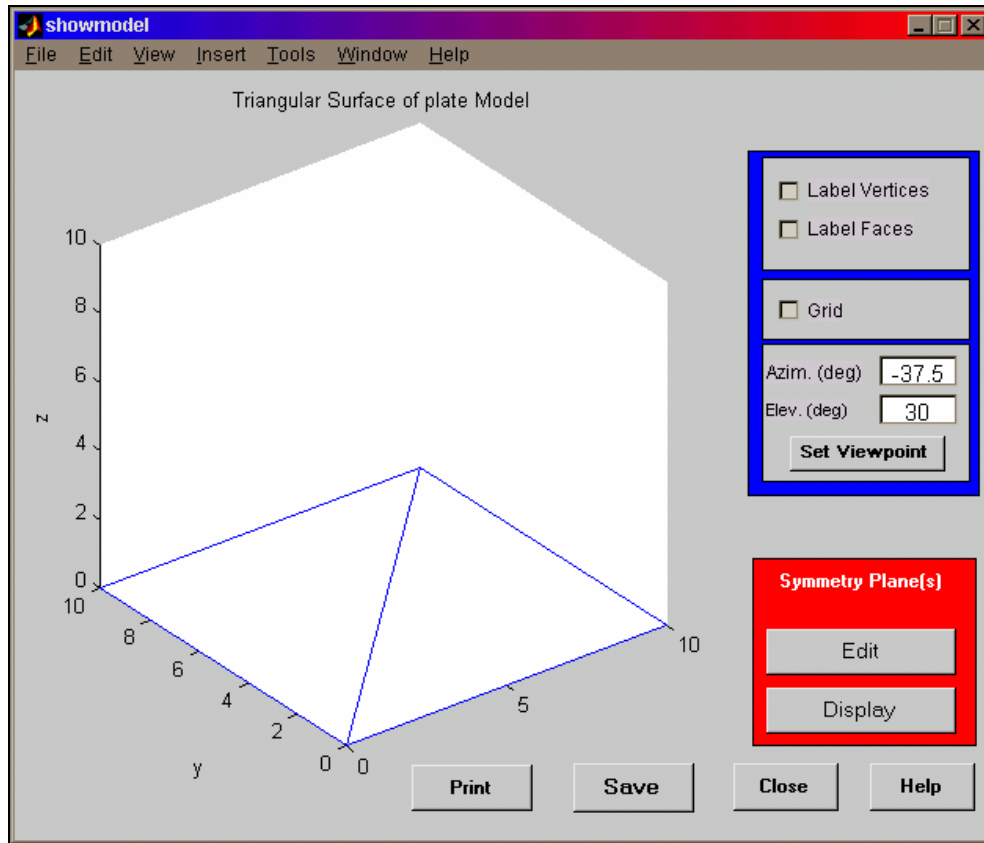


Figure 19. Plate Model Display

The user can now view the model in three dimensions: change viewpoint, label the vertices and/or facets and decide whether to save and/or print the model or make further changes. At this point, the user can also add symmetry planes to the model, which the following chapter discusses.

The Manual Model Design GUI, as was shown in Figure 16, also has provisions for the application of a specific surface resistivity value to all the model facets and the scaling of the model. It also allows the user to add comments or text descriptions to the facets, whose importance will be explained in Section F of this chapter. Finally, the user can apply specific materials or coating to the facets. The following chapter describes this option as it pertains to the new computational capabilities of the program.

3. Results

Generally, the process of manually designing a complex model proved tedious, error-prone and time consuming. When a model was comprised of more than 20 facets, a significant amount of time and effort had to be spent on entering coordinate values and

facet definitions. In conclusion, the manual model design is a good approach for small, simple models such as the plate model described above, or for making detailed changes to specific vertices or facets of an existing model.

Figure 20 depicts the manually designed model of a simple dart target, consisting of 11 vertices and eight facets.

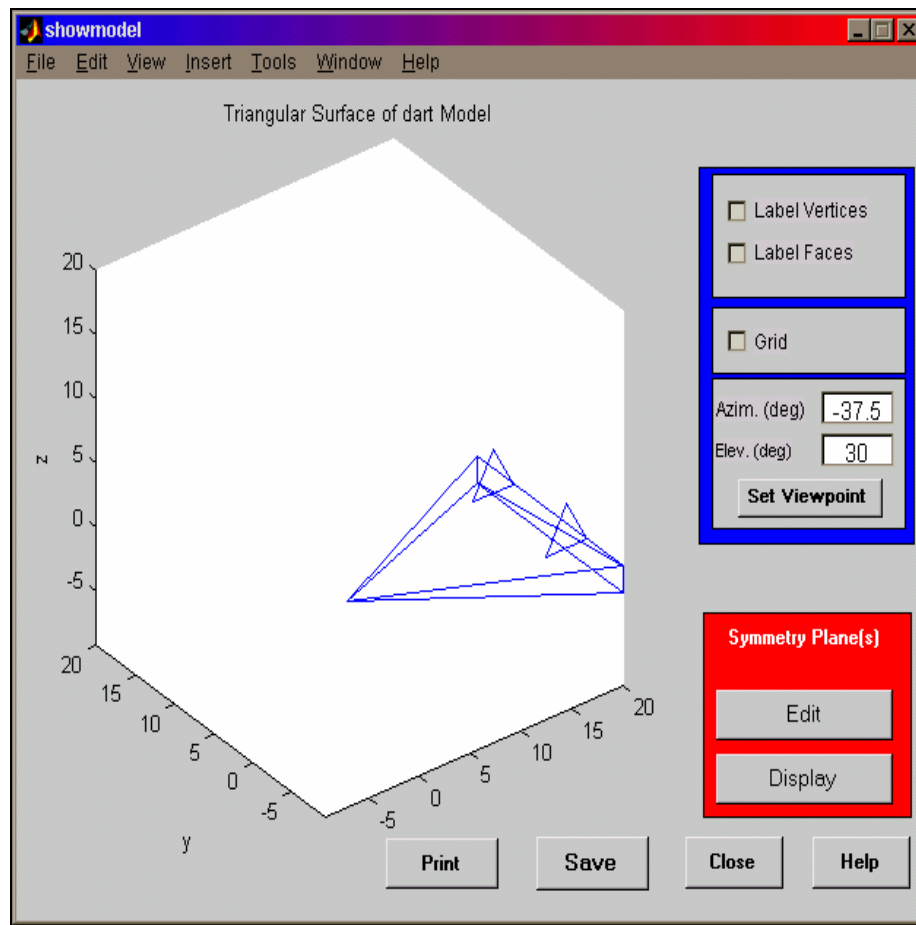


Figure 20. Dart Model Display

D. GRAPHICAL MODEL DESIGN

1. Rationale

The discussion of the manual model design approach revealed that it could not be efficiently used to design large, complex models. Even simple geometrical models, such as spheres, cylinders or cones, when described with triangular facets, would result in a large number of facets in order to approximate their surface curvature. Thus, the manual model design would involve extensive preparatory work in the form of calculations of

coordinates and time-consuming work to enter the coordinates to the program. Therefore, a graphical, automated approach to model design was necessary to produce complex models with minimum user workload.

2. Procedure

Since all standard geometrical shapes can be described with mathematical equations, many of which are implemented by standard MATLAB functions, the whole process of model design could be easily automated by using these equations to find the values of vertex coordinates. Once the coordinates are derived, the right-hand facet definition approach can be used to produce the facet arrays

Figure 21 depicts the Graphical Model Design GUI form, which displays a model of a cylinder.

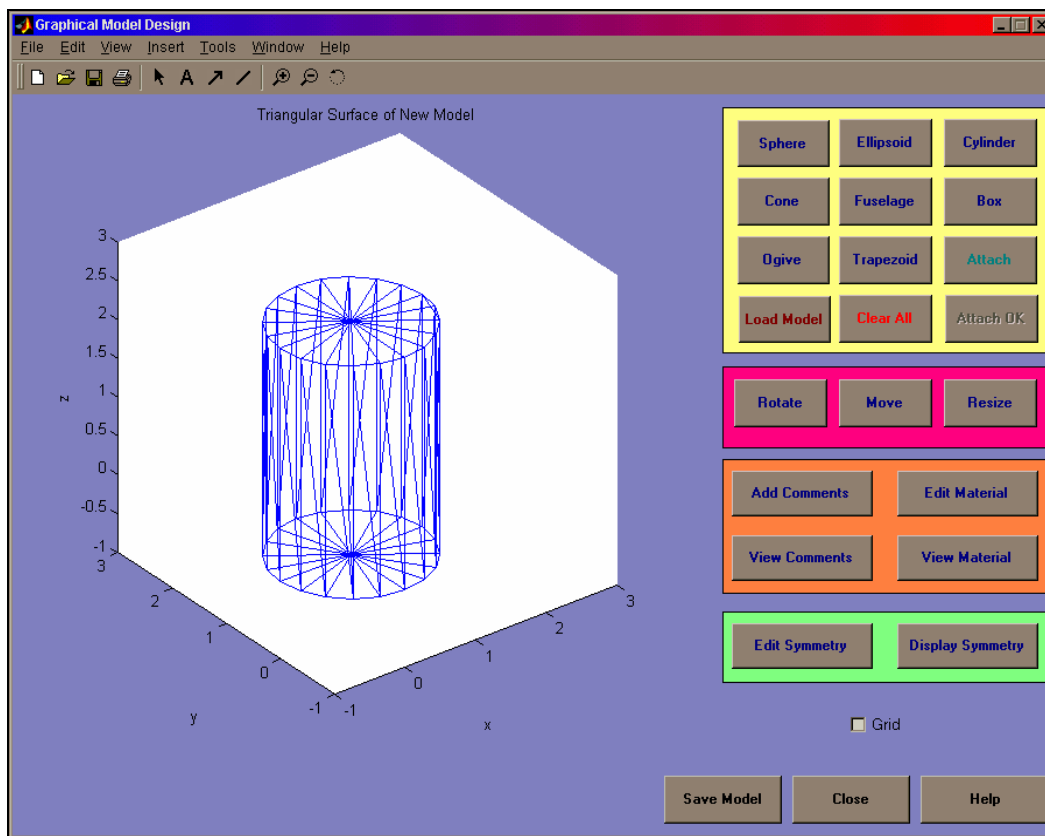


Figure 21. Graphical Model Design GUI Form

This form can be used to create a new model or to make changes to an existing model. As shown in Figure 21, there are provisions for the automatic model design of the

following standard shapes: Spheres, Ellipsoids, Cylinders, Cones, Fuselages, Boxes, Ogives, and Trapezoids. In each of these cases, the user selects the parameters of the model and the number of points used to approximate curved surfaces.

For example, Figure 22 depicts the dialog box that allows the user to select the radius of the model of a sphere and the number of points approximating a circle on the sphere's circumference. Figure 23 depicts the resulting sphere model.



Figure 22. Sphere Parameters

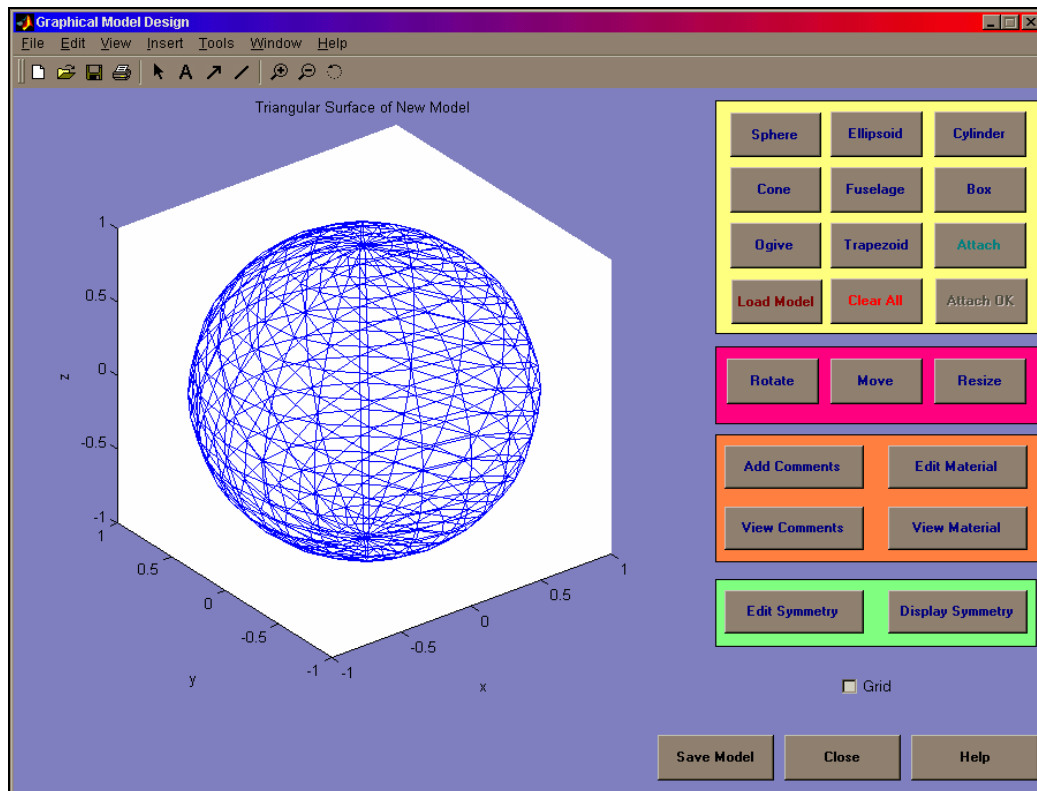


Figure 23. Sphere Model (20 Points per Circle)

When the same sphere is designed using 40 points per circle, the resulting model is depicted in Figure 24. Obviously, this model consists of a larger number of vertices and facets.

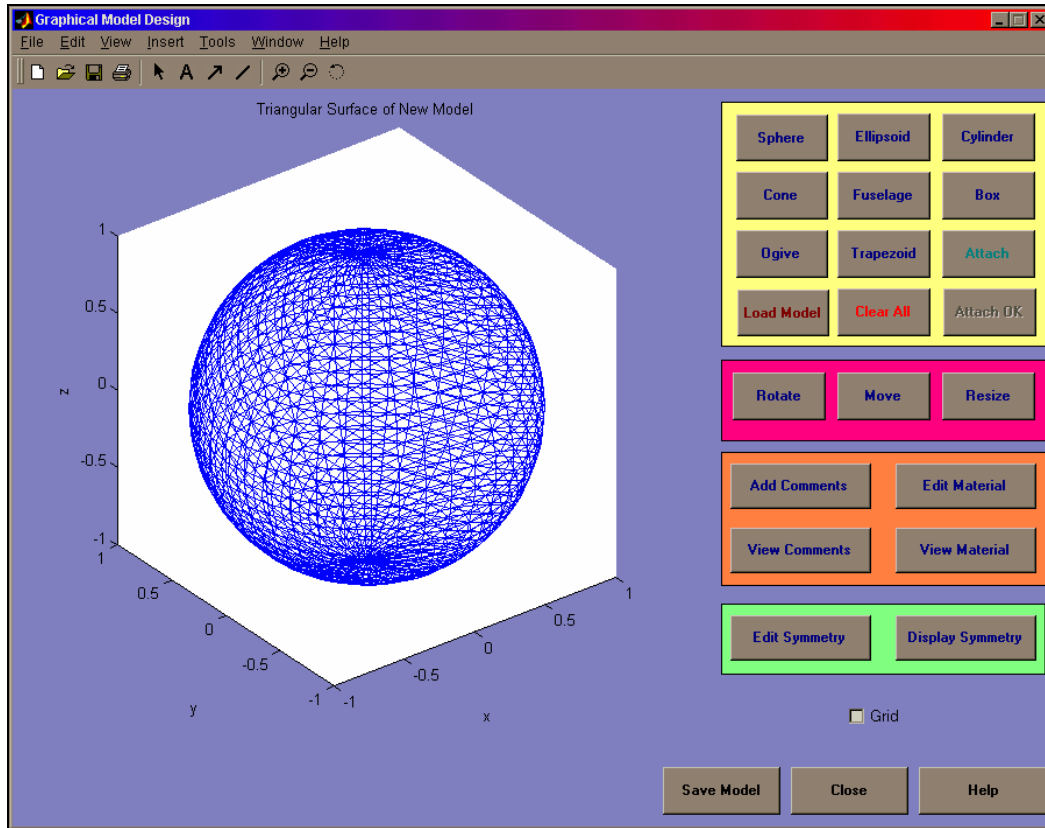


Figure 24. Sphere Model (40 Points per Circle)

Once a model is created or loaded, it can undergo certain standard geometrical manipulations. For example, the user can select to rotate the model around one or more axes by entering the desired value of the rotation angle(s) in degrees, in the dialog box shown in Figure 25.

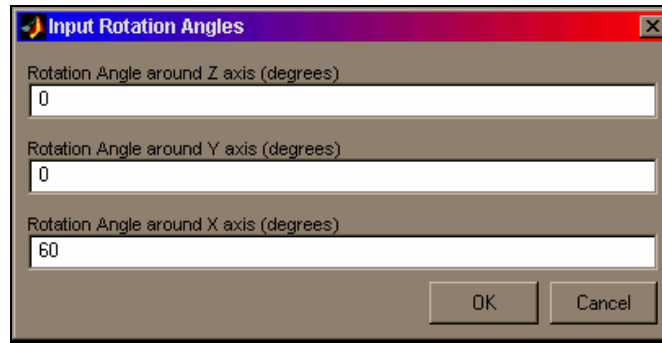


Figure 25. Model Rotation Dialog Box

Thus, the cone model shown in Figure 26(a), resulted in the model shown in Figure 26(b), when rotated by 60 degrees around the x axis. The GUI form buttons shown in the previous figures were omitted and the grid was added for clarity.

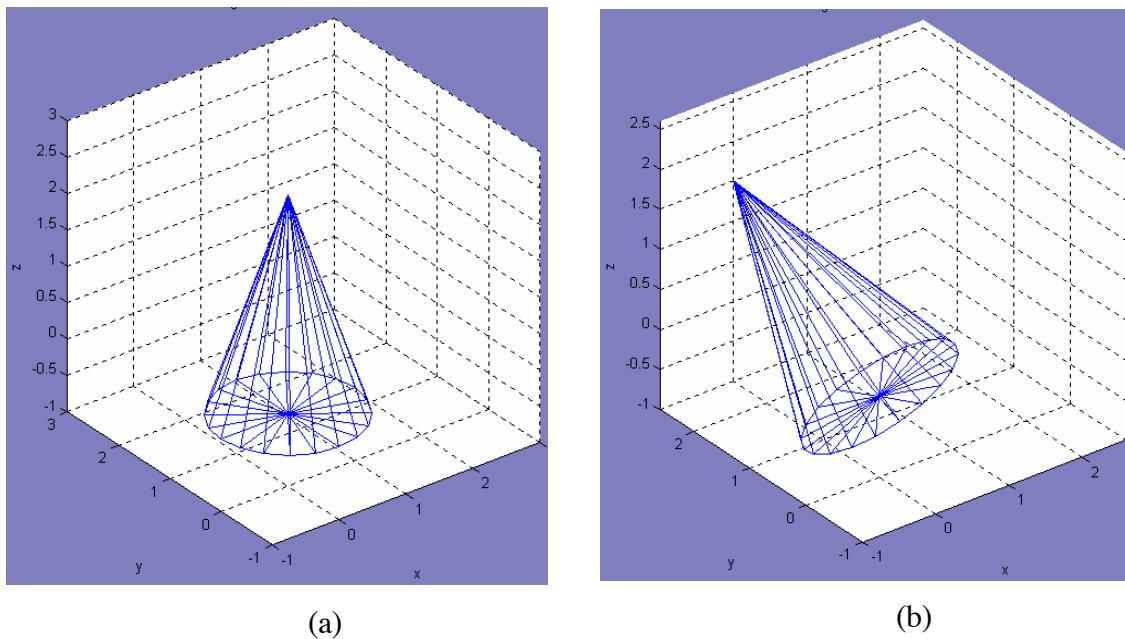


Figure 26. (a) Cone Model, (b) Rotation of 60 Degrees Around X Axis

Other geometrical manipulations include the resizing of the model in one or more axes by a user-selectable amount, resulting in either the increase or decrease of the model's size, and the movement of the model in any desired direction in space by a user-selectable distance.

The user can also add symmetry planes to the model and apply specific materials or coating to the facets. The following chapter discusses both options. Comments or text descriptions to the facets can also be added here, which Section F of this chapter discusses.

3. Results

The Graphical Model Design GUI provides the user with the capability to create models with standard geometrical shapes, selecting both the shape parameters and, when applicable, the required approximation to curved surfaces. The creation of these shapes is, in most cases, almost instantaneous. However, in the case of curved shapes, the amount of time required for their creation rapidly increases with the number of points used per circle. For example, the sphere model shown in Figure 23 (20 points per circle) took less than one second to complete, while the sphere model shown in Figure 24 (40 points per circle) took almost nine seconds to complete.

Generally, the Graphical Model Design GUI was used almost exclusively for the creation of most of the new models that accompany the 3.0 version of the POFACETS program.

Figure 27 depicts four models created with the Graphical Model Design GUI.

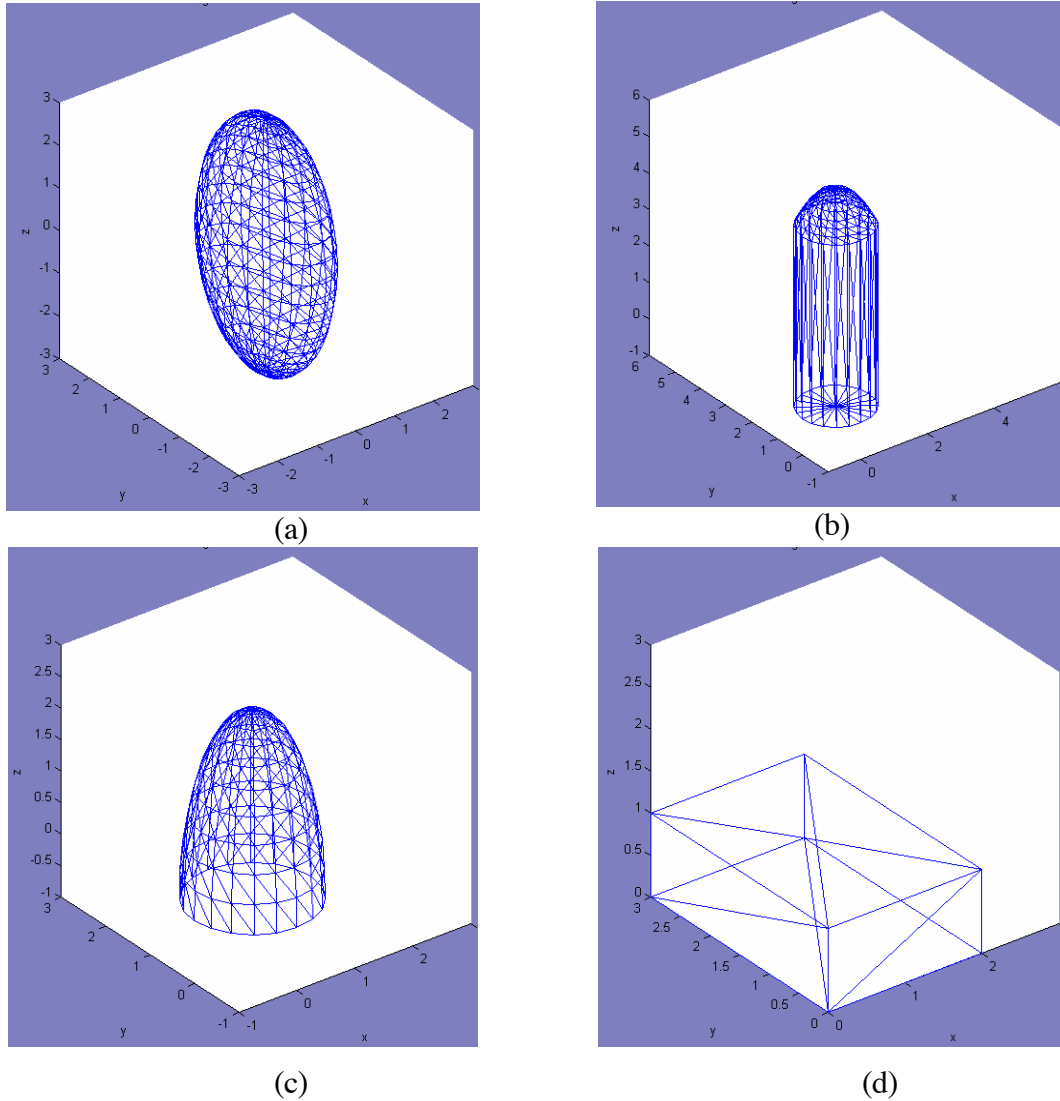


Figure 27. Graphically Designed Models (a) Ellipsoid, (b) Fuselage, (c) Ogive, (d) Box

E. IMPORT/EXPORT OF MODELS

1. Rationale

The Graphical Model Design GUI provided new options for the automated design of models with standard geometrical shapes. However, its capabilities in the manipulation of the geometrical shapes and the tools it provided could not be compared to those available in commercial design software, such as AUTOCAD. These software packages not

only provide the user a wide variety of tools and options for designing new models, but quite often, they also include libraries of pre-designed models.

Hence, the capability of importing models created in commercially available design software into the POFACETS, would greatly enhance the program's versatility and provide it with real-life target models. Since the AUTOCAD software was considered the most prominent among the Computer Aided Design software available, it was decided to create an option for importing model files designed with AUTOCAD.

In addition, model files created by other software packages used by RCS professionals were examined. The defining factor in the model file type selection was whether there were sufficient data available for a specific file type structure to allow successful import of a model to POFACETS and, secondly, successful export of a POFACETS model to this file format.

In addition, a standard MATLAB model design toolbox, called *pdetool*, was also considered a candidate for importing models into the POFACETS. The models created by *pdetool* can be used for RCS prediction of two-dimensional shapes with another software package, which uses the Method of Moments with the Rao-Wilton-Glisson (RWG) basis functions.

2. Procedure

The Model Import/Export functions of POFACETS were incorporated in the Utilities GUI form. They are implemented through the circled buttons shown in Figure 28. The GUI provides options for importing models from:

- AUTOCAD files saved in stereo-lithographic text format (*.stl). This file format can be only applied to AUTOCAD models consisting of shapes defined as solids and not in models consisting of surfaces.
- Files saved in ACADS or DEMACO facet format (*.facet and *.dem files). These file formats are only available through the ACADS and CIPHER software packages. They are often used by RCS engineers and their format facilitates translation into the triangular facet format used in the POFACETS models.
- Surface mesh files created by MATLAB's *pdetool*.

The GUI allows POFACETS to export models in ACADS and DEMACO facet formats. Although models could also be easily exported to stereo-lithographic format and

pdetool mesh format, these options are not provided in the GUI, since AUTOCAD cannot import the stereo–lithographic format and POFACETS’ three–dimensional models could not be imported to the *pdetool*.

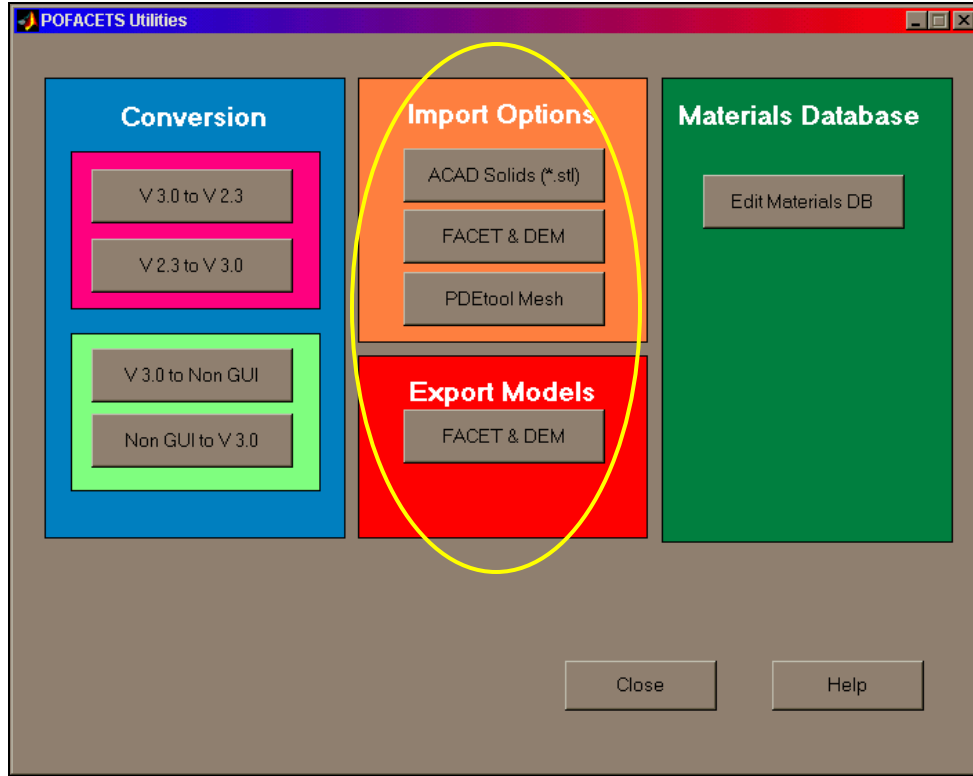


Figure 28. Import/Export Options (circled)

3. Results

The following sequence of figures depicts various models imported from the AUTOCAD, ACADS, CIFER and *pdetool*, utilizing the model file types described above. As these figures clearly demonstrate, the complexity and detail of models that can be imported to POFACETS is on the same level as the complexity and detail of models produced by the respective CAD program. This is especially evident in the models imported from ACADS and DEMACO files.

Figure 29 depicts a cylinder, designed as a solid body in AUTOCAD, saved in stereo–lithographic text format and imported into POFACETS. Notice the difference in facet definition, as compared to the cylinder model of Figure 21.

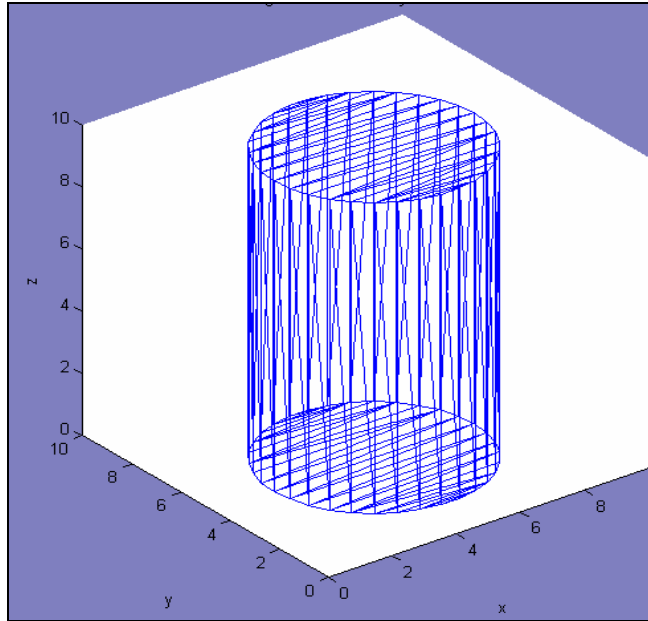


Figure 29. Cylinder Model Imported from Stereo-Lithographic Format

Figure 30 depicts the model of a T-62 Armored Fighting Vehicle (AFV) imported from the ACADS file format.

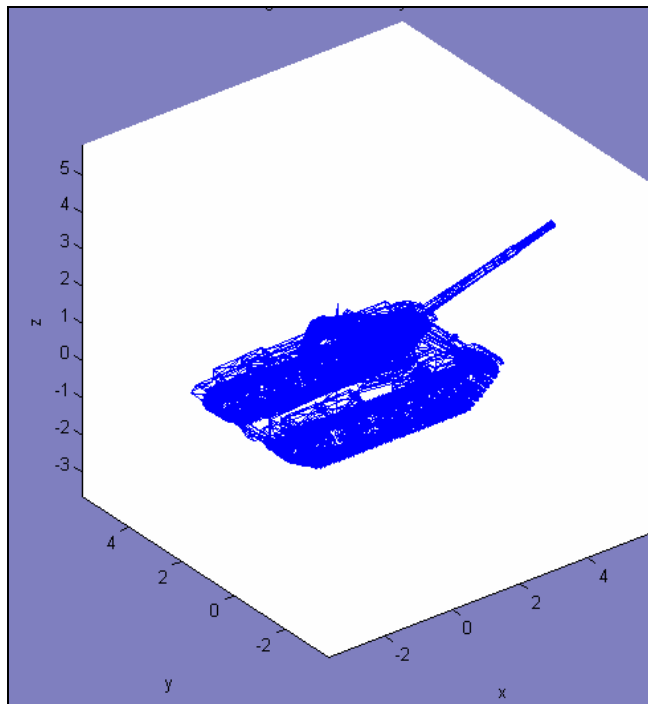


Figure 30. T-62 AFV Model Imported from ACADS Format

Figure 31 depicts the model of the X-29 aircraft imported from the DEMACO file format.

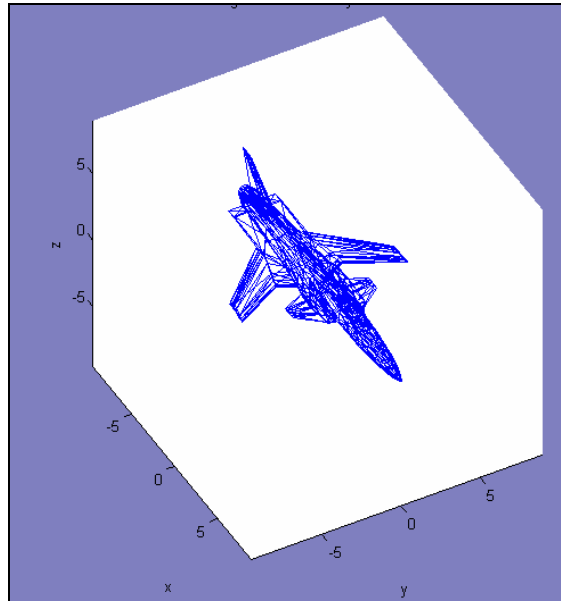


Figure 31. X-29 Aircraft Model Imported from DEMACO Format

Figure 32 depicts the model of a star-shaped two-dimensional model, imported from MATLAB's *pdetool*.

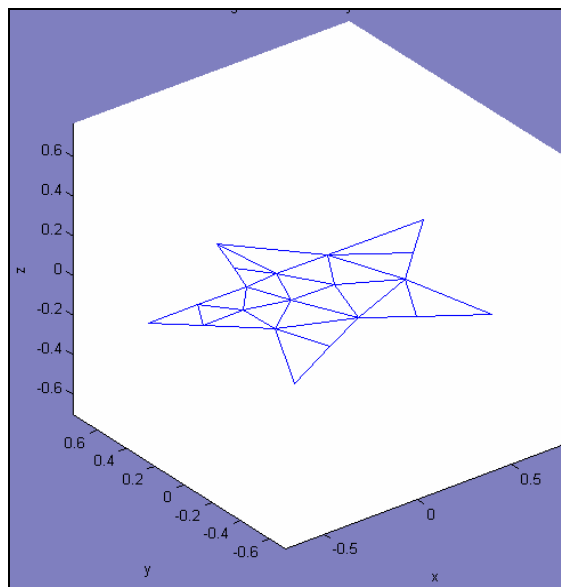


Figure 32. Star-Shaped Model Imported from *Pdetool*

F. COMBINATION OF MODELS

1. Rationale

As discussed previously, the implementation of the Graphical Model Design GUI and the development of code allowing the user to import into POFACETS models designed in commercially available software provided significant versatility to the POFACETS model management capabilities.

The next logical step was to provide code that would allow the combination of existing models. The goal here was twofold. First, a complex target model could be built by combining simpler models. For example, a simple Unmanned Air Vehicle (UAV) can be modeled through a combination of a fuselage, two trapezoidal wings and two parallelepipeds as stabilizers. Second, additional or optional parts could be added to a standard target model to evaluate the effects on its RCS. For example, the RCS of an aircraft could be evaluated with or without external stores and armament.

2. Procedure

The combination of models is accomplished using the Graphical Model Design GUI, through the Attach buttons, which are circled in Figure 33.

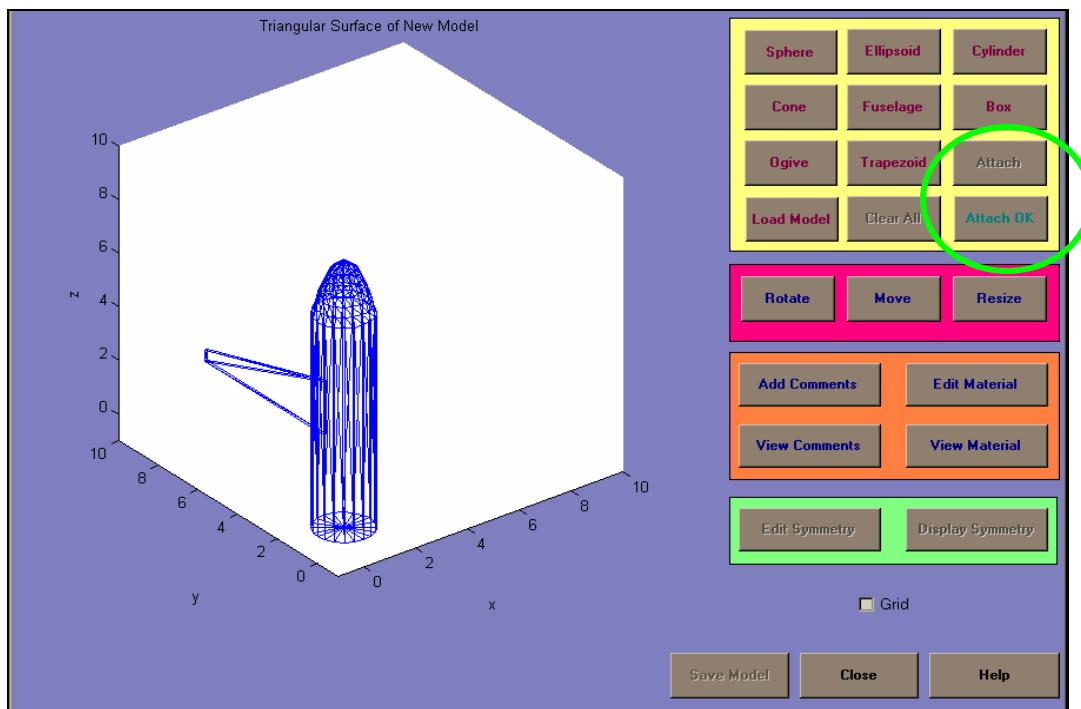


Figure 33. Model Combination (circled)

In the example depicted in Figure 33, a fuselage of a UAV has been initially modeled. Next, a trapezoid was defined to serve as one of the wings of the UAV. After the trapezoid was modeled, it was appropriately moved and rotated as described in Section D of this chapter in order to be placed in its final location. Following this process, the final model of the UAV, comprised of a fuselage, two wings and two stabilizers is depicted in Figure 34.

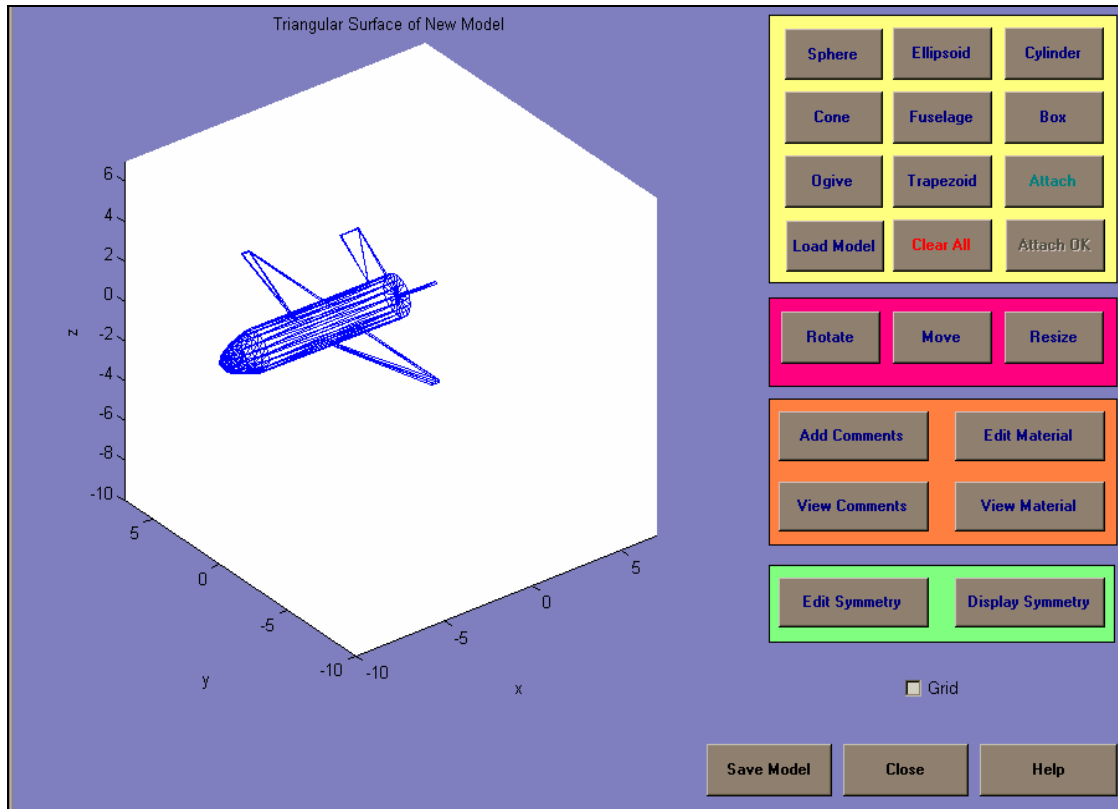


Figure 34. UAV Model

At this point, as the models designed by the POFACETS were becoming more complex, it was considered necessary to provide the user with some means to distinguish facets belonging to different components or parts of the model. This would be helpful not only for future modifications of the model, but for the application of different materials to various parts of the model as well.

In order to provide this capability, an array containing the description of the major part or component to which each facet belongs was added to the model file structure. When a model is automatically generated through the use of the Graphical Model Design

GUI, standard descriptions are added to this array. Subsequently, the user can view or modify these descriptions by using the appropriate buttons provided both on the Graphical Model Design GUI and on the Manual Model Design GUI.

Figure 35 depicts some of the descriptions for the facets of the UAV depicted in Figure 34. The user can easily determine that facets with numbers up to 20 form the fuselage base, while facets with numbers 21 and higher pertain to the fuselage body itself. Similar descriptions can be viewed for the wings and the stabilizers. Notice that the user can modify these descriptions to describe a part or component better.

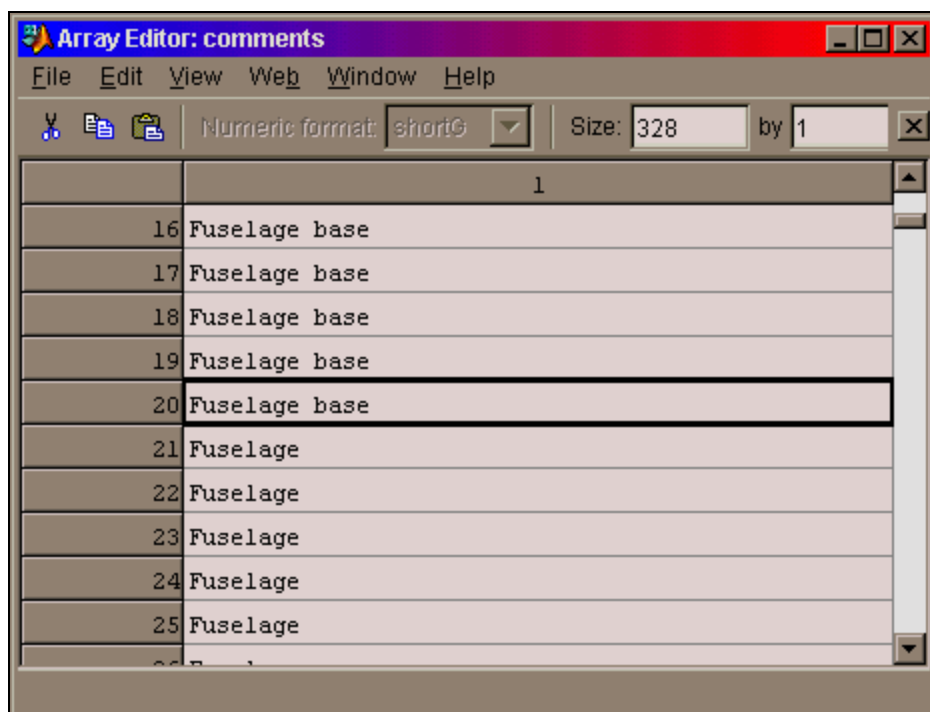


Figure 35. Facet Descriptions

3. Results

The option to combine existing models in POFACETS adds new capabilities to model management and manipulation. Specifically, it allows for distributed model design, with different users being able to implement sub-components or parts of a design independently, and then combining their work to produce a final, complex model.

The results of the application of this capability are portrayed in the example shown in Figures 36 and 37. Figure 36 shows several target models designed by different

users, using different tools. Figure 36(a) shows the X-29 aircraft model, imported from a DEMACO file. Figure 36(b) depicts a model of an AIM-9 Sidewinder missile, which was manually designed in the previous version of POFACETS. Figure 36(c) depicts a model of the AGM-84 Harpoon Anti-Ship Missile, which was designed using the Graphical Model Design GUI of POFACETS. Notice that the scale of the models, as shown in the graphs' axes, is correct, regardless of the manner in which they are depicted.

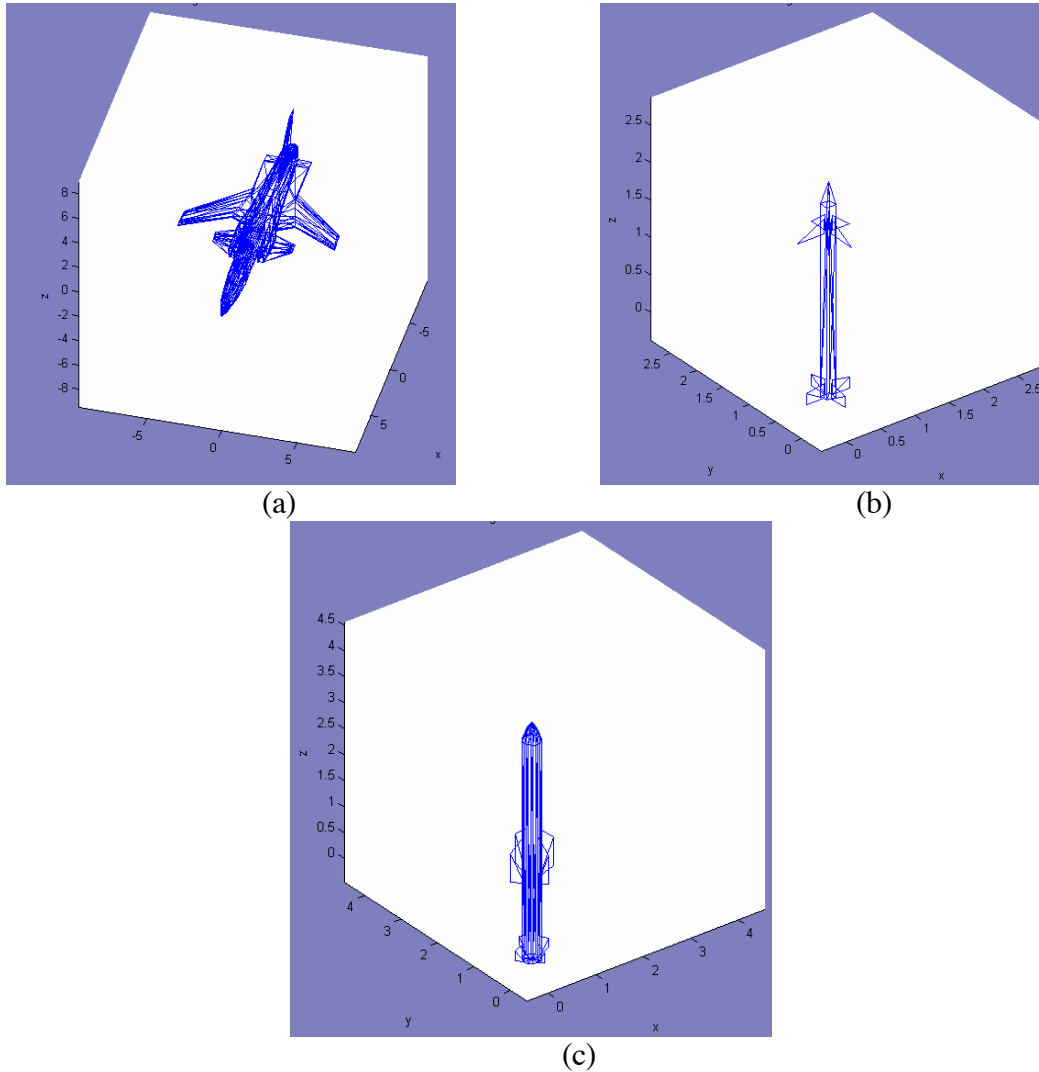


Figure 36. Various Models (a) X-29, (b) AIM-9, (c) AGM-84

Figure 37 depicts a combination of the X-29 aircraft model with two AIM-9 models and two AGM-84 models. The four missiles were attached to the wings of the aircraft. The whole process took less than 10 minutes. Other stores and armament configurations could be easily implemented as well.

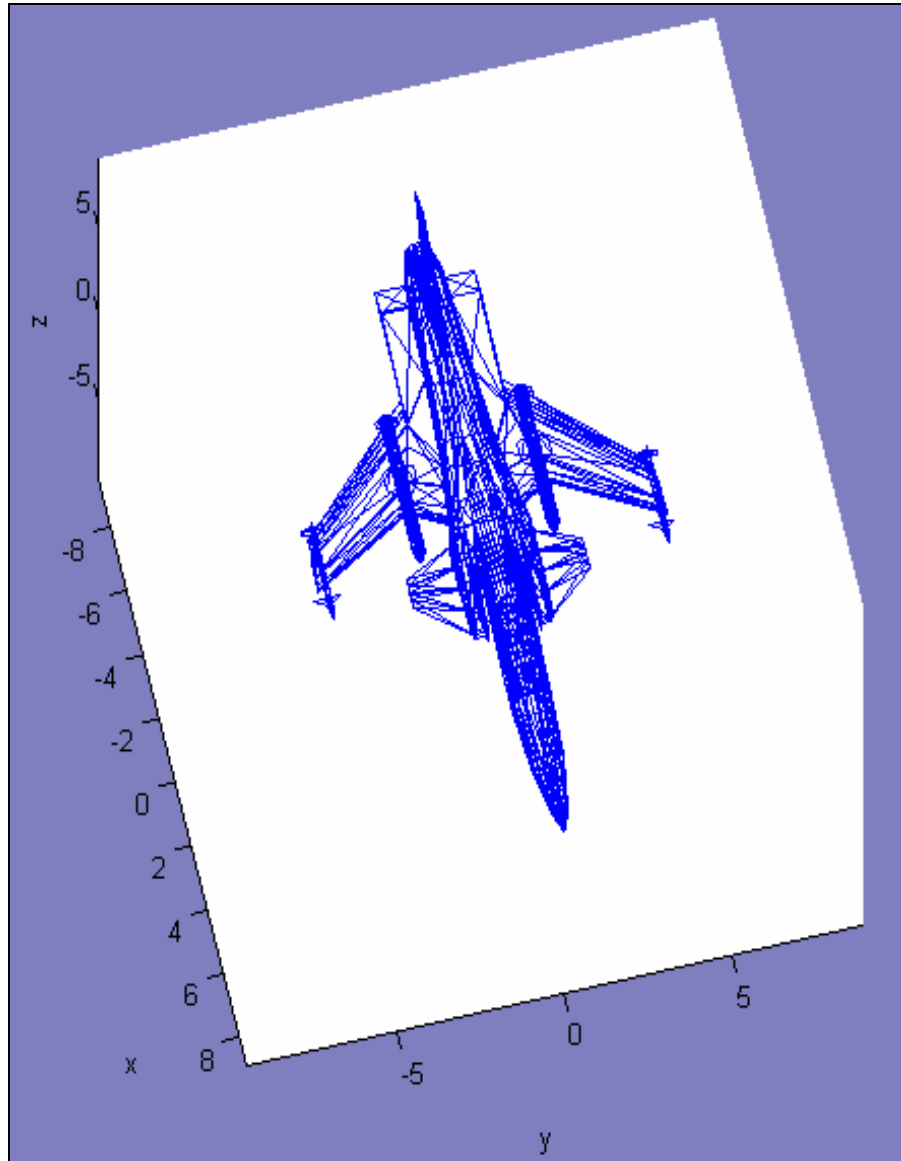


Figure 37. Armed X-29 Aircraft Model

G. RCS COMPUTATION OPTIONS

1. Rationale

The work described so far was aimed at upgrading the existing POFACETS GUI, improving its models database, and providing new options and additional versatility in

the design of new models or the modification of existing models. All these features are necessary in order to implement better and more efficiently the main goal of this program, which is the prediction of the RCS of target models.

The POFACETS version 2.3 program provided the user with two main options regarding the calculation of the RCS of a model, monostatic (i.e., the radar transmitter and receiver are collocated) and bistatic (i.e., the radar transmitter and the radar receiver are placed in different locations). The calculation of RCS was performed relative to the spherical coordinates angles of observation, θ and ϕ , for a fixed frequency, which was selected by the user. This type of RCS computation is the one that appears most often in the relevant literature and, of course, it was maintained in the new POFACETS version, with certain new computational capabilities being added, as described in the next chapter.

The monostatic and bistatic RCS computations were also expanded in the new version of POFACETS to include the calculation of RCS versus frequency for a fixed, user-selectable, observation angle. This option can be used to predict the RCS behavior of a model over a selected range of frequencies, while it can also provide an additional verification of RCS results obtained for standard target models.

2. Procedure and Results

a. RCS versus Observation Angles

The RCS computation versus the observation angles was implemented in POFACETS version 2.3. Its GUIs are briefly discussed here, in order to provide a complete description of the program's functionalities. Figure 38 depicts the Monostatic RCS Computation GUI.

First, the user selects and loads the model for which the RCS calculation will be performed. The model is displayed, so that the user can review it and verify that this is the desired model. Next, the user must select the parameters that will be used in the RCS calculations. Specifically, the user enters values for the following parameters:

- Observation angle θ starting and ending values (from -360 to 360 degrees), and increment value
- Observation angle ϕ starting and ending values (from -360 to 360 degrees), and increment value

- Incident wave polarization (selectable between Transverse Magnetic and Transverse Electric)
- Frequency
- Taylor Series Number of Terms and Length of Region
- Surface Roughness Correlation Distance and Standard Deviation.

Many of these parameters have standard predefined values, so in those cases, the user simply enters the desired frequency and observation angles. Notice that in the case of observation angles, one of the two can be constant, as shown in Figure 38 for the ϕ angle, resulting in a ϕ –cut or a θ –cut.

The user can also select to add a ground plane on the (x,y) plane or exploit symmetry planes in the model (if any). These options are discussed in the next chapter. Finally, the user can select the types of RCS plots that will be produced as a result of the calculations.

CALCULATE MONOSTATIC RCS

Calculation of Monostatic RCS for the plate model

Load File

☐ Ground Plane XY?

☒ PEC

Rel. Permittivity: 4

☐ Use Symmetry?

Surface Roughness

Correlation Dist.(m): 0

Standard Dev. (m): 0

Computational Parameters

Taylor Series

Length of Region: 0.05

Number of Terms: 5

Incident Polarization: Theta (TM-z)

Frequency: 1 GHz

☐ Show 3D Display ☐ Show Polar Graph

Calculate RCS Print Close Help

Theta **Phi**

Starting Angle: 0 deg 0 deg

Ending Angle: 360 deg 0 deg

Increment Angle: 1 deg 1 deg

Figure 38. Monostatic RCS Calculation GUI

Once all parameters are entered, the user initiates the RCS computation by the appropriate button. Upon completion of the calculations, the selected RCS plot is displayed. For example, a 1 m by 1 m PEC plate located on the (x,y) plane, when illuminated with a TM wave at 1 GHz, with ϕ being constant at 0 degrees, produced an RCS graph versus angle θ , as shown in Figure 39.

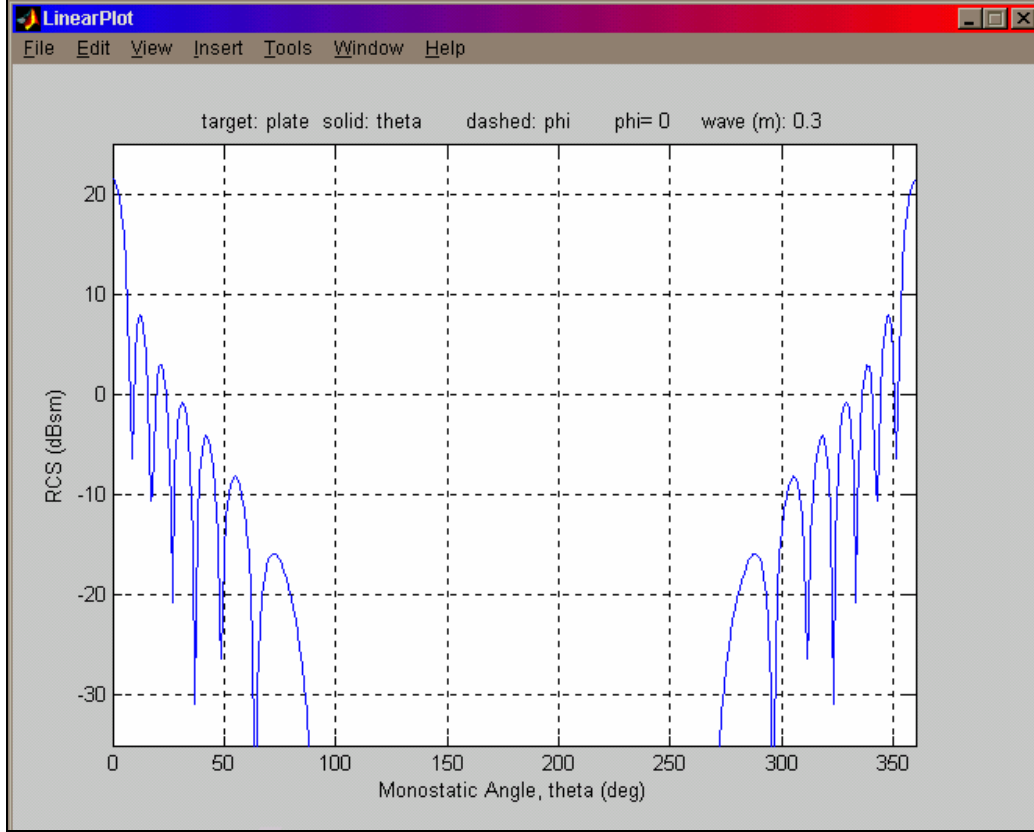


Figure 39. RCS of a 1 m by 1 m PEC Plate at 1 GHz, TM wave, for $\phi=0$

For θ between 90 and 270 degrees, the RCS is zero, since that part of the plate is considered its back side and, therefore, it cannot be illuminated. The RCS curve in Figure 39 follows the closed form solution for the RCS of a 1 m^2 plate (Ref. 2):

$$\sigma = \frac{4\pi}{\lambda^2} \cos^2 \theta \cdot \text{sinc}(ku) \cdot \text{sinc}(kv) \quad (4.1)$$

where λ is the wavelength, $k = 2\pi/\lambda$, $u = \sin\theta \cos\phi$ and $v = \sin\theta \sin\phi$. Indeed, in this case, the frequency is 1 GHz, yielding a wavelength of $\lambda = 0.3 \text{ m}$ and for $\theta = 0$ degrees, the RCS is computed to be $\sigma = 4\pi / (0.3)^2 = 139.62 \text{ m}^2 \rightarrow 21.44 \text{ dBsm}$. Moreover, the *sinc* function form of the RCS curve is clearly visible in the graph in Figure 39. Notice that the solid blue curve in Figure 39 corresponds to the RCS component in θ direction. According to the graph, a dashed line would correspond to the RCS component in the ϕ direction. This line does not appear, which means that the RCS component in this direction is zero (i.e., no change in polarization occurs).

When both angles of observation θ and ϕ can vary, the resulting RCS plot takes the form depicted in Figure 40. This graph pertains to the same 1 m by 1 m PEC plate, for a 1 GHz, TM polarized incident wave, with θ varying from 0 to 360 degrees in 2 degree steps and ϕ varying from 0 to 180 degrees in 2 degree steps. Notice that the graph now is made versus U and V , where $U \equiv u = \sin\theta \cos\phi$ and $V \equiv v = \sin\theta \sin\phi$. Again, the *sinc* function format is clearly visible in two dimensions for the RCS component in the θ direction, while the RCS component in the ϕ direction is zero (i.e., no change of polarization occurs).

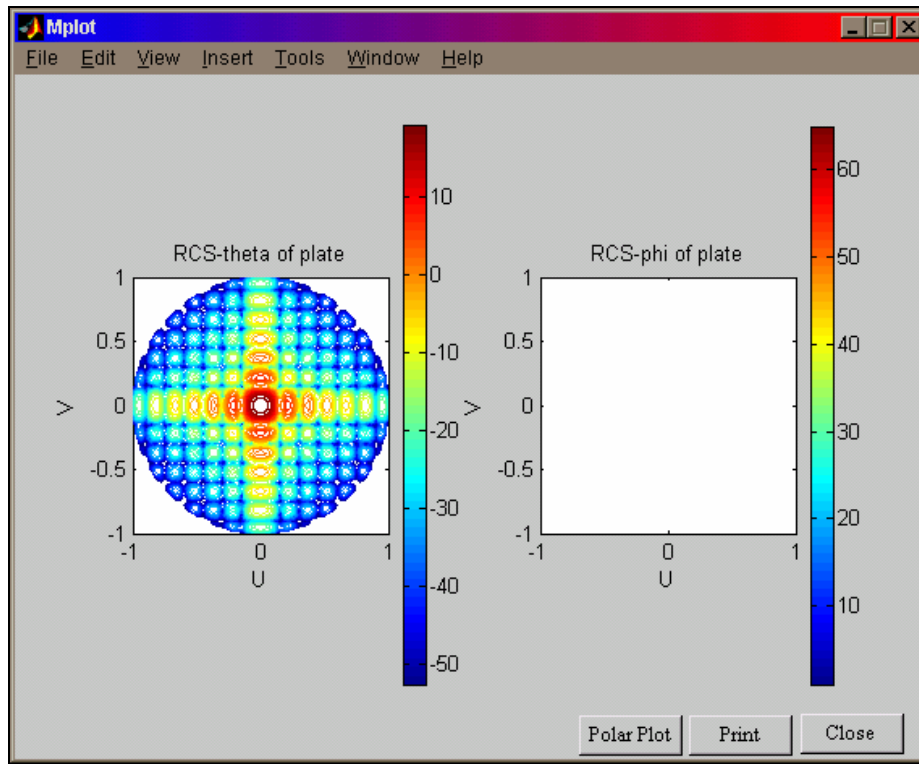


Figure 40. RCS of a 1 m by 1 m PEC Plate for at 1 GHz, TM Wave

For the bistatic RCS case, the GUI form depicted in Figure 41 allows the user to enter values for the various computation parameters. All the parameters mentioned in the monostatic case are included here. In addition, the user must now enter an incidence angle (i.e., the radar transmitter is located at a fixed angle to the target, while the angle of observation is varied as desired).

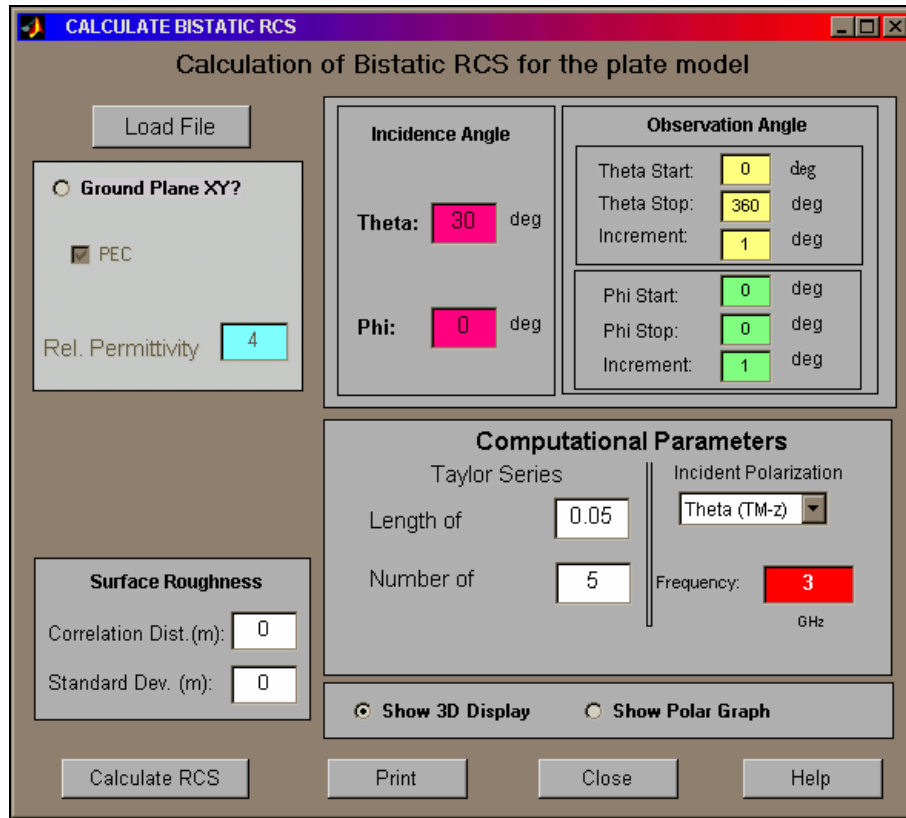


Figure 41. Bistatic RCS Calculation GUI

For example, a 3 GHz, TM polarized wave, incident on a 1 m by 1 m PEC plate from $\theta = 30$ degrees and $\phi = 0$ degrees produces an RCS curve versus angle θ for $\phi = 0$ degrees shown in Figure 42.

The nulls in the graph occur for $\theta = 90$ and $\theta = 270$ degrees (i.e., in the two directions parallel to the plate). The two peaks in the RCS curve correspond to the specular reflection on the plate and the forward scatter from the plate.

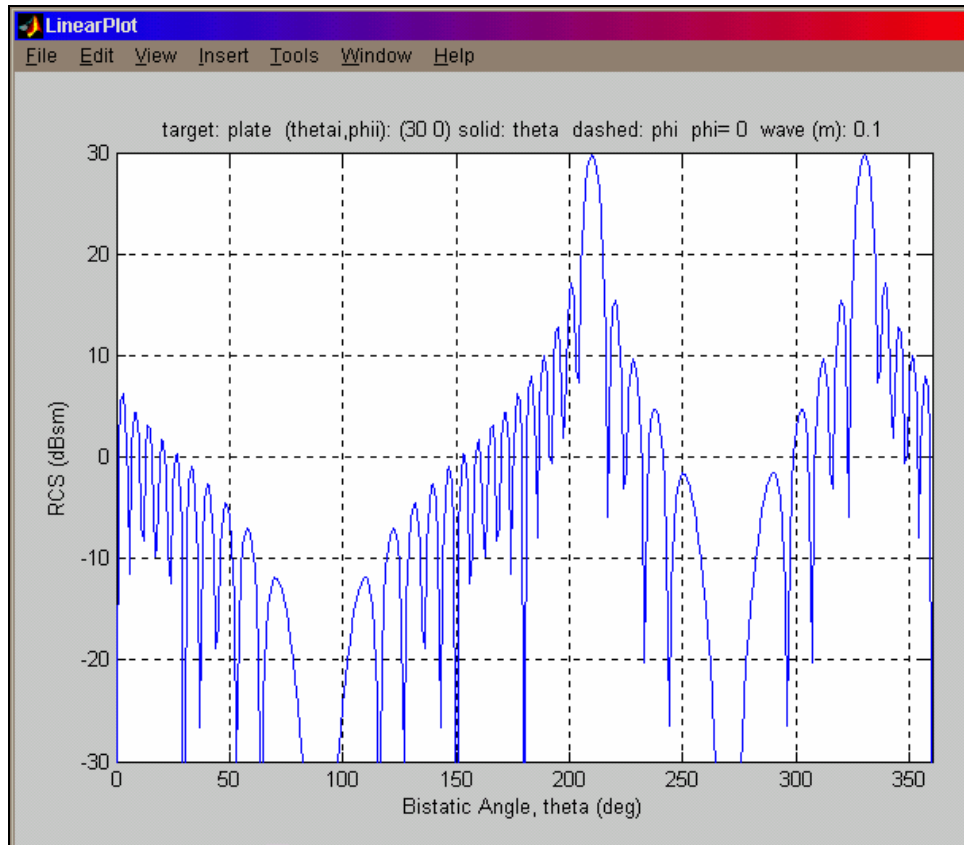


Figure 42. Bistatic RCS Example

Indeed, the specular reflection in the $\phi = 0$ plane occurs at $\theta = 360 - 30 = 330$ degrees, while the forward scatter occurs at $\theta = 180 + 30 = 210$ degrees, illustrated in Figure 43.

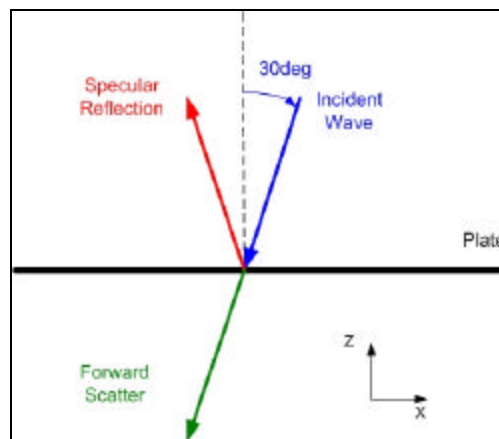


Figure 43. Specular Reflection and Forward Scatter from a Plate

b. RCS versus Frequency

Figure 44 depicts the RCS versus Frequency GUI for the monostatic case. The user again selects a model to be loaded and enters computational parameters, as previously described. The user specifies starting and ending frequencies, frequency increment step and uses the sliders to select the angles of observation. Once these angles are specified, they remain fixed throughout the calculations, with only the frequency being varied as specified.

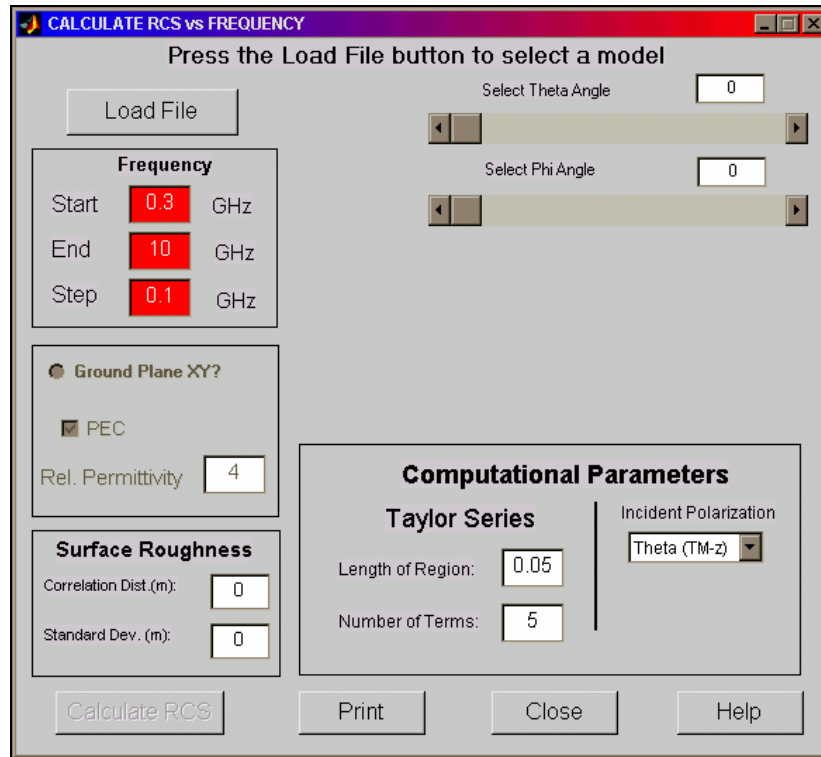


Figure 44. Monostatic RCS versus Frequency GUI

Continuing the example with the 1 m by 1 m PEC plate located on the xy plane, its RCS versus frequency was calculated for observation angles of $\theta = 0$ and $\phi = 0$ (i.e., vertical incidence). Figure 45 shows the resulting graph. Indeed, the RCS of a plate increases with the square of frequency, as predicted by Equation (4.1). Of course, in Figure 45, a logarithmic increase is observed, since the RCS is expressed in dBsm (i.e., logarithmic scale).

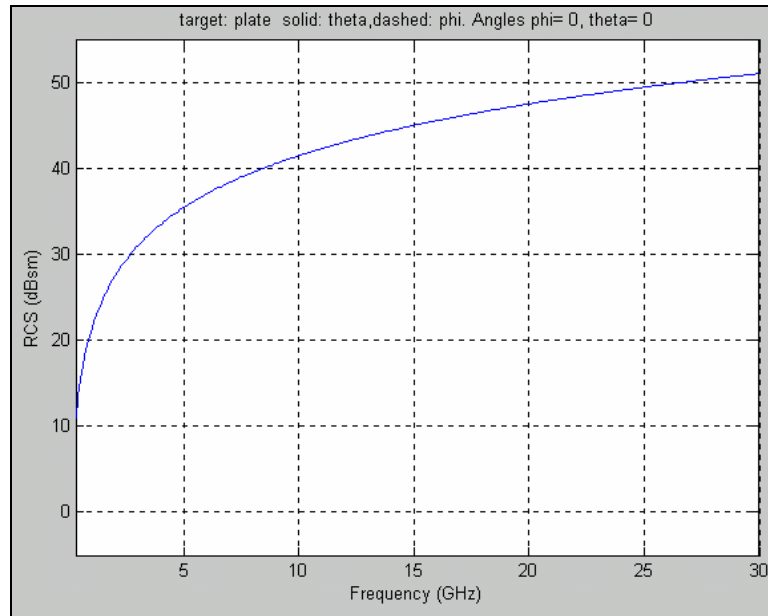


Figure 45. RCS of a 1 m by 1 m PEC Plate versus Frequency (Vertical Incidence)

Figure 46 depicts the RCS versus Frequency GUI for the bistatic case. Here, the user must also specify a fixed incidence angle in addition to all other parameters previously discussed.

Figure 46. Bistatic RCS versus Frequency GUI

H. RCS RESULTS DISPLAY OPTIONS

1. Rationale

Section G of this chapter presented the RCS displays of the POFACETS 2.3 version. Two types of displays were available, depending on whether only one or both angles θ and ϕ were used as parameters for RCS calculations. The displays were configured to present a dynamic range of 60 dBsm. However, in some cases, this resulted in small RCS values not being displayed at all (when the variations of the RCS exceeded 60 dBsm), while in other cases (when the variations of the RCS were in the order of 10 or 20 dBsm), details in the RCS plot were hard to detect.

Thus, the first improvement in the RCS display was to add a user-selectable dynamic range, so that the plot could be configured according to the users needs. This was implemented for the plots in which one of the angles θ or ϕ was constant (i.e., not in the contour of graphs like the one displayed in Figure 40).

Since the most common way to calculate the RCS of a target is versus angles θ , ϕ or both, a Polar Plot was added as an optional way to display the RCS, as angles are more naturally represented in polar format.

Finally, a combination plot, which includes the target model superimposed on its RCS, was added as an optional display. The goal was to illustrate how the incidence and observation angles were related to the target and, thus, assist the user in performing analysis of the RCS results and identifying the parts of the target that contribute to high RCS values.

2. Procedure and Results

a. User-Selectable Dynamic Range

In order to allow the user to manually select the dynamic range that best suits the RCS plot displayed, a slider was added in the GUI that presents the RCS plots in the case when one of the angles θ or ϕ is constant. Figure 47 depicts the same results as Figure 39 (i.e., RCS of a 1 m by 1 m PEC Plate at 1 GHz, TM wave, for $\phi = 0$ and θ varying from 0 to 360 degrees). In this case, however, the dynamic range, as indicated by the slider on the bottom of the GUI, was set to 100 dB. This resulted in less apparent dif-

ferences between the lobes of the RCS curve, but also illustrated that the RCS for values of θ between 90 and 270 degrees was indeed zero and not a small value, which was not displayed because of the 60-dB dynamic range limitation.

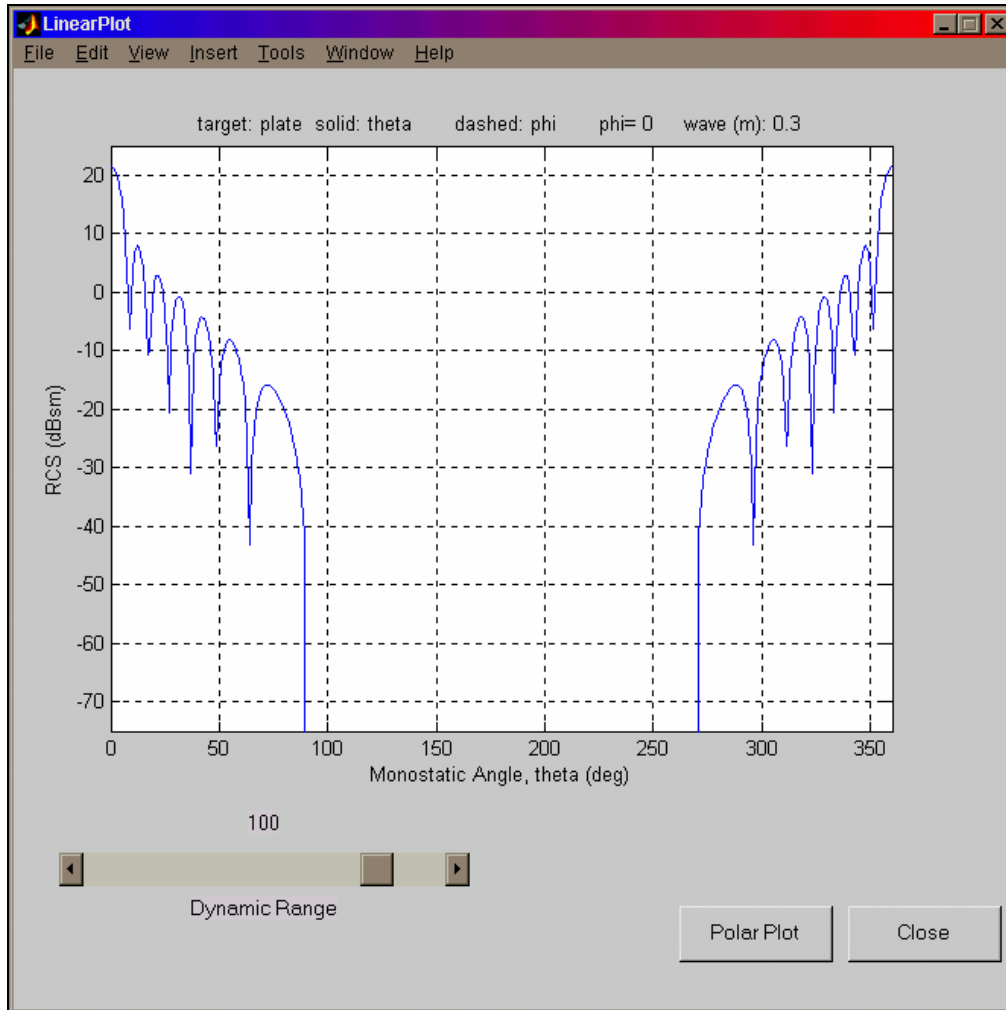


Figure 47. Dynamic Range Effects

b. Polar Plots

As previously stated, polar plots provide a more natural way to present angles, as the 0 and 360 degree points coincide, rather than being on the extreme locations of a linear graph. Indeed, when viewing Figure 47, as well as all other RCS plots presented thus far, always keep in mind that the two ends of the graph coincide.

However, this becomes immediately apparent in a polar plot, such as that depicted in Figure 48. The graph presents the same information as the RCS plot in Fig-

ures 39 and 46. Angle θ varies from 0 to 360 degrees, as indicated by the numbered sectors on the circle. Again, for θ between 90 and 270 degrees RCS is 0. The value of the RCS is read on the concentric circles in the graph.

Notice that the user can also adjust the dynamic range for a more suitable display. In addition, while both angles θ and ϕ can vary, the user can select to generate a plot by using the sliders to specify a value for ϕ (or θ) and then selecting a ϕ -cut (or a θ -cut).

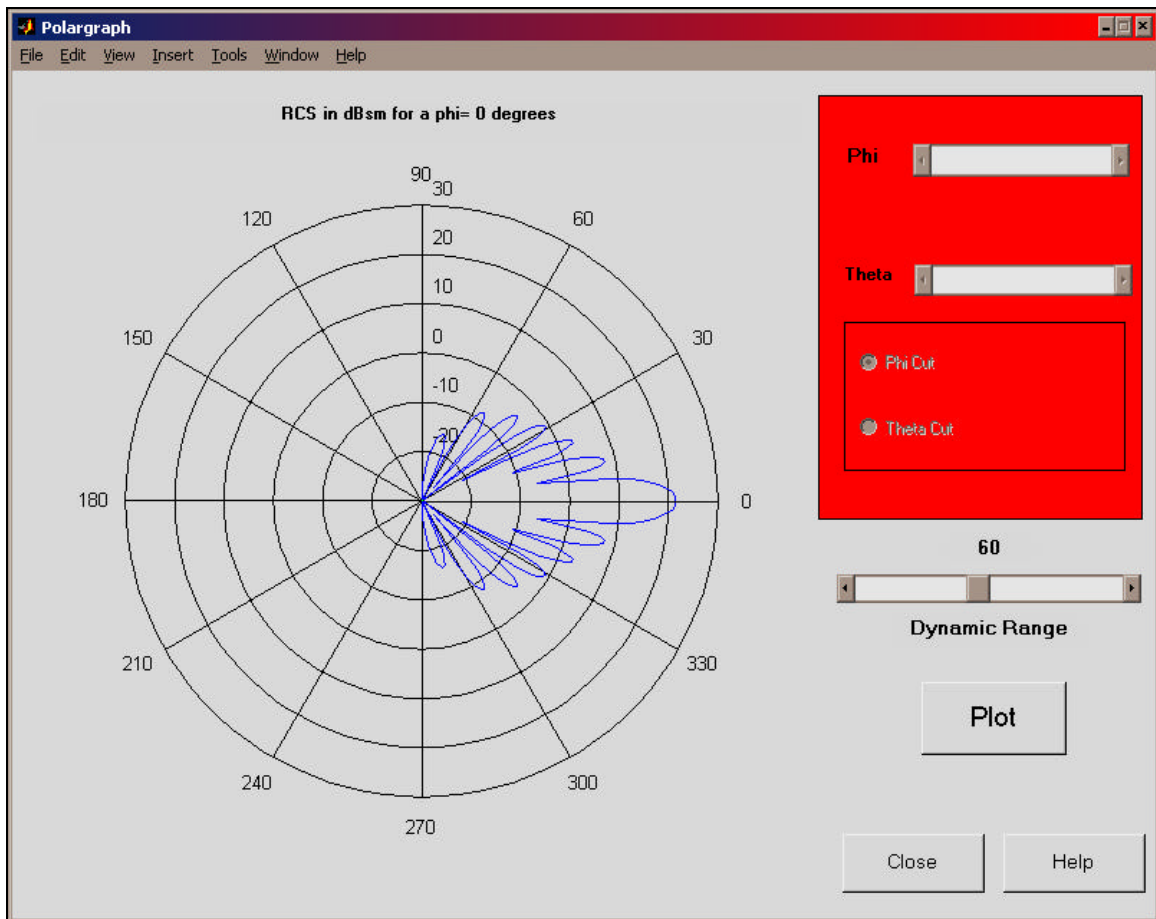


Figure 48. Polar Plot

c. Combination Plots

These plots superimpose the RCS of a model in space with the model itself. Thus, the various RCS lobes, peaks or details can be interpreted and associated with specific areas or features of the model.

It must be noted that since the resulting graph contains both the model and its RCS, the RCS values have to be normalized to take values in the order of the model's size, so that everything can be visible simultaneously. Thus, the RCS curve should not be interpreted at face value, but only used to associate specific target characteristics with specific RCS curve details. The exact RCS values should always be obtained from RCS plots such as those depicted in Figures 47 and 48.

Figure 49 depicts the combination plot for the RCS of the 1 m by 1 m PEC plate located on the xy plane for 1 GHz, TM polarized incident wave. Both the plate itself and the RCS curve, similar to that depicted in Figure 48, are visible.

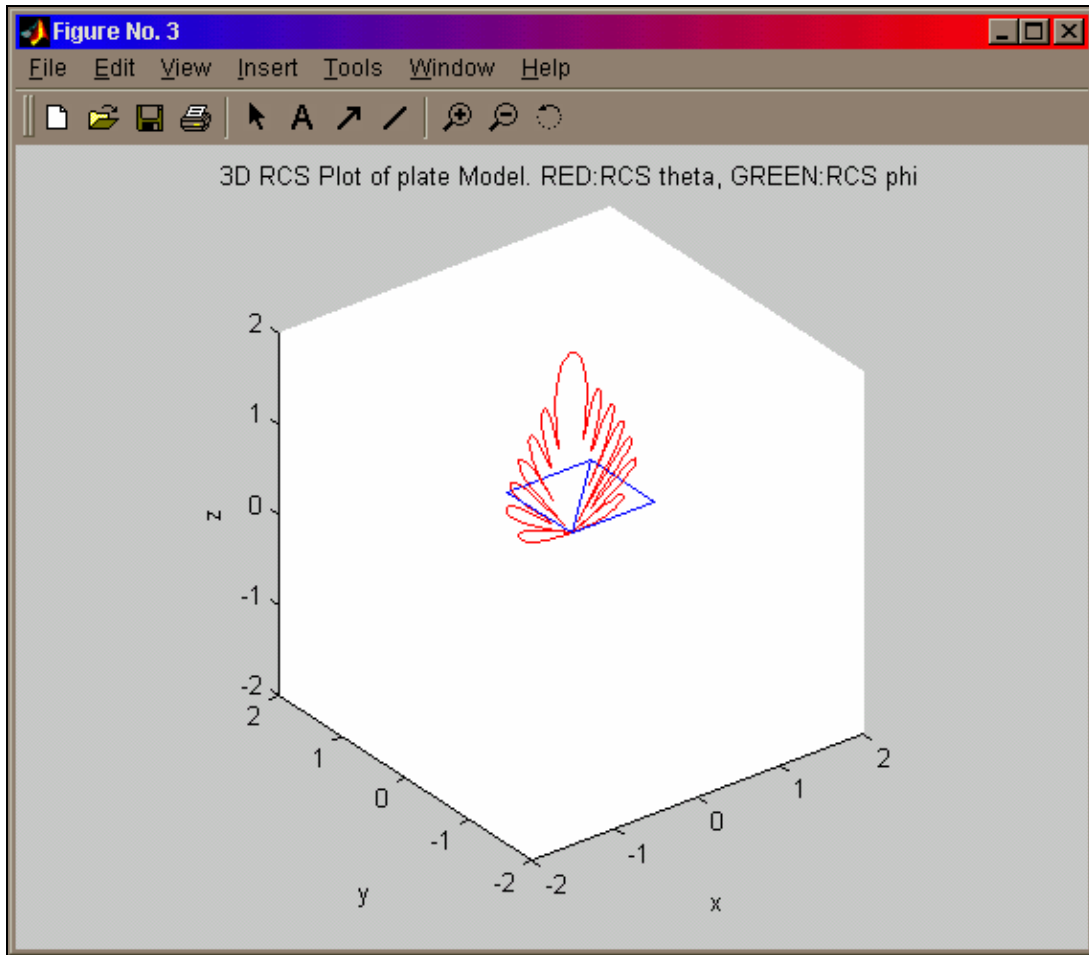


Figure 49. Combination Plot

Figure 50 depicts a combination plot for the monostatic RCS of the UAV model shown in Figure 34. Its RCS was computed for a 10 GHz, TM polarized incident

wave, with angle θ being equal to 90 degrees and angle ϕ varying from 5 to 355 degrees (i.e., the radar is located at the (x,y) plane and rotates around the z axis). The range of ϕ angles from 355 to 5 degrees was intentionally omitted, since the flat surface of the fuselage base yielded very high RCS values which, due to the normalization of the RCS curve, would make other RCS details more difficult to detect.

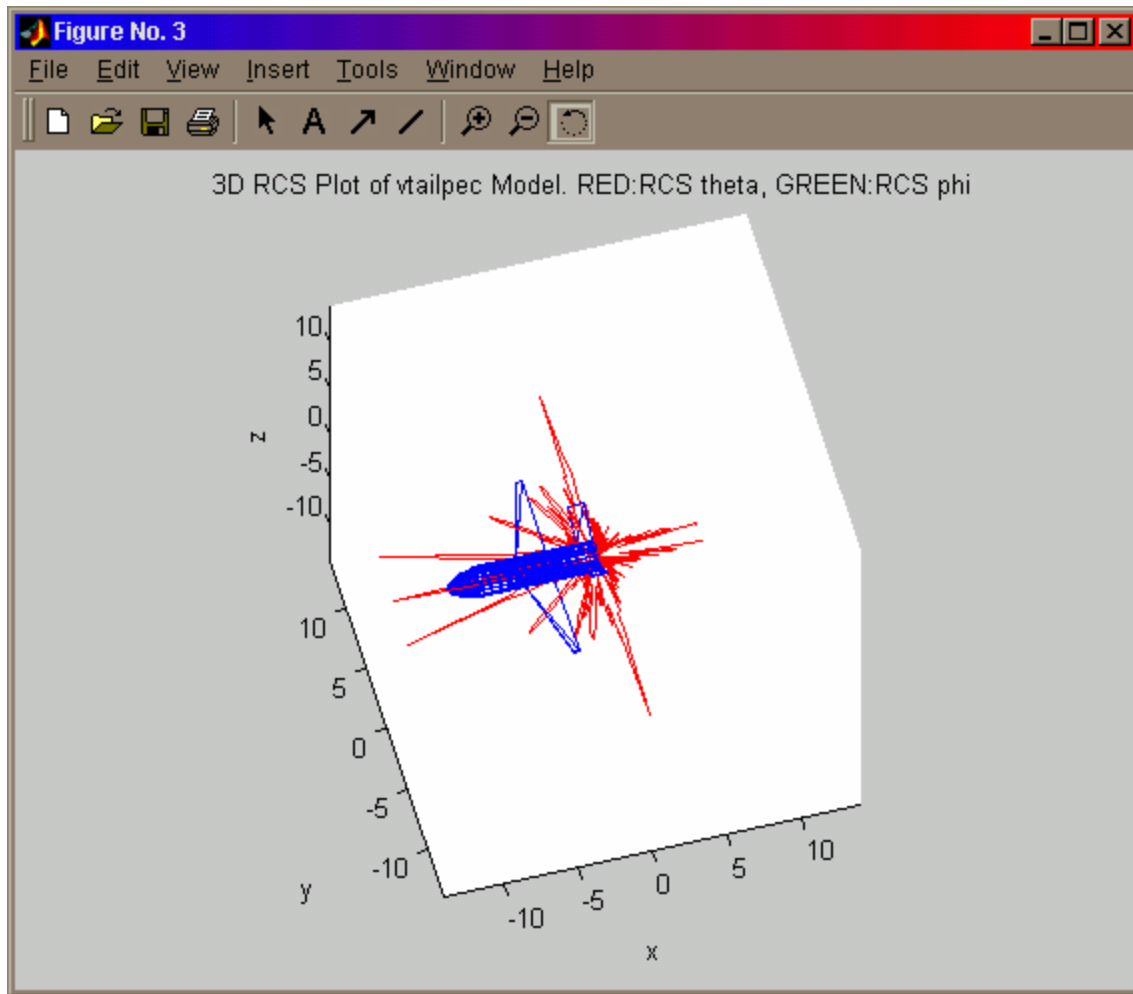


Figure 50. Combination Graph of the UAV Model

Keeping in mind that the RCS value is represented by the distance of any point on the RCS curve from the origin of the axes, which in this case coincides with the center of the fuselage base, it is easy to identify the major RCS contributors on this model. In the head-on direction, the radome and the front facets of the stabilizers create a high RCS value. The leading edges of the wings create two strong RCS spikes approxi-

mately 20 degrees around the centerline of the UAV. Two strong returns occur at broadside, at $\phi = 90$ and $\phi = 270$ degrees. These are probably due to the fuselage body itself and the wingtips. Finally, as previously mentioned, the effect of the fuselage base can be discerned in the large RCS lobe at the back of the UAV.

Although other RCS spikes appear in the graph, these have considerably lower values (more than 20 dB below the highest value), as indicated in the annotated graph in Figure 51, which depicts the absolute values of the RCS curve of Figure 50.

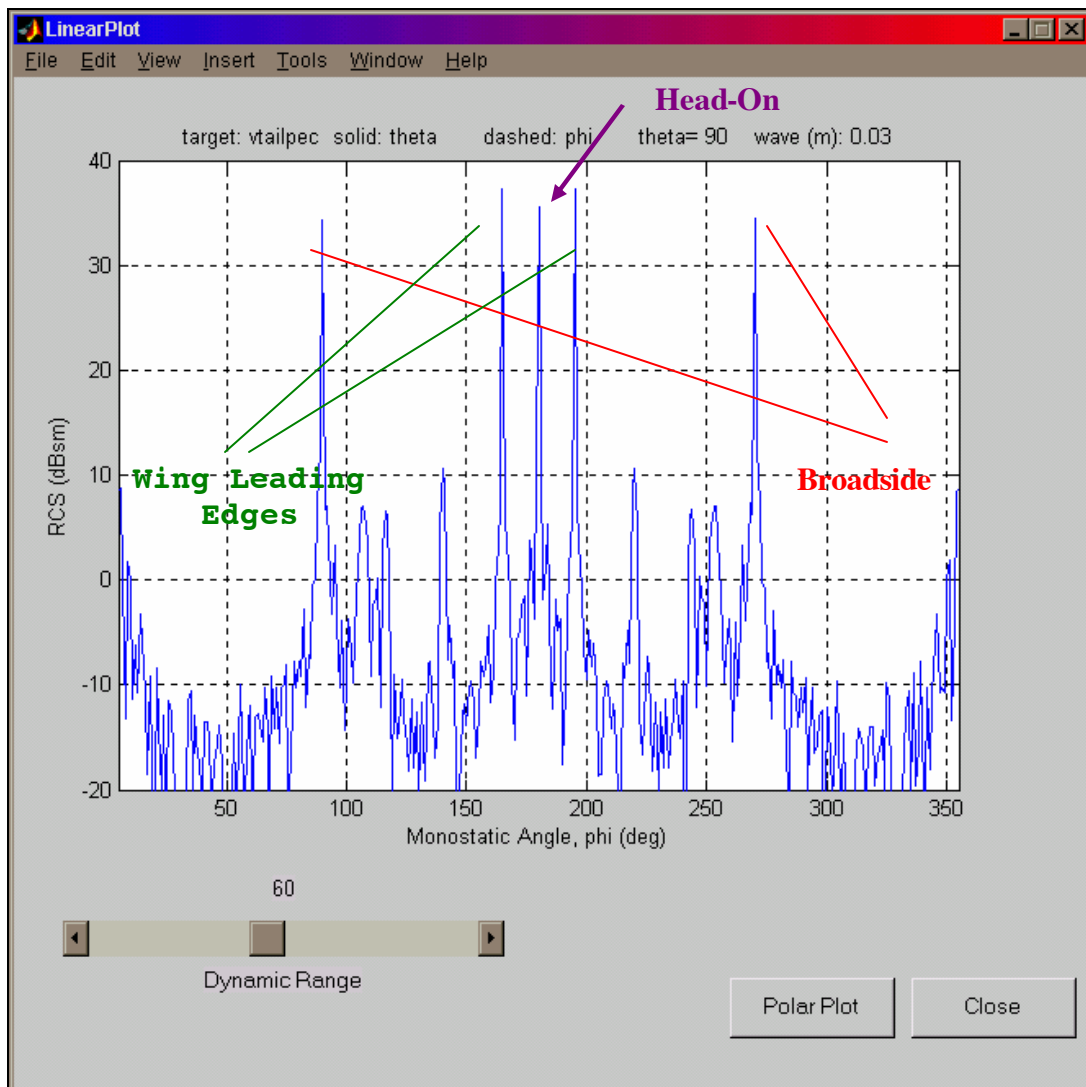


Figure 51. Annotated UAV RCS Plot

I. SUMMARY

This chapter presented the improvements and the new functionalities incorporated in the POFACETS. Specifically, the GUI and model database upgrade, the manual and graphical model design options, the model import/export capabilities, the model combination capabilities, the RCS calculation options, and the RCS display options were described. The following chapter discusses the new RCS computational capabilities of the program.

V. NEW COMPUTATIONAL CAPABILITIES ADDED TO THE POFACETS PROGRAM

This chapter describes the new RCS computation capabilities added to the POFACETS program as a result of this thesis. These include the exploitation of symmetry planes in models, the calculation of the effects of various materials and coatings, and the calculation of the effects of the ground on the RCS of the targets. For each case, a brief rationale is provided regarding the development of the specific capability, followed by the theoretical background upon which the software is based, the implemented program features, and the RCS results obtained.

A. EXPLOITATION OF SYMMETRY PLANES

1. Rationale

As previously mentioned, the main advantage of the Physical Optics method is that it requires minimum computing resources and results in convenient program run-times. However, as the number of facets in a model increases, the run-time increases proportionally. On the other hand, a larger number of facets may be desirable or even necessary to model curved surfaces more accurately, as Figures 23 and 24 have illustrated for the case of spheres.

In order to reduce the total run-time for models with a large number of facets, one obvious method is to take advantage of existing symmetries in the model. Indeed, for the monostatic case, the RCS at two observation angles, which are symmetrical relative to the model's symmetry planes, will have the same value. Thus, if the RCS is computed for one angle, the calculations do not need to be repeated for the symmetric angle, but the same RCS value can be directly assigned to the symmetric angle.

Therefore, the goal of this effort was to provide POFACETS the capability to define symmetries in target models and then exploit these symmetries in the calculation of the monostatic RCS. Symmetry planes were not implemented for the bistatic RCS case.

2. Background

The first step was to determine how to define symmetries for target. An object may have planes, lines or points of symmetry. For this thesis, it was decided to use planes

of symmetry, because they could be defined by existing program structures and the basic mathematical and software formulations for their exploitation were already available in other program sections. When more complex symmetries are present in a target, they can be described by an appropriate combination of fundamental symmetry planes.

Consider the scenario depicted in Figure 52. A wave, whose direction of propagation is represented by the thick blue arrow, is incident from global spherical coordinate angles θ and ϕ . The target has a plane of symmetry defined by points P_1 , P_2 and P_3 (whose coordinates in the global coordinate system are known) and represented by the shaded purple triangle. The local coordinates of the symmetry plane are defined so that the plane is identified with the (x'', y'') plane. Hence, the unit normal vector \hat{n} of the plane of symmetry is identified with axis z'' .

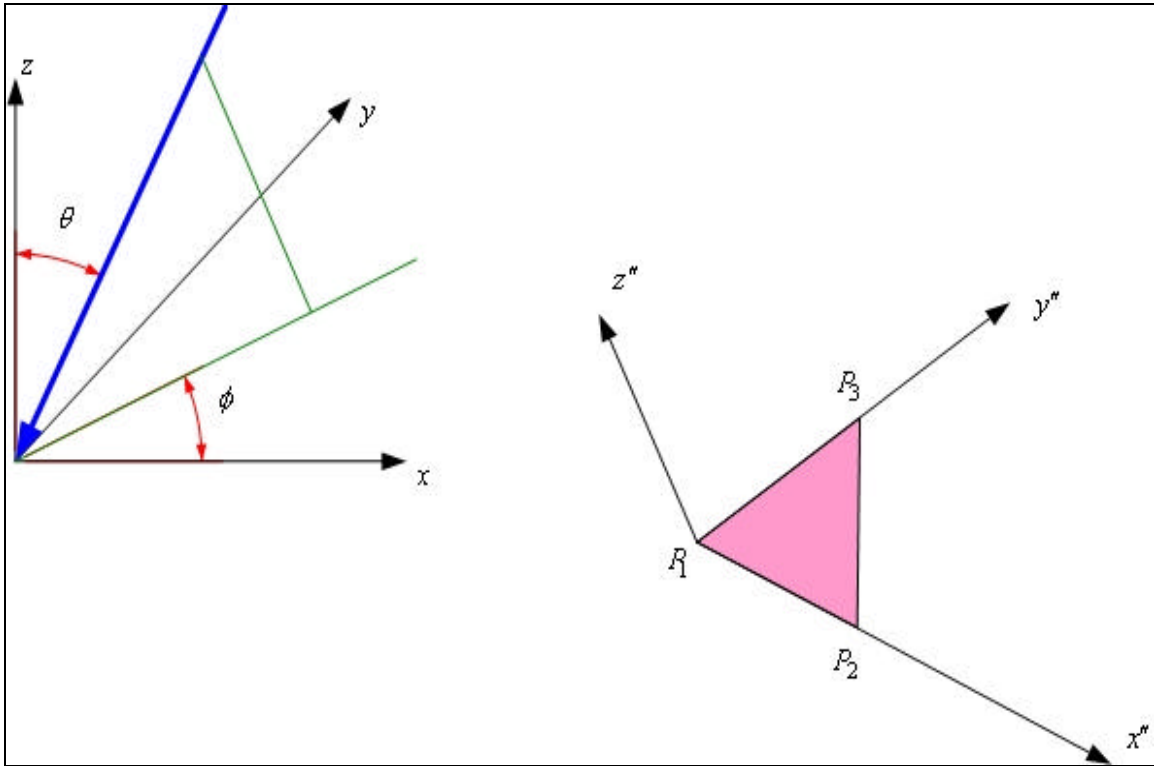


Figure 52. Symmetry Plane Scenario – Global Coordinates

Using standard transformations between Cartesian and spherical coordinates, and vice versa, along with Equation (3.20), it is possible to convert angles θ and ϕ from the global coordinates to the local symmetry plane coordinates. Let the angles of incidence at

the local symmetry plane coordinates be θ'' and ϕ'' . These angles are depicted in Figure 53. The shaded purple triangle is still used to illustrate the symmetry plane, i.e., the (x'', y'') plane better.

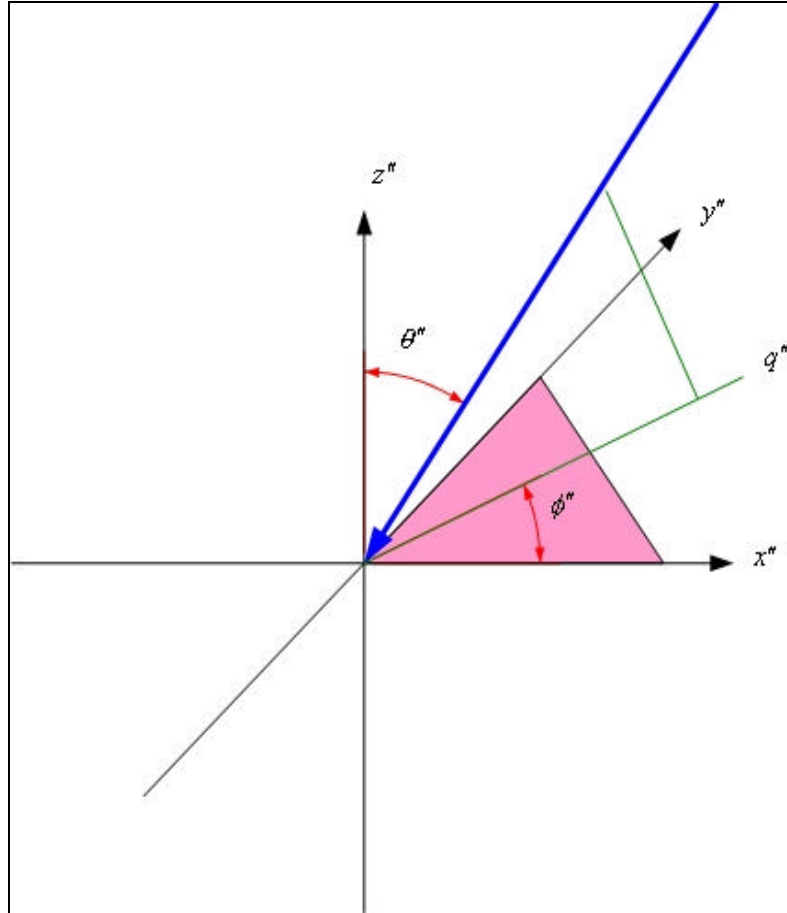


Figure 53. Symmetry Plane Scenario – Local Coordinates

Let q'' be the projection of the wave propagation vector on the $x''y''$ plane, as shown in Figure 53. In order to facilitate the discussion and simplify the graphs, the situation can now be depicted on the $z''q''$ plane. In this way, the ϕ'' angle can be omitted, and only the angle θ'' needs to be discussed.

The scenario is now presented in Figure 54. Notice that the symmetry plane is no longer visible, as this plane is now normal to the plane of the page. Two cases can be distinguished, based on the value of the θ'' angle. If θ'' is between 0 and 90 degrees (Case 1), this is considered a valid incidence angle and, therefore, normal RCS computations

can be executed. If θ'' is between 90 and 180 degrees (Case 2), this angle is symmetric to the $\pi - \theta''$ angle. Hence, if the RCS for the $\pi - \theta''$ angle has been already computed, this RCS value can be directly assigned to the θ'' direction as well.

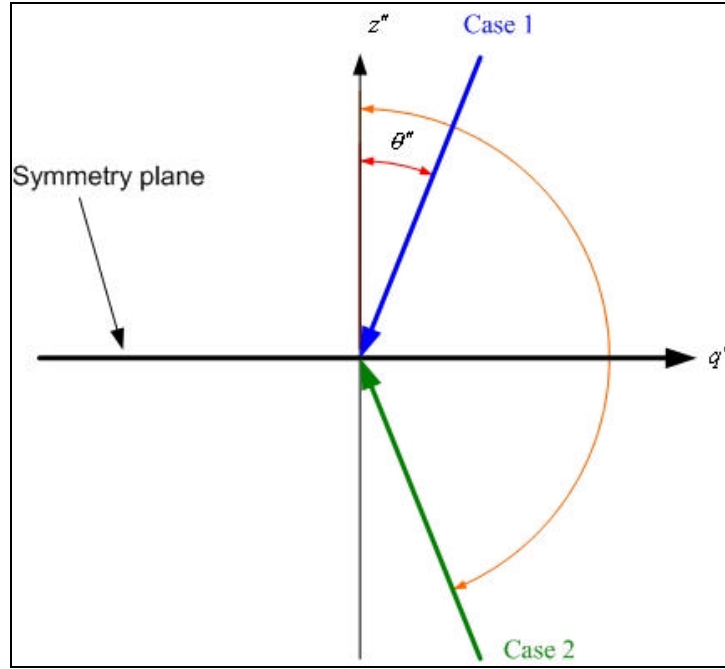


Figure 54. Cases of Incidence Angle in Local Coordinates

It is now possible to outline the process that exploits the symmetry planes of a model to expedite RCS calculations as follows:

- a. The program reads the planes of symmetry of a model, which were previously specified by the user
- b. The RCS computation algorithm starts to execute. For each combination of angles of incidence θ and ϕ , the following steps are executed.
- c. Angles θ and ϕ are converted from global coordinates to local coordinates, resulting in angles θ'' and ϕ'' .
- d. If θ'' is between 90 and 180 degrees, it is replaced by $\theta_1'' = \pi - \theta''$.
- e. Angles θ_1'' and ϕ'' are converted back to global coordinates, resulting in angles θ_c and ϕ_c .

- f. Steps c to e are repeated for all symmetry planes, with each new repetition being applied to the θ_c and ϕ_c angles that were produced by the previous repetition. After the process has been repeated for the last symmetry plane, a final pair of θ_c and ϕ_c angles has been produced from the initial θ and ϕ angles.
- g. If the RCS has already been computed for the θ_c and ϕ_c angles, that value is directly assigned to the RCS for incidence angles θ and ϕ .
- h. If the RCS has not already been computed for the θ_c and ϕ_c angles, normal RCS computations are executed.

3. Procedure

The first step for the exploitation of symmetry planes in models in the POFACTS is to allow the user to define the symmetry planes and store them with the rest of the model data (coordinates, facets, parts descriptions). Appropriate controls were added to both the Manual Model Design GUI and the Graphical Model Design GUI. Figure 55 depicts the controls on the Graphical Model Design GUI.

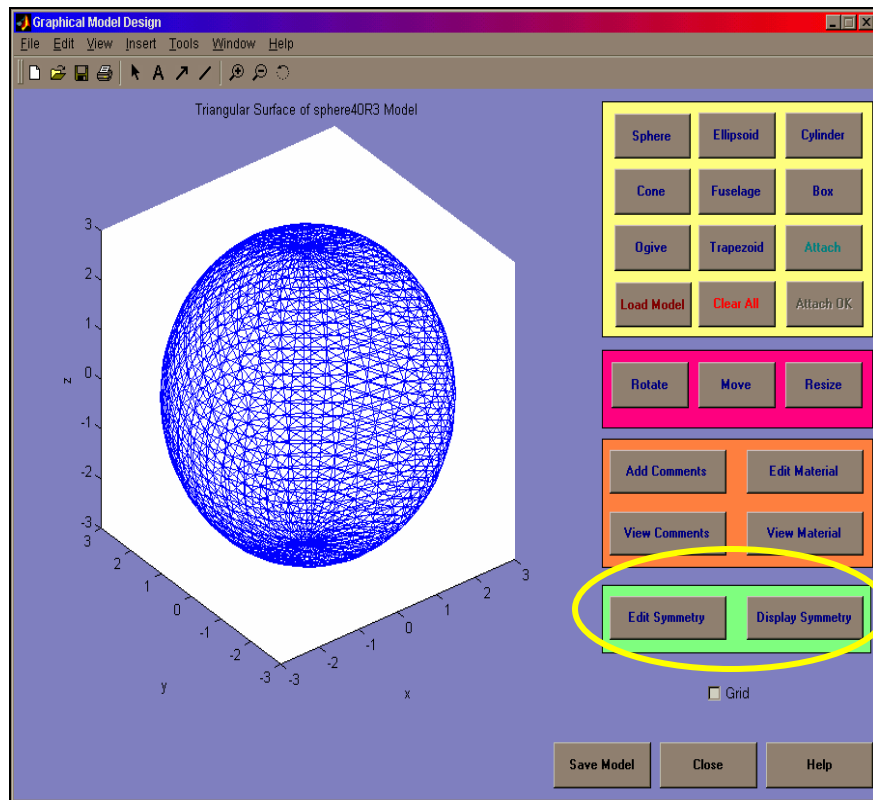


Figure 55. Symmetry Controls in the Graphical Model Design GUI (circled)

The user describes each symmetry plane using MATLAB's array editor by entering three points for each symmetry plane. Figure 56 depicts an array of points defining three symmetry planes. Each column represents the coordinates of a point in x , y , and z . Each row represents a point, and each group of three rows represents a symmetry plane. The sequence by which each plane is defined follows the right-hand rule, so that the right hand points to the outward normal of the plane. Up to three symmetry planes can be defined for each model.

	1	2	3
1	0	0	0
2	1	0	0
3	0	1	0
4	0	0	0
5	0	1	0
6	0	0	1
7	0	0	0
8	0	0	1
9	1	0	0

Figure 56. Symmetry Plane Definition

Once the symmetry planes have been defined, they are superimposed on the model display in the form of triangles of different colors. Figure 57 shows the three symmetry planes for a sphere model with a radius of 3 m and 40 points per circle.

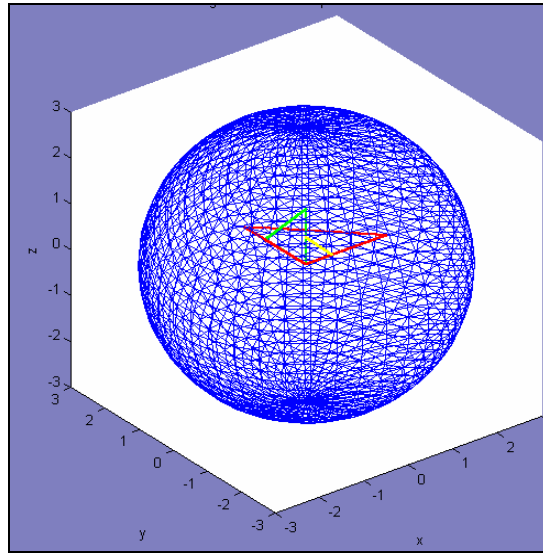


Figure 57. Symmetry Planes for a Sphere Model

When a model that contains symmetry planes is loaded for the computation of its monostatic RCS, the Use Symmetry checkbox in the Monostatic RCS Calculation GUI is enabled, as shown in Figure 58. If no symmetry planes exist, the checkbox remains disabled.

CALCULATE MONOSTATIC RCS

Calculation of Monostatic RCS for the sphere40R3 model

Load File

☐ Ground Plane XY?

☒ PEC

Rel. Permittivity

☒ Use Symmetry?

Surface Roughness

Correlation Dist.(m):

Standard Dev. (m):

Computational Parameters

Taylor Series

Length of Region:

Number of Terms:

Incident Polarization:

Frequency: GHz

☐ Show 3D Display ☐ Show Polar Graph

Calculate RCS Print Close Help

Theta Phi

Starting Angle deg deg

Ending Angle deg deg

Increment Angle deg deg

Figure 58. Symmetry Selection for Monostatic RCS Calculations (circled)

The user can select to use the symmetry of the model by selecting the checkbox. Generally, the use of symmetry has significant effects on the program execution time when a model consists of a large number of facets (hundreds of facets or more).

4. Results

The sphere model with a radius of 3 m and 40 points per circle, for a total of 3120 facets, which is shown in Figure 56, was used as a test-case for the comparison of program execution times with and without the exploitation of symmetry planes. The RCS was computed for 18 GHz, TM polarized wave, with θ held constant at 90 degrees and ϕ varying between 0 and 360 degrees in increments of 4.5 degrees. This value was se-

lected as half of the extent of a facet, which is $\frac{360 \text{ degrees}}{40 \text{ facets}} = 9 \text{ degrees/facet}$.

Both executions, with and without exploitation of the symmetry planes, gave the same RCS results, shown in Figure 59. The fluctuations between the two values are expected, since even and odd multiples of the 4.5 degrees increment step result in slightly different configuration of facets being illuminated by the incident wave.

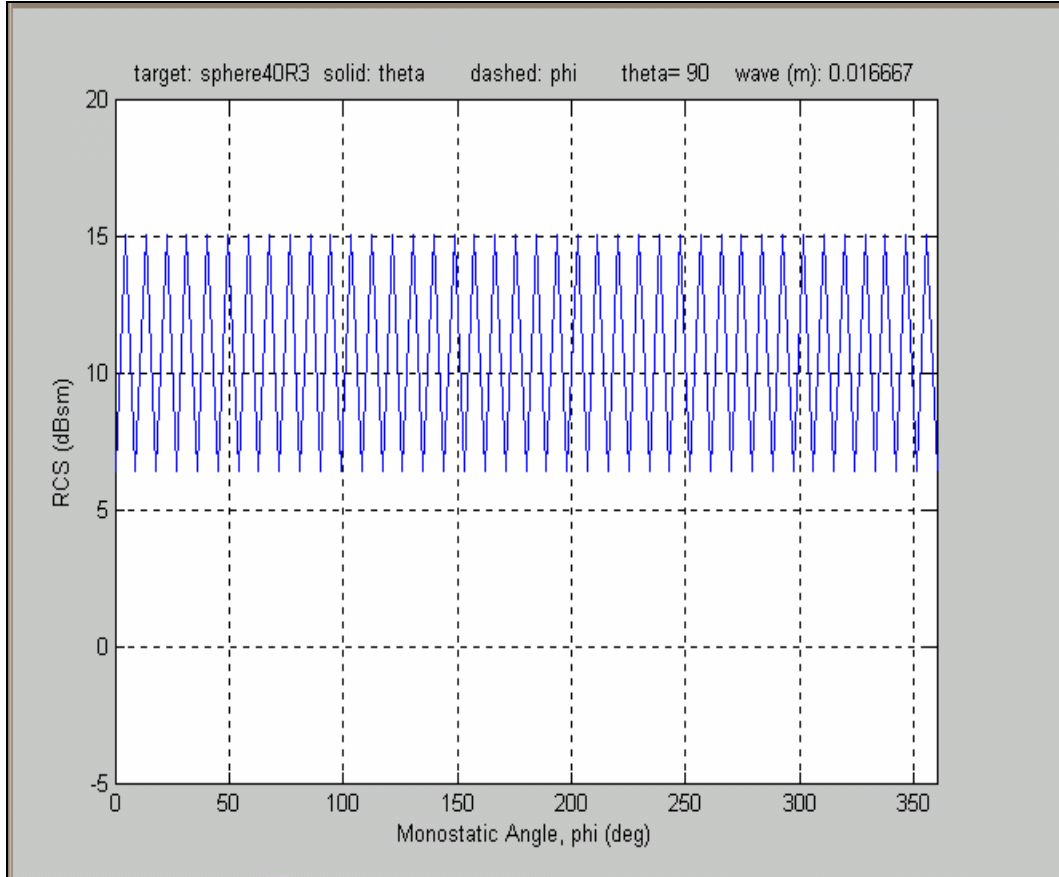


Figure 59. Monostatic RCS of a Sphere with Radius of 3 m at 18 GHz

When the program was run without exploitation of symmetry planes, it was completed in 130 seconds. When using the symmetry planes, the RCS computations were executed in 35 seconds, resulting in a decrease of 73% in run-time.

B. EFFECTS OF MATERIALS AND COATINGS ON RCS

1. Rationale

The POFACETS 2.3 version allowed the user to use different materials on the facets of a model by specifying the value of the surface resistivity R_s for each facet. This

meant that, since the known parameters for any material are its constitutive parameters (i.e., its relative electric permittivity and its relative magnetic permeability), the user would have to use these parameters to calculate the surface resistivity in order to enter it in the program. These calculations would have to be performed each time a new material was used in a model. Moreover, it would be very difficult to implement more complex configurations of facet materials, such as multiple layers and coatings on PEC.

Therefore, it was decided to add the necessary features to POFACETS to allow the user to directly select materials for the facets of the model (utilizing the material description) and provide different options regarding the application of these materials to the model. These options include single composite material, composite material layer on PEC, multiple composite layers and multiple composite layers on PEC. These are sufficient to account for most of the usual cases of materials on “real-world” targets.

For the convenience of the user, a database of materials has been created that includes the description of common materials and their constitutive parameters. The user can also update the database to include new types of material.

2. Background

As previously mentioned, the program allows four different types of material configurations for a facet: (1) single composite material, (2) composite material layer on PEC, (3) multiple composite layers, and (4) multiple composite layers on PEC. The theoretical framework for each of these cases is discussed below. The discussion begins from the multiple composite layers case and the composite layer on PEC case. The formulas for the other two cases are derived as special cases of the formulas of the first two cases. For each case, the goal is to compute the reflection coefficients for parallel and perpendicular polarization, so that they can be directly used in Equations (3.30) and (3.31).

Notice that the electric permittivity is

$$\epsilon = \epsilon_0 \epsilon_r = \epsilon_0 (\epsilon'_r - j\epsilon''_r) = \epsilon_0 (\epsilon'_r - j\epsilon'_r \tan \delta) \quad (5.1)$$

where ϵ_0 is the electric permittivity of free space, ϵ'_r the real part of the relative electric permittivity of the material and $\tan \delta$ the electric loss tangent of the material. Similarly, the magnetic permeability of the material is

$$\mu = \mu_0 \mu_r = \mu_0 (\mu'_r - j\mu''_r) \quad (5.2)$$

where μ_0 is the magnetic permeability of free space, μ'_r the real part of the relative magnetic permeability of the material and μ''_r the imaginary part of the relative magnetic permeability of the material.

a. Case 1: Multiple Composite Layers

Consider the configuration shown in Figure 60. A wave represented by c_1 , traveling to the positive z direction, is incident on a body comprised of N different layers. The material in front of layer 1 is free space. The constitutive parameters of layer n are ϵ_n (electric permittivity) and μ_n (magnetic permeability). The thickness of each layer is t_n . Symbols c and b represent the waves incident and reflected at each boundary, respectively. The reflection coefficient between region 0 (i.e., free space) and region 1 is Γ_1 , while the reflection coefficient between region $n-1$ and region n is Γ_n . Similarly, the transmission coefficient between region 0 (i.e., free space) and region 1 is τ_1 , while the transmission coefficient between region $n-1$ and region n is τ_n .

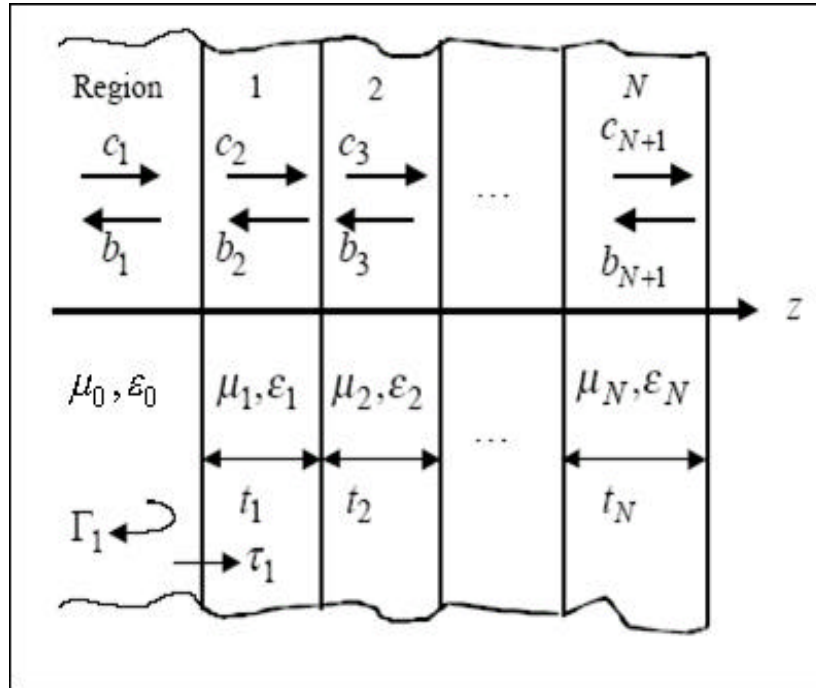


Figure 60. Wave Incident on Multiple Layers (After Ref. 8.)

Using the formulations of Ref. 8, it is thus possible to write the incident and reflected waves at the first boundary as

$$\begin{bmatrix} c_1 \\ b_1 \end{bmatrix} = \prod_{n=1}^N \frac{1}{\tau_n} \begin{bmatrix} e^{j\Phi_n} & \Gamma_n e^{-j\Phi_n} \\ \Gamma_n e^{j\Phi_n} & e^{-j\Phi_n} \end{bmatrix} \begin{bmatrix} c_{N+1} \\ b_{N+1} \end{bmatrix} \equiv \begin{bmatrix} A_{11} & A_{12} \\ A_{21} & A_{22} \end{bmatrix} \begin{bmatrix} c_{N+1} \\ b_{N+1} \end{bmatrix} \quad (5.3)$$

where

$$\Phi_n = \beta_n t_n = \frac{2\pi}{\lambda_n} t_n \quad (5.4)$$

with λ_n being the wavelength in the layer n . Now, the overall reflection coefficient is

$$\Gamma = \frac{b_1}{c_1} = \frac{A_{21}}{A_{11}}. \quad (5.5)$$

When the last layer extends to infinity, as is the case with multiple layers of materials with free space on both sides, then $b_{N+1} = 0$ and we can arbitrarily use $\Phi_N = 0$ (Ref. 8).

Notice that formulas (5.3) and (5.5) must be used twice: once for the perpendicular polarization case (Γ_{\perp}) and once for the parallel polarization case (Γ_{\parallel}). The following formulas give the reflection coefficients at boundary n (boundary between layer $n-1$ and layer n) (Ref. 8):

$$\Gamma_{\perp} = \frac{\eta_n \cos \theta_i - \eta_{n-1} \cos \theta_t}{\eta_n \cos \theta_i + \eta_{n-1} \cos \theta_t} \quad (5.6)$$

$$\Gamma_{\parallel} = \frac{\eta_n \cos \theta_t - \eta_{n-1} \cos \theta_i}{\eta_n \cos \theta_t + \eta_{n-1} \cos \theta_i} \quad (5.7)$$

where

$$\eta_n = \sqrt{\frac{\mu_n}{\epsilon_n}} \quad (5.8)$$

and

$$\sqrt{\mu_{n-1} \epsilon_{n-1}} \sin \theta_i = \sqrt{\mu_n \epsilon_n} \sin \theta_t. \quad (5.9)$$

Figure 61 shows the angles θ_i and θ_t .

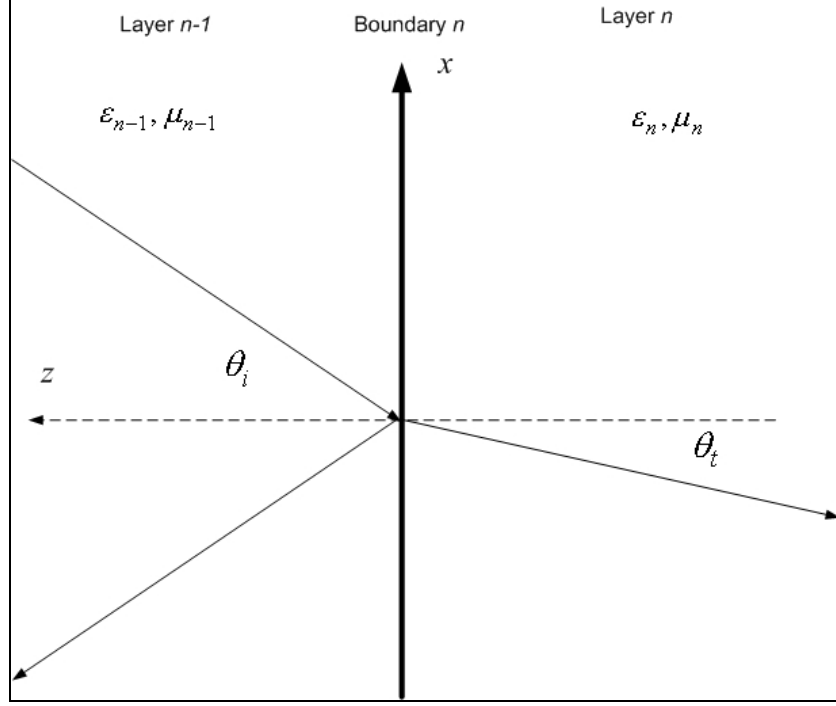


Figure 61. Incidence and Transmission Angles at the Boundary Between Two Layers

b. Case 2: Composite Layer on PEC

Figure 62 depicts a composite layer of thickness t on a Perfect Electric Conductor. The following formula gives the reflection coefficient for both the perpendicular and the parallel polarization (Ref. 2):

$$\Gamma = \frac{Z_{in} - 377}{Z_{in} + 377} \quad (5.10)$$

where

$$Z_{in} = \sqrt{\frac{\mu}{\epsilon}} \tanh(\gamma t) \quad (5.11)$$

with $\gamma = j\omega\sqrt{\mu\epsilon}$, $\omega = 2\pi f$, and f the frequency of the wave in Hertz. In Equation (5.10) the value of 377 is the impedance of free space in Ohms. Although Equations (5.10) and (5.11) are valid for normal incidence, they are used in the program as an approximation for all angles of incidence.

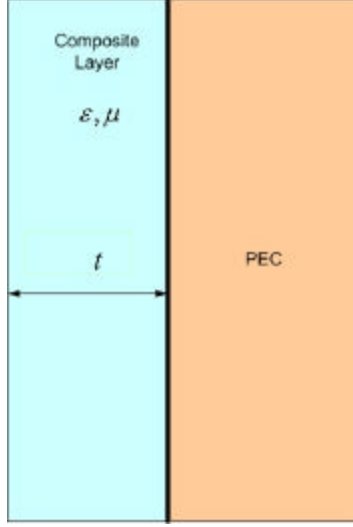


Figure 62. Composite Layer on PEC

c. Case 3: Composite Layer

A single layer of composite material can be considered as a special case of the Multiple Layers case with $N = 2$ (the second layer being the free space at the back-side of the material). Thus, Equations (5.3) and (5.5) can be applied to compute the reflection coefficients for perpendicular and parallel polarizations.

d. Case 4: Multiple Layers on PEC

This case can be considered as a combination of Cases 1 and 2. Assuming there are N layers of composite material on PEC, Equations (5.3) and (5.5) are used to compute the overall reflection coefficient of the $N - 1$ first layers. Let this coefficient be Γ' . Since this reflection coefficient refers to the boundary between free space and the $N - 1$ first layers space, an equivalent impedance (Z') of the $N - 1$ first layers can be computed. Specifically:

$$\Gamma' = \frac{Z' - Z_o}{Z' + Z_o} = \frac{Z' - 377}{Z' + 377} \Rightarrow \Gamma' Z' + \Gamma' 377 = Z' - 377 \Rightarrow Z' = 377 \frac{1 + \Gamma'}{1 - \Gamma'} \quad (5.12)$$

where Z_o is the impedance of free space, 377 ohms.

The input impedance Z_{in} of the combination of the last layer and the PEC is given by Equation (5.11). The reflection coefficient on the boundary between the combination of the $N - 1$ first layers and the combination of the last layer and the PEC is

$$\Gamma_N = \frac{Z_{in} - Z'}{Z_{in} + Z'}. \quad (5.13)$$

Now Γ_N can be used in Equation (5.3) to calculate the overall reflection coefficient. Of course, this process is executed once for the perpendicular polarization case and once for the parallel polarization case.

3. Procedure

The materials database can be accessed through the Utilities GUI. Figure 63 depicts the Materials Database Management GUI.

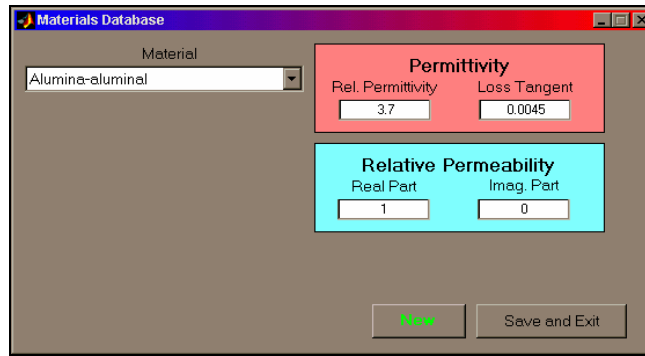


Figure 63. Materials Database Management GUI

The user can select a material by its description in the list box in Figure 63 and then view and edit its constitutive parameters, which are comprised of the relative electric permittivity, the loss tangent, and the real and imaginary part of the magnetic permeability. The user can also add new materials to the database through the GUI depicted in Figure 64.

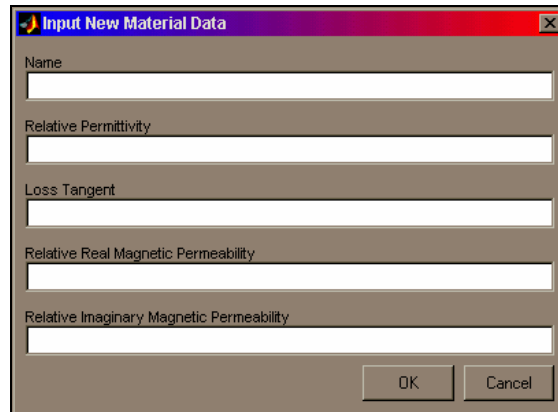


Figure 64. New Material Data Input GUI

The POFACETS 3.0 materials database is already provided with a library of more than 20 composite materials that are often used in military applications. The user can apply these materials to the facets of a model by using the Material Application GUI shown in Figure 65. This GUI can be called from either the Manual Model Design GUI or the Graphical Model Design GUI.

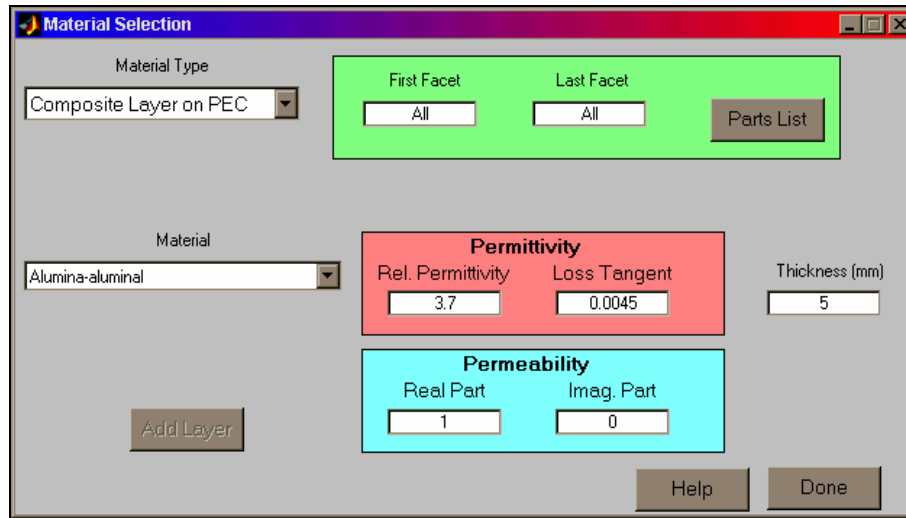


Figure 65. Material Application GUI

The user selects the type of material configuration that will be applied to the facets, choosing Composite, Composite Layer on PEC, Multiple Layers, or Multiple Layers on PEC from the Material Type listbox. Next, the specific Material is selected from the Material listbox. For each material selected, its constitutive parameters are displayed, so that the user can decide whether a certain material is desirable. The thickness of the layer is also specified in millimeters. The user can also select whether to apply a certain material type to all or some of the facets of a model, by specifying the first and the last facet number for which this material type is to be applied. At this point, the user may need to view the descriptions of the major parts to which the facets belong in order to identify the correct facet numbers to which the material will be applied.

When a material or layers of materials have already been applied to a model, the user can use the Graphical Model Design GUI to view both the application of the material and the materials' constitutive parameters. Figure 66 depicts the Material View GUI

that is used to present these data. In this example, the first facet of the model has two layers of materials, whose constitutive parameters and thicknesses are displayed.

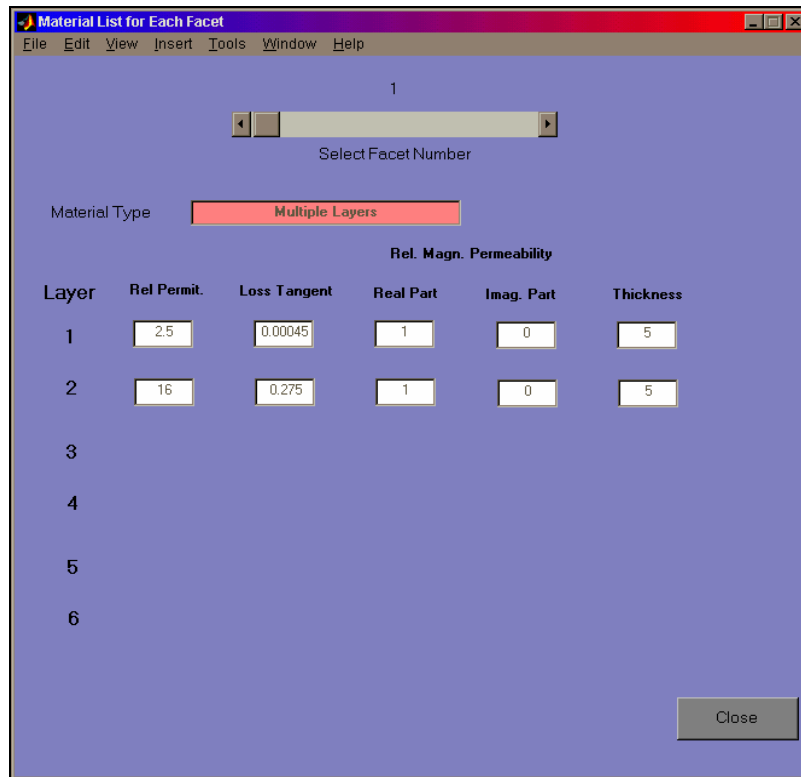


Figure 66. Material View GUI

Once the user has applied the selected material or layers of materials to the model, their effects on its RCS can be evaluated by using the RCS calculation GUIs described in Chapter IV. The effects of materials on RCS can be computed for monostatic and bistatic RCS versus angle or versus frequency. Figure 67 depicts the dialog box that prompts the user to select the type of material to be used during RCS calculations.

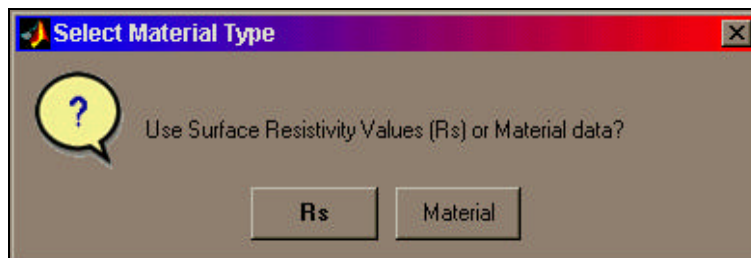


Figure 67. Material Type Selection Dialog Box

The user can either select the surface resistivity values stored in the facet definition array and ignore the data stored in the material array, or select the data in the material array and ignore the surface resistivity values.

4. Results

In order to compare the effects of different materials and material applications on a model, the monostatic RCS versus frequency of a 1 m by 1 m PEC plate, located on the (x,y) plane for a TM polarized incident wave from the direction $\theta = 0$ and $\phi = 0$ degrees (i.e., normal to the plate) was computed, as shown in Figure 68. As previously explained in Equation (4.1), the RCS increases with the square of the frequency.

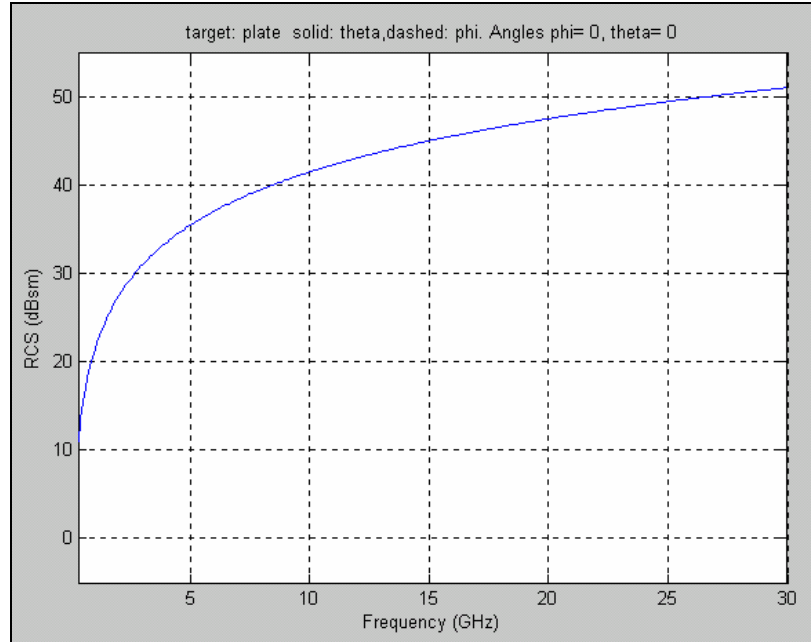


Figure 68. RCS vs. Frequency of a 1 m by 1 m PEC Plate (normal incidence)

Various materials were applied to the plate and the resulting RCS was computed versus frequency for the same angle of incidence and polarization. First, a single composite material with $\epsilon'_r = 16$, $\tan\delta = 0.275$, $\mu'_r = 1$, $\mu''_r = 0$ and 5 mm thickness was applied to all the facets of the plate.

Figure 69 shows the effects on its RCS.

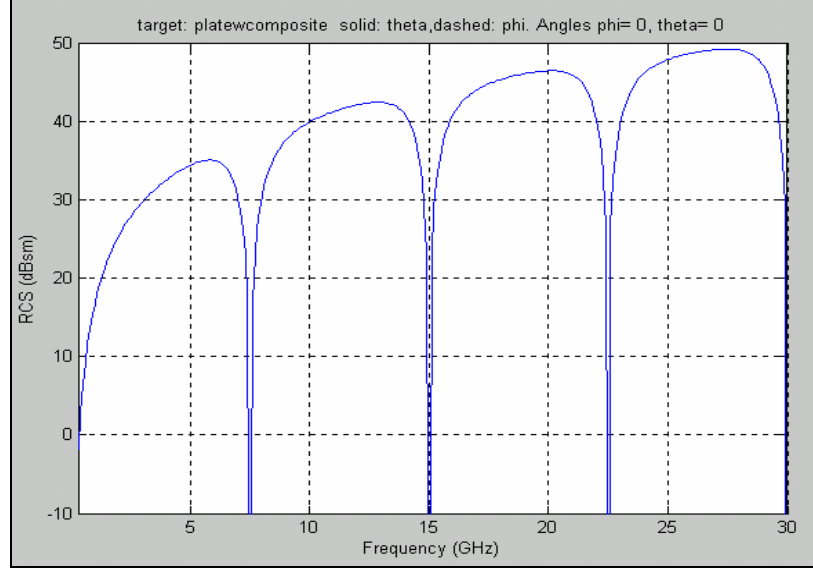


Figure 69. RCS vs. Frequency of a 1 m by 1 m Plate with One Composite Layer (normal incidence)

Notice that nulls have appeared in multiples of 7.5 GHz. The wavelength at this

frequency is $\lambda = \frac{3 \times 10^8}{7.5 \times 10^9 \sqrt{\epsilon_r'}} = 0.01 \text{ m} = 10 \text{ mm}$, which is equal to the round trip of the

wave in the material, indicating that the wave components at the air/material interface cancel out, yielding reflection coefficients equal to zero and, hence, low RCS values at this frequency and its harmonics.

Next, two layers of composite materials were applied to all facets of the model.

Both layers were 5 mm thick. The material parameters for the first layer were

$\epsilon_r' = 2.5$, $\tan \delta = 0.00045$, $\mu_r' = 1$ and $\mu_r'' = 0$. The material parameters of the second layer were. $\epsilon_r' = 16$, $\tan \delta = 0.275$, $\mu_r' = 1$ and $\mu_r'' = 0$.

Figure 70 depicts the RCS of the plate versus frequency. Since the material of the second layer is exactly the same as that resulting in the RCS plot of Figure 69, some similarities appear in the plots of Figures 69 and 70. However, in the two-layer case, the first layer has affected the overall reflection coefficients. Thus, the nulls at 7.5 GHz and its harmonics have been replaced by a reduction in RCS which varies from a few dBsm at

approximately 7.5 GHz to almost 20 dBsm at approximately 15 GHz. Also, notice that, due to the added layer, the locations of these low RCS values have been slightly shifted from their original frequencies.

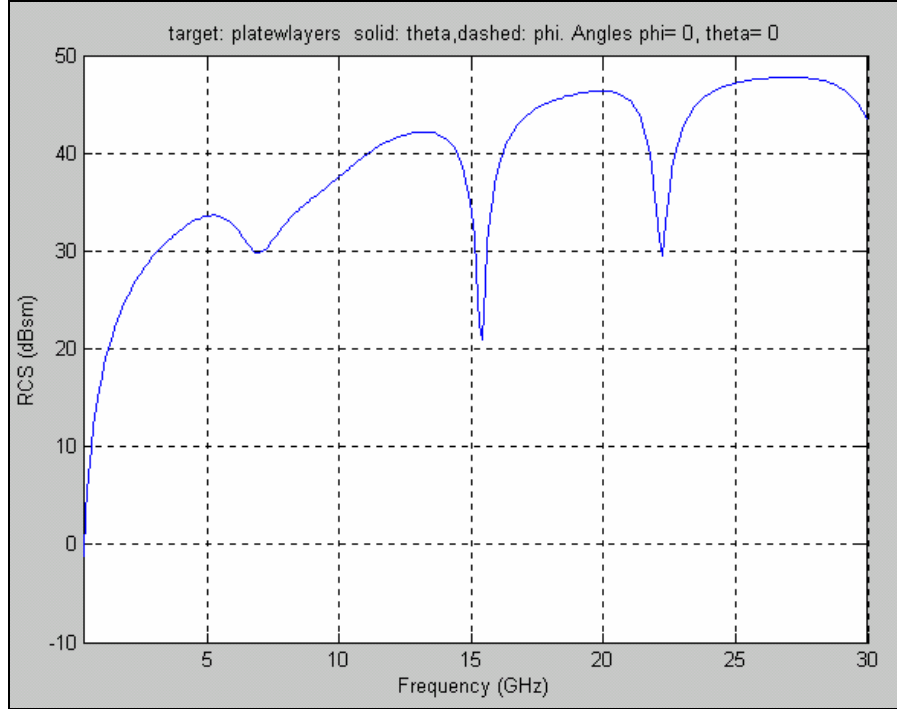


Figure 70. RCS vs. Frequency of a 1 m by 1 m Plate with Two Composite Layers (normal incidence)

Next, a single layer of composite material on PEC was applied to all facets of the model. The material parameters were $\epsilon'_r = 16$, $\tan \delta = 0.275$, $\mu'_r = 1$ and $\mu''_r = 0$, while its thickness was 6.25 mm.

Figure 70 depicts the RCS of the plate versus frequency. At approximately 3 GHz, a reduction in RCS of almost 20 dB occurs. At this frequency, the wavelength

$$\text{is } \lambda = \frac{3 \times 10^8}{3 \times 10^9 \sqrt{\epsilon'_r}} = 0.025 \text{ m} = 25 \text{ mm} . \text{ The thickness of the material is equal to } \lambda/4 ,$$

which makes it a Dallenbach layer at this frequency. The behavior of a Dallenbach layer (Ref. 2) versus frequency closely follows the pattern depicted in Figure 71.

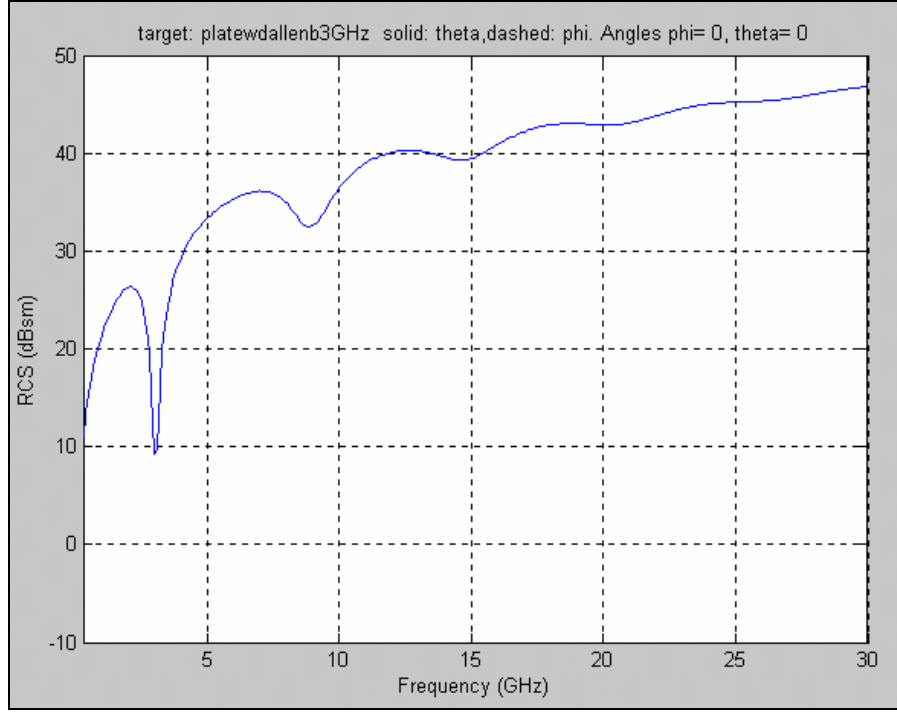


Figure 71. RCS vs. Frequency of a 1 m by 1 m Plate with One Composite Layer on PEC (normal incidence)

Finally, two layers of composite materials on PEC were applied to all the facets of the model. The first layer was 5 mm thick and its material constitutive parameters were $\epsilon'_r = 2.5$, $\tan \delta = 0.00045$, $\mu'_r = 1$ and $\mu''_r = 0$. The second layer was 6.25 mm thick and its parameters were $\epsilon'_r = 16$, $\tan \delta = 0.275$, $\mu'_r = 1$ and $\mu''_r = 0$.

Figure 72 depicts the RCS of the plate versus frequency. The existence of two layers significantly affects the RCS of the plate. The reduction in RCS at 3 GHz is now approximately 15 dB. However, there is a reduction of approximately 25 dB in the RCS at 9 GHz. The reduction of RCS at this frequency was approximately 5 dB for the single layer on PEC case.

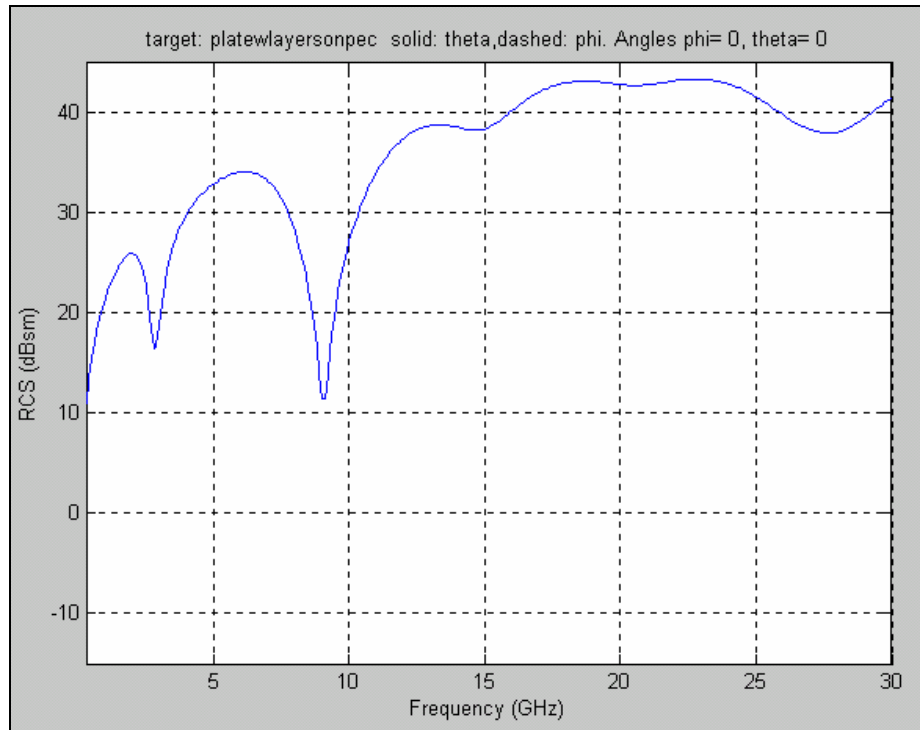


Figure 72. RCS vs. Frequency of a 1 m by 1 m Plate with Two Composite Layers on PEC (normal incidence)

C. EFFECTS OF GROUND

1. Rationale

Up to this point, the RCS of the targets was calculated with the assumption that the target was located in free space and away from the ground. This is true only in those cases where the target is an airborne vehicle flying very high above the ground or an airborne vehicle flying near the ground and the radar antennas have high directivity. However, when airborne targets fly low, as in the case for helicopters and aircraft performing terrain following, and the radar antennas do not have high directivity, the effects of the ground must be taken into consideration. In addition, when the targets are located on the ground (e.g., ground vehicles, buildings, etc.), or in the case of naval targets, the effects of the ground or the sea respectively should always be taken into account.

Given that the ground can take many different forms (e.g., woods, deserts, mountains, planes, etc.), it was decided not to model it in a unique way, but rather allow the user to select certain characteristics relating to its reflection coefficients. The same rationale holds true for the sea, since different sea states can demonstrate different scatter-

ing behaviors. Thus, the ground or sea beneath the target is modeled as a material whose relative electric permittivity can be adjusted by the user. In addition, in order to simplify the necessary calculations, the assumption is that the ground or sea always lies on the xy plane.

2. Background

Consider the situation depicted in Figure 73. A target, represented by the shaded cyan shape, is located at height h above an infinite ground plane. The radar transmitter and receiver can be anywhere above the ground plane. If no restriction is imposed on angle ϕ , then angle θ can vary from 0 to 90 degrees for the monostatic case. For the bistatic case, when this limitation is imposed on the RCS observation angle, the incidence angle will have no limitations on angle ϕ and angle θ can vary from -90 to $+90$ degrees. The following discussion uses the monostatic case example, but is also applicable to the bistatic case.

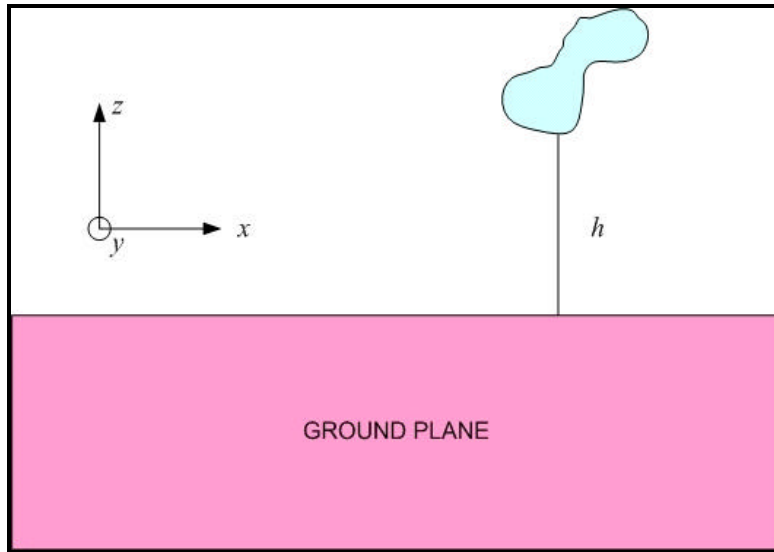


Figure 73. Target Over Infinite Ground Plane

The presence of the ground plane below the target will affect both the incident and the scattered radiation. The following equations give the ground reflection coefficients for the perpendicular and the parallel polarizations (Ref. 8):

$$\Gamma_{\perp} = \frac{\eta \cos \theta_i - 377 \cos \theta_t}{\eta \cos \theta_i + 377 \cos \theta_t} \quad (5.14)$$

$$\Gamma_{\parallel} = \frac{\eta \cos\theta_t - 377\cos\theta_i}{\eta \cos\theta_t + 377\cos\theta_i} \quad (5.15)$$

where $\eta = \sqrt{\mu/\epsilon}$ and angles θ_i and θ_t were defined in Figure 61.

Thus, the target is illuminated both by radiation coming directly from the radar transmitter and by radiation reaching the target after it is reflected on the ground. Similarly, the radar receiver antenna is illuminated both by radiation coming directly from the target and by radiation reaching the receiver location after it is reflected on the ground.

Therefore, four different cases can be distinguished. In the first case, both the incident and the scattered radiation are not reflected on the ground. This is depicted in Figure 74. Obviously, both the angle of incidence and the angle of RCS observation are equal to θ . This case is identical to the monostatic RCS computation case discussed in Chapter III.

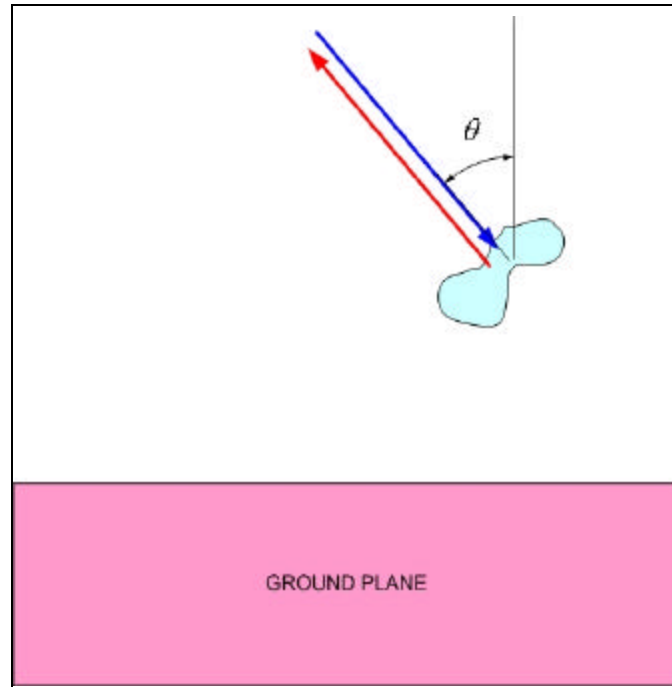


Figure 74. Direct Incident – Direct Scattered

In the second case, only the scattered radiation is reflected on the ground, with the incident radiation coming directly from the radar transmitter with no ground reflection, as depicted in Figure 75. In this case, the angle of incidence is equal to θ , but the scattered

radiation must be calculated in the $\pi - \theta$ direction, as illustrated in Figure 75. Additionally, the scattered radiation must be multiplied by the appropriate ground reflection coefficients.

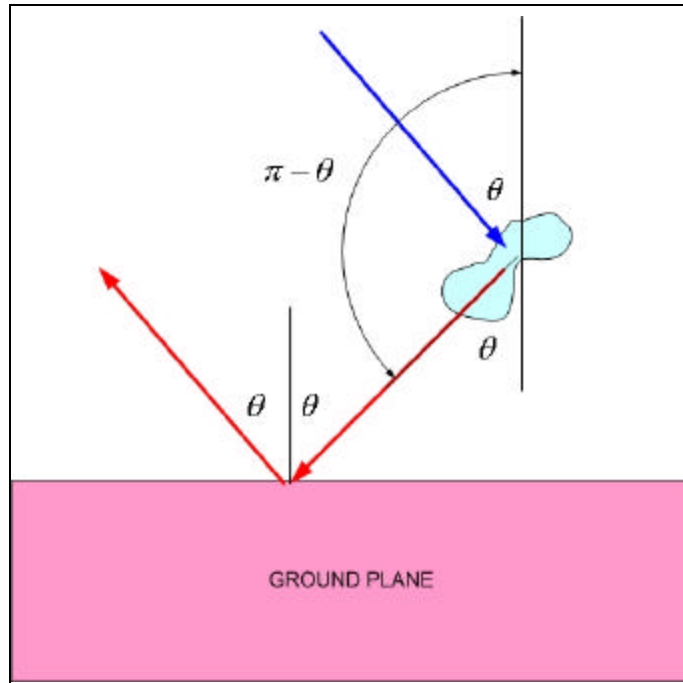


Figure 75. Direct Incident – Reflected Scattered

In the third case, only the incident radiation is reflected on the ground, with the scattered radiation reaching the radar receiver with no ground reflection, as depicted in Figure 76.

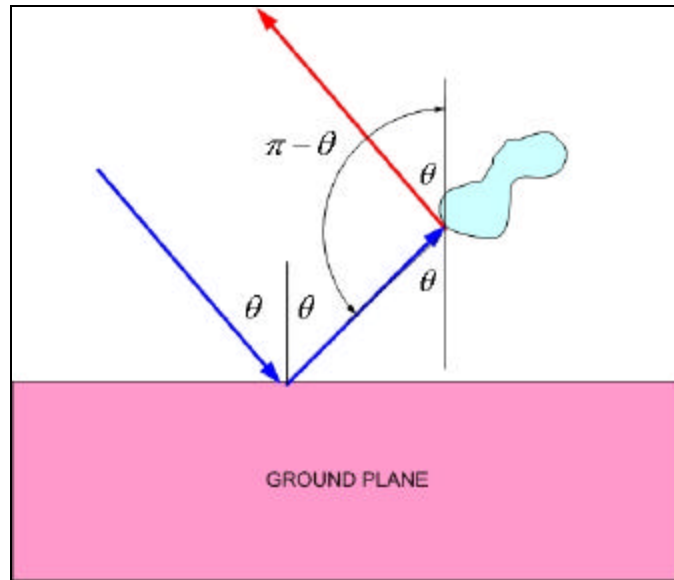


Figure 76. Reflected Incident – Direct Scattered

In an alternate approach using the Method of Images (Ref. 2), this case is replaced by its equivalent, which creates an “image” target, with the ground plane being the “mirror.” As evident in Figure 77, in the equivalent scenario, the incident field coming from angle θ must be first multiplied by the appropriate ground reflection coefficients and then the scattered field can be computed from the image target in the direction of angle $\pi - \theta$.

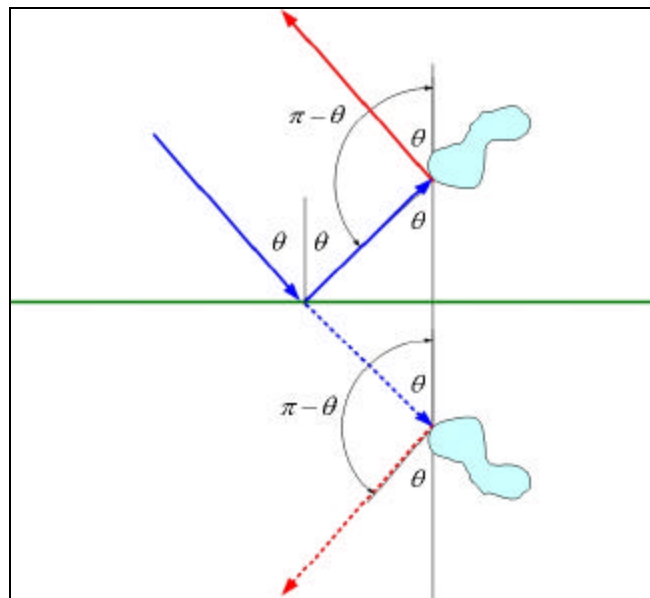


Figure 77. Reflected Incident – Direct Scattered Equivalent Scenario

In the fourth case, both the incident and the scattered radiation are reflected on the ground, as depicted in Figure 78.

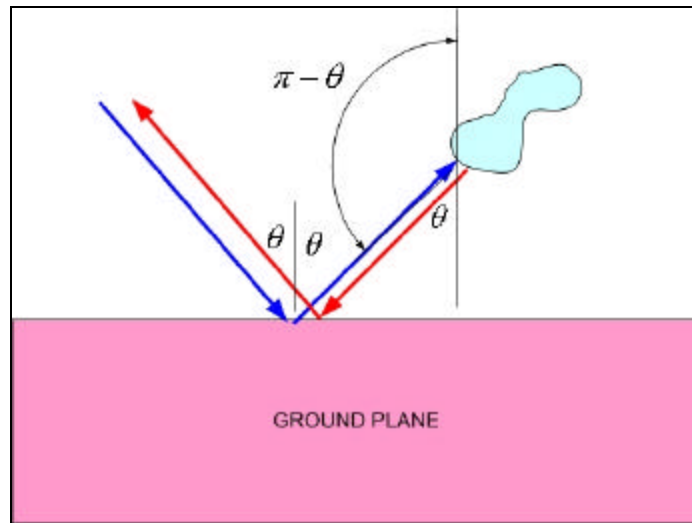


Figure 78. Reflected Incident – Reflected Scattered

Following the same alternate approach as in the previous case, the equivalent scenario is presented in Figure 79. Again, the incident field, coming from angle θ , must be first multiplied by the appropriate ground reflection coefficients. Then, the scattered field can be computed from the image target in the direction of angle θ and also be multiplied with the appropriate ground reflection coefficients.

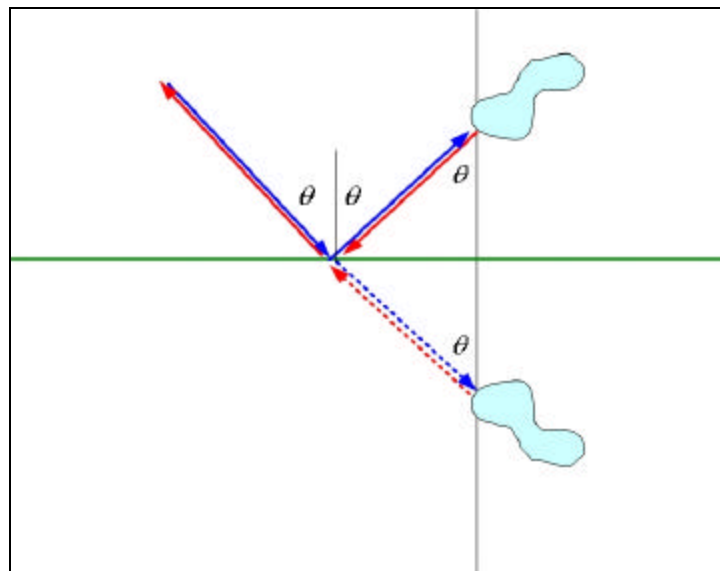


Figure 79. Reflected Incident – Reflected Scattered Equivalent Scenario

Summarizing, the following procedure can compute the approximate effects of the ground on RCS:

- a. A symmetric model is created relative to the xy plane.
- b. For the incident radiation, the scattered radiation is computed from the original model at the θ angle (i.e., first case)
- c. For the incident radiation, the scattered radiation is computed from the original model at the $\pi - \theta$ angle and multiplied by the ground reflection coefficients (i.e., second case)
- d. The incident radiation is multiplied by the ground reflection coefficients. The scattered radiation is computed from the symmetric model at the $\pi - \theta$ angle (i.e., third case)
- e. The incident radiation is multiplied by the ground reflection coefficients. The scattered radiation is computed from the symmetric model at the θ angle and multiplied by the ground reflection coefficients (i.e., fourth case)
- f. The scattered radiation from steps b, c, d, and e is vector summed.
- g. The RCS can be computed

3. Procedure

As previously discussed, the ground plane, when used, is always limited to the xy plane, indicating that the model must be placed at the desired height over this plane. This is accomplished by utilizing the Move button in the Graphical Model Design GUI, as described in Section D of Chapter IV.

Once the target is placed at the desired height, the user can select whether to include the use of ground plane in the computations of monostatic or bistatic RCS versus angle or versus frequency, or to perform RCS computations neglecting the ground. The controls by which the user can make this selection are circled in Figure 80, which pertains to the calculation of monostatic RCS versus frequency. Similar controls appear in the GUIs used for the other cases of RCS calculation.

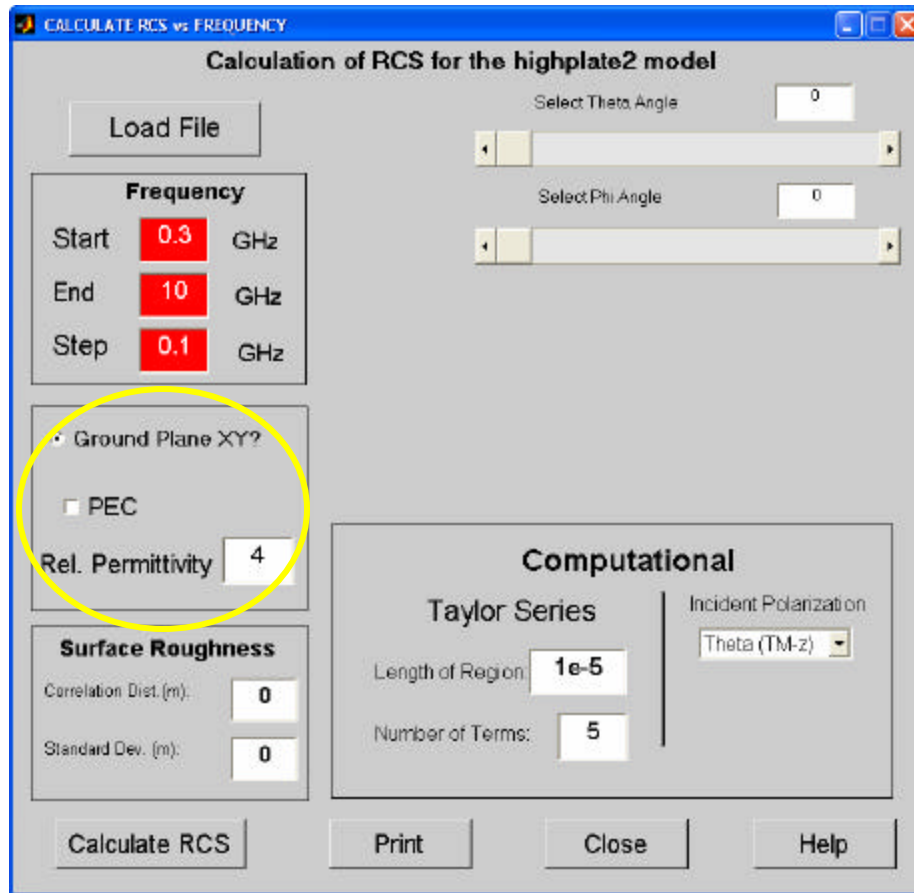


Figure 80. Ground Plane Controls (circled)

Once the user enables the use of ground plane in the RCS computation, the program automatically limits the range of available incidence and reflection angles to the values described earlier in this section. The user can then select whether the ground plane will be PEC or enter a relative electric permittivity value for the material of the ground plane.

4. Results

Figure 81 depicts the RCS of a 1 m by 1 m PEC plate lying parallel to the xy plane at $z = 9.25$ m. When no ground plane is used, the RCS of this plate versus frequency (from 0.3 to 3 GHz) for a TM polarized wave incident from angles $\theta = 0$ and $\phi = 0$ degrees (i.e., normal to the plate) is that depicted in Figure 81. This is similar to Figure 68, as the position of the plate relative to the origin does not affect its RCS. Notice that, in that case, the frequency was varied from 0.3 to 30 GHz.

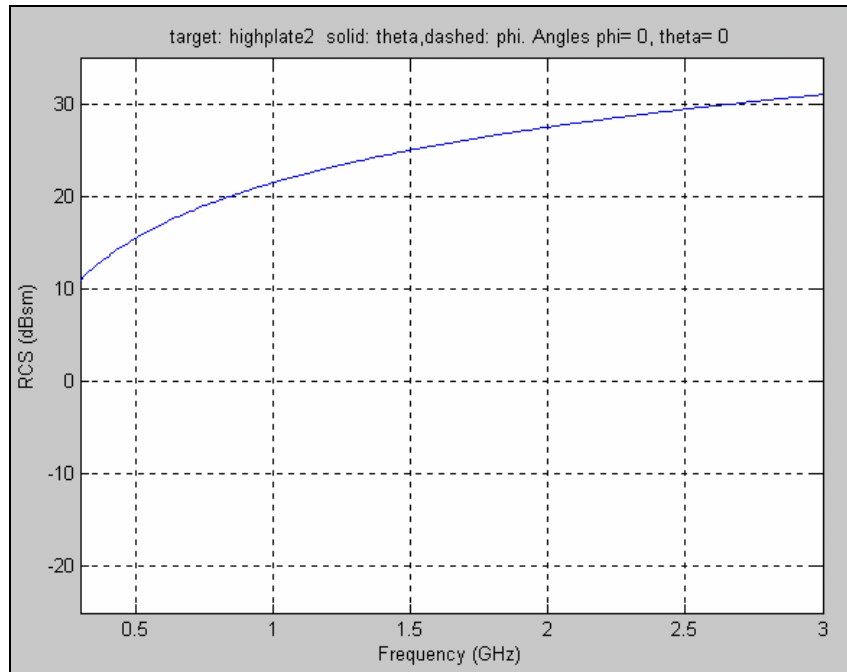


Figure 81. RCS vs. Frequency of a 1 m by 1 m PEC Plate (normal incidence)

Next, the use of ground plane was enabled and the ground plane was also defined as PEC. Figure 82 shows the resulting plot of RCS versus frequency.

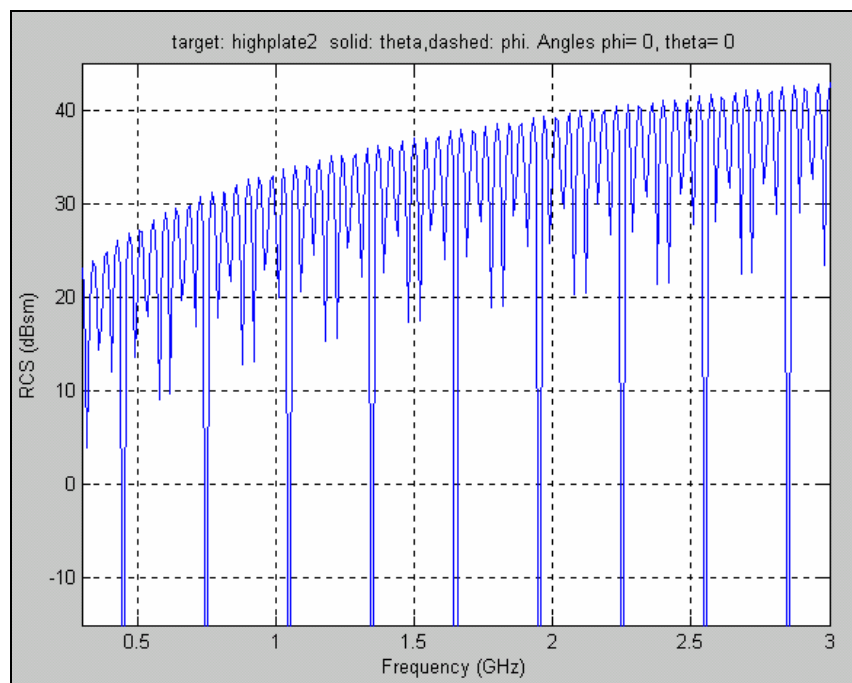


Figure 82. RCS vs. Frequency of a 1 m by 1 m PEC Plate (normal incidence) with PEC Ground Plane 9.25 m Below the Plate

It is obvious that once again the maximum value of the RCS is increasing with the square of frequency, following the pattern depicted in Figure 81. However, the vector sum of the scattered fields from the four cases described previously (i.e., Direct Incident/Direct Scattered, Direct Incident/Reflected Scattered, Reflected Incident/Direct Scattered, and Reflected Incident/Reflected Scattered) has produced significant variations in the RCS values.

Indeed, depending on the frequency of the incident wave, those four scattered fields can have the same phase, resulting in constructive interference. Then, the total scattered field is increased by a factor of four, which increases the total RCS by a factor of 16, since RCS is proportional to the square of the scattered field, as shown in Equation (2.5). This corresponds to an increase of approximately 12 dBsm. Indeed, a comparison of Figures 81 and 82 reveals that the difference in the highest RCS values at the same frequency is approximately 12 dBsm.

For other frequency values, the four scattered fields might cancel each other, resulting in zero total scattered field, which is represented by the nulls that appear in the RCS plot in Figure 82. Moreover, for other frequencies, the vector sum of the four scattered fields can produce RCS values higher or lower than those depicted in Figure 81. These are represented by the variations of the RCS in Figure 82 between the maximum values and the nulls.

D. SUMMARY

This concludes the description of the new computational capabilities added to the POFACETS program. The theoretical background, the implementation and the results for the exploitation of symmetry planes, the use of different materials and coatings on models, and the effects of the ground have been presented and discussed. The next and final chapter summarizes the work of this thesis and suggests further potential improvements to the program.

THIS PAGE INTENTIONALLY LEFT BLANK

VI. SUMMARY AND RECOMMENDATIONS

A. SUMMARY

The objective of this thesis was to improve the existing POFACETS RCS prediction software tool. This objective was achieved by providing new functionalities and adding new computational capabilities to the POFACETS 2.3 version.

The new functionalities include the GUI and model database upgrade, the improvement of the manual model design options, the creation of a graphical model design GUI, the inclusion of capabilities for importing and exporting models compatible with commercial CAD programs, the inclusion of capabilities for a combination of existing models, the computation of RCS versus frequency, and the creation of new options for the display of RCS results.

The new computational capabilities include the exploitation of symmetry planes in target models to decrease run-time for RCS prediction, the development of a user-updateable database of materials which can be applied to models in one or multiple layers, the computation of the effects of materials and coatings in the model RCS, and the approximate effect of the ground on the RCS of a model.

Overall, the program is now user-friendlier, by providing easy-to-use GUIs and familiar controls, while minimizing the possibility for erroneous input. Moreover, the creation of complex models was facilitated through the use of an automated standard model design and the new capabilities, which allow the program to combine existing models and share models with CAD software. Despite the new improvements and computational capabilities, minimal effect occurred to the required program execution time, while the option for the exploitation of symmetry planes, when these exist, can drastically decrease execution time.

The versatility of the program was enhanced by allowing the capability for RCS computation versus frequency and providing a broader range of options for RCS display. Indeed, these capabilities allow the use of the program not only for RCS prediction, but for RCS analysis as well.

Finally, the capability to use very complex models, the materials database, the capability to apply different types of materials and coatings to the models' surfaces and the inclusion of the effects of the ground on RCS, have made the POFACETS 3.0 a much more useful tool regarding real-world RCS prediction and analysis problems.

B. RECOMMENDATIONS

The POFACETS 3.0 program is implemented in the current version of the MATLAB software. Thus, it can be easily modified and upgraded through the wide variety of tools that this software package provides. There are two areas of potential improvements that could further enhance the value and usefulness of the POFACETS program.

The first area pertains to the enhancement of the capabilities for importing models from other CAD software. Other commercial CAD or RCS prediction software packages can be considered as candidates for importing models. In addition, the capability to import AUTOCAD standard files, and not just text stereo-lithographic format, would be a significant addition to the features of the program.

The second area pertains to the limitations in the RCS prediction, which are inherent to the Physical Optics method. As previously discussed, certain significant scattering mechanisms, such as second reflections, diffraction, and traveling waves are not included in the calculations. These mechanisms, of course, would have a significant effect on program execution time, especially on large, complex models. Thus, it would be possible to implement them in the program as options, allowing the user to decide which of these mechanisms to enable, depending on model complexity and the desired accuracy of results.

APPENDIX. POFACETS FILES AND MODEL DATABASE STRUCTURE

The purpose of this Appendix is to provide basic information regarding the framework of the POFACETS 3.0 program and the structure of its data files. This was necessary, since the new functionalities and computational capabilities added to POFACETS resulted in a complex program, consisting of 39 MATLAB script files and 16 MATLAB figure files. The following information provided aims mainly to help the reader understand how the program operates, rather than serve as a user manual, since the program itself incorporates detailed user instructions either through dialog boxes or through help screens.

The Appendix consists of three parts. The first part presents the general framework of the program, providing information about the interconnections between the various script and figure files. The second part contains an alphabetical list of the script and figure files comprising POFACETS 3.0, along with a brief description of the functions performed by each file. The third part contains the description of the data structures in the model database files and in the materials database file.

A. POFACETS FILE FRAMEWORK

The complete file framework of POFACETS 3.0 is presented in graphical form in Figures 83 through 89. Each script file is represented by a cyan box, which contains the name of the file. Each figure file is represented by a yellow box, which also contains the name of the file. When a script and a figure file with the same name are attached, this means that they comprise a pair of files which implements a GUI form. For each file or pair of files, a brief description of its functionality is provided.

Execution flows from the top to bottom of the figures. Files are interconnected through blue and red lines. Blue lines indicate that a script file is executed or a figure is activated, as a result of an action in the higher-level file (e.g., a button is pressed). Red lines indicate that one or more functions of the lower-level file are called from the higher-level file.

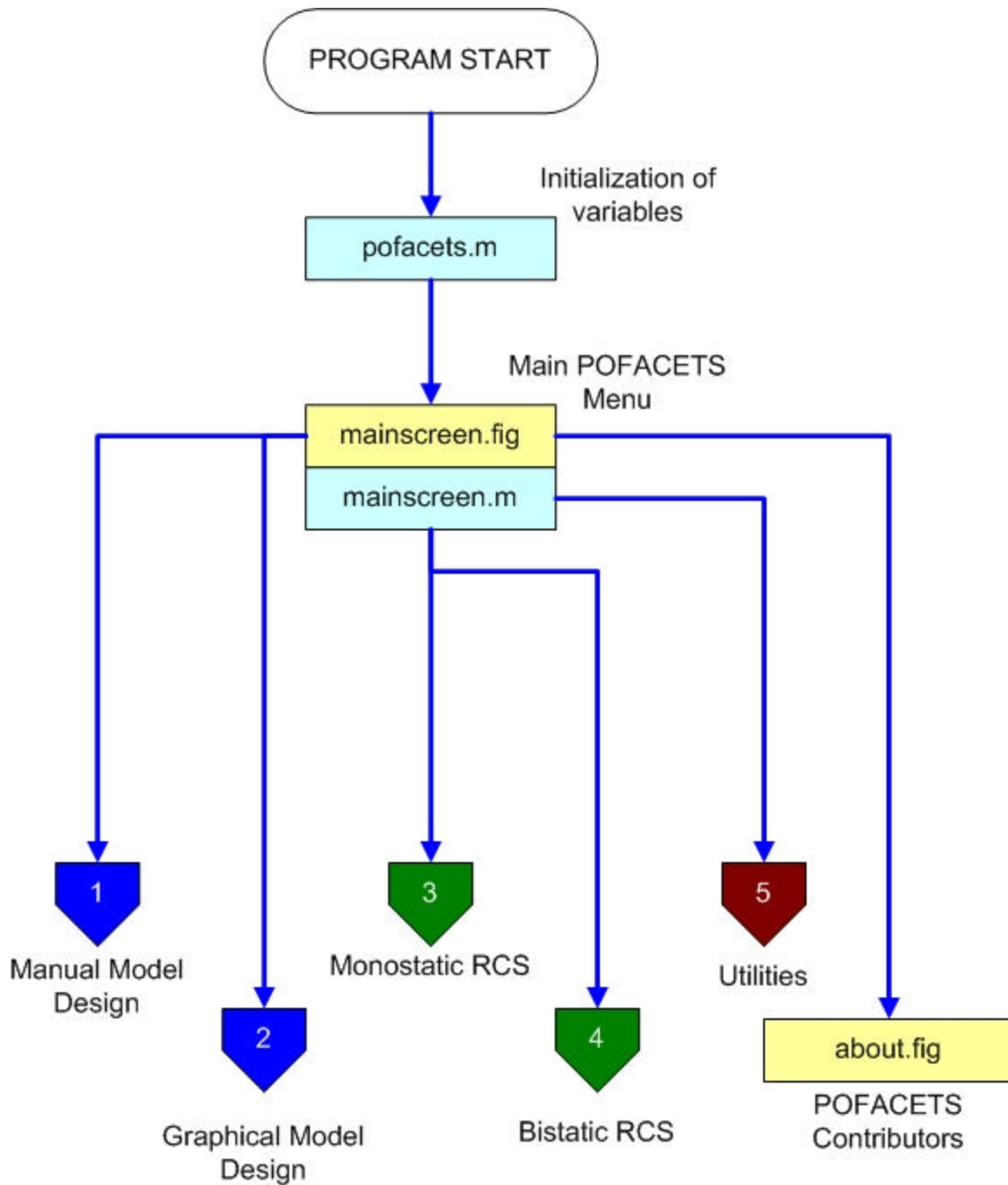


Figure 83. POFACTS Main Screen File Framework

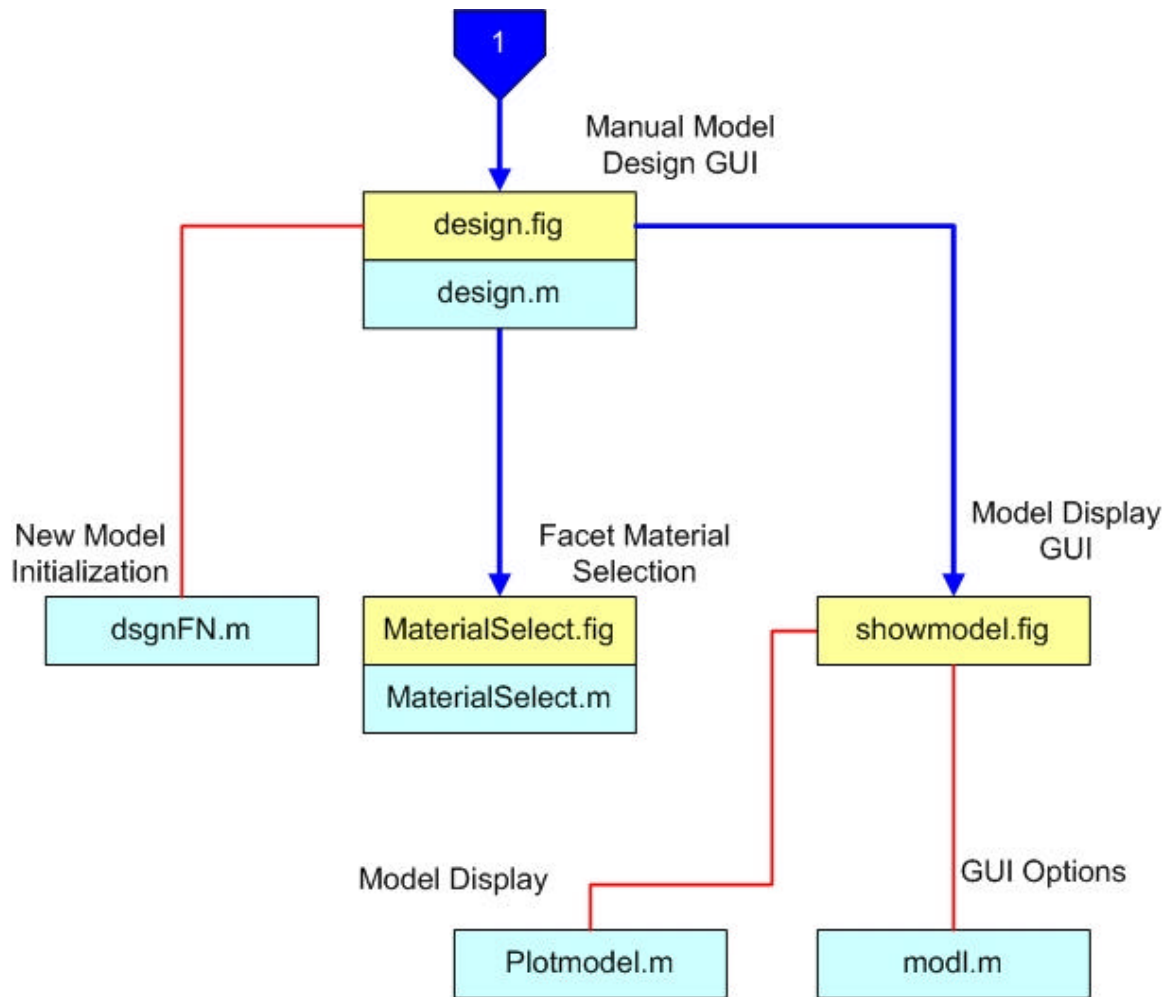


Figure 84. Manual Model Design File Framework

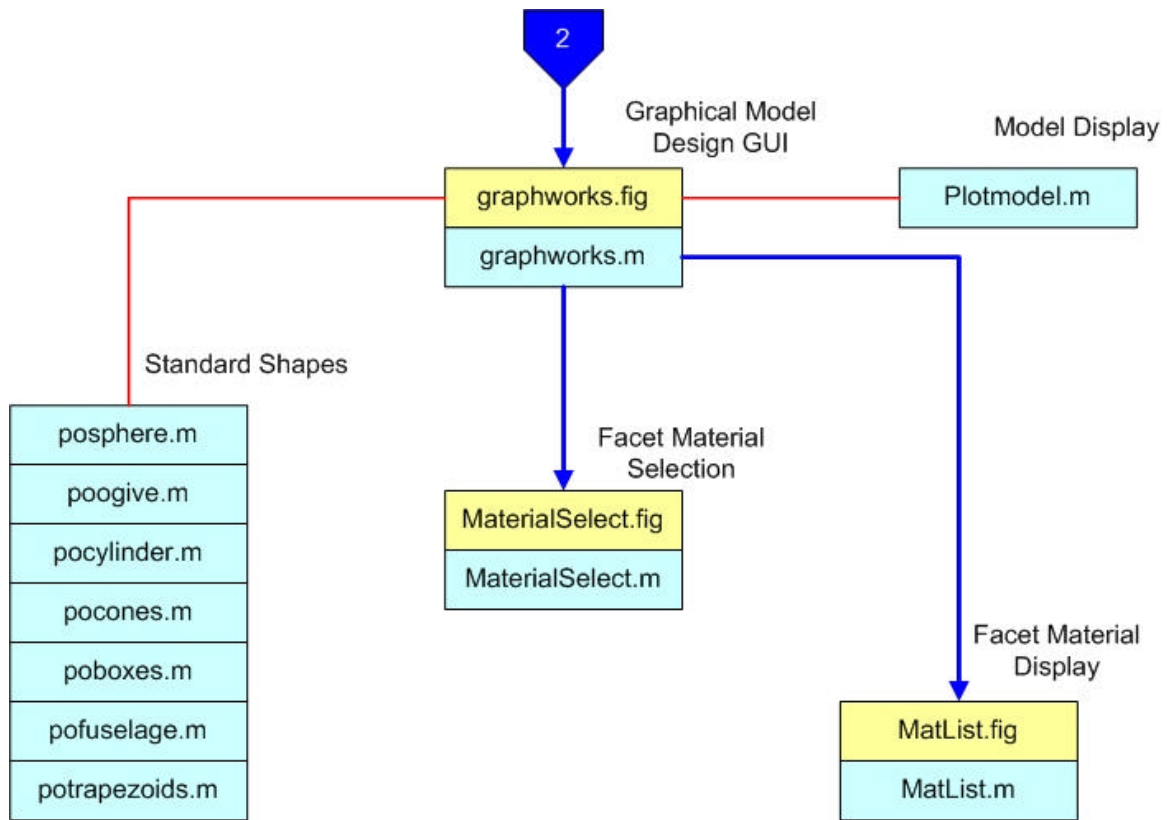


Figure 85. Graphical Model Design File Framework

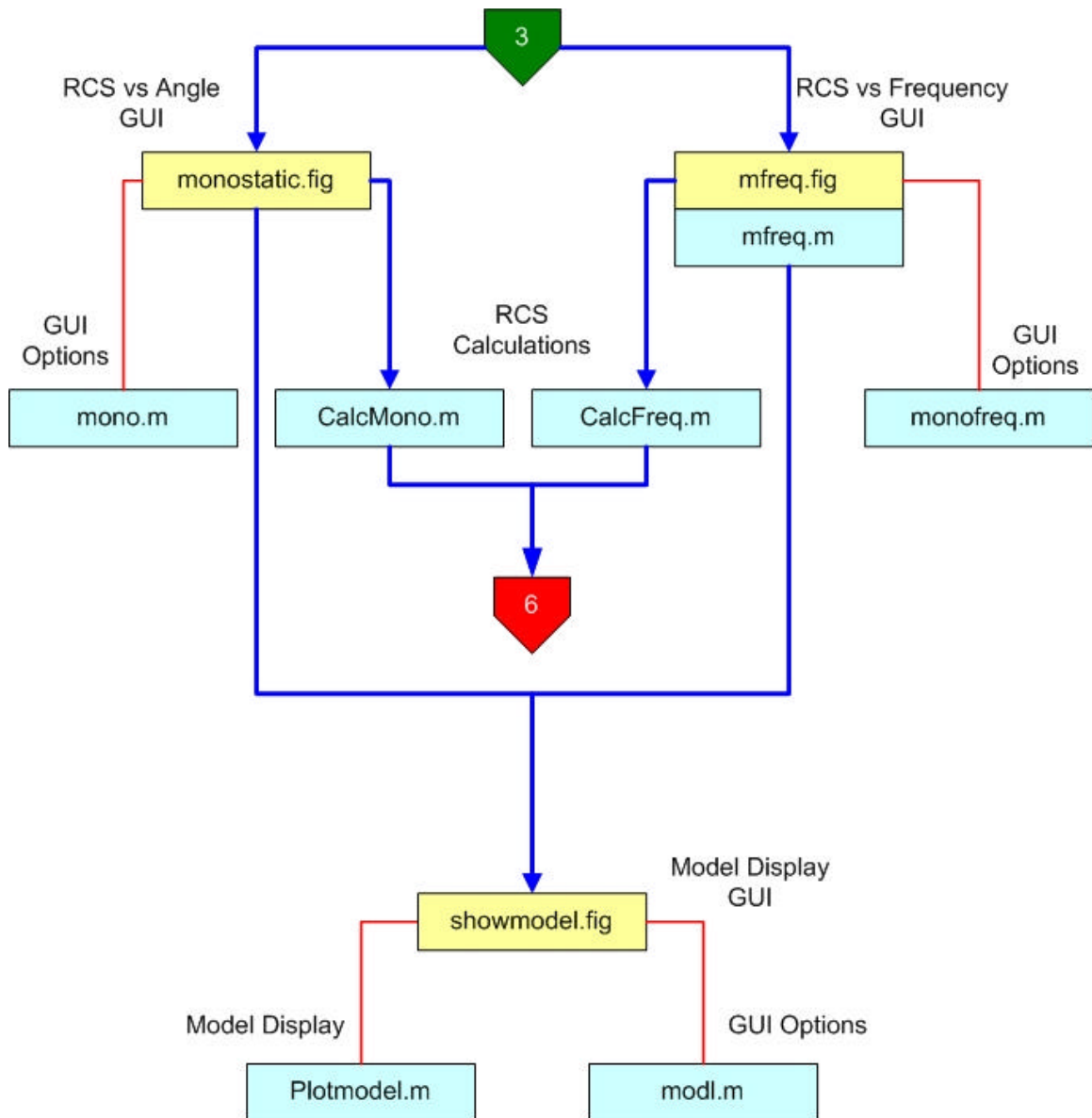


Figure 86. Monostatic RCS Calculation File Framework

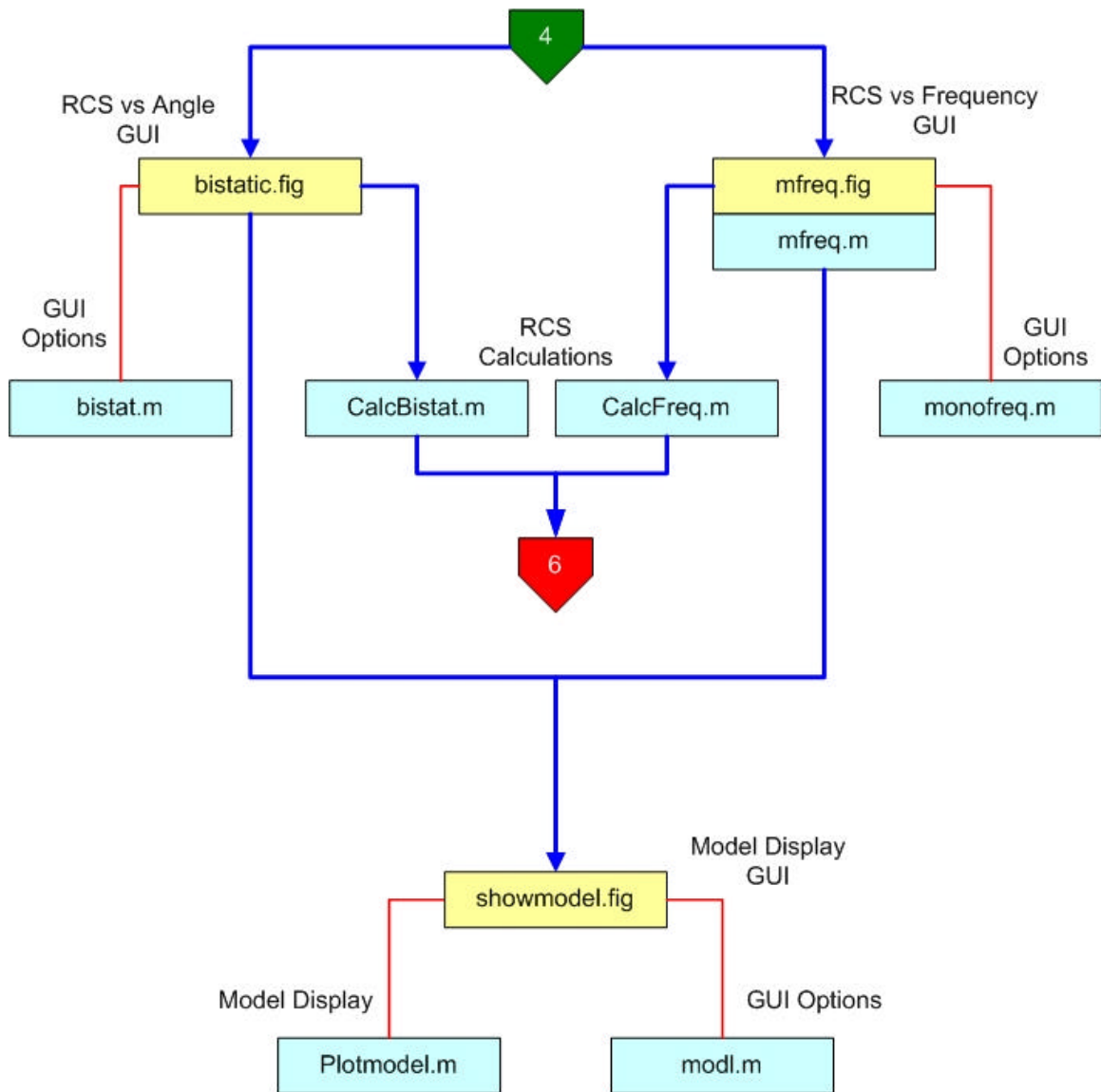


Figure 87. Bistatic RCS Calculation File Framework

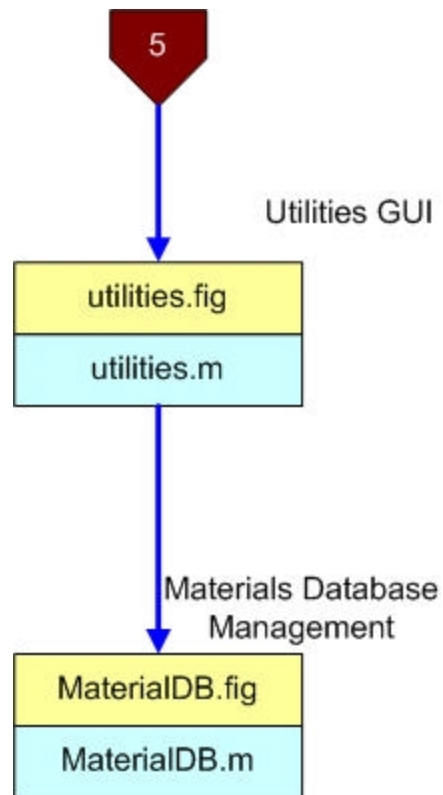


Figure 88. Utilities File Framework

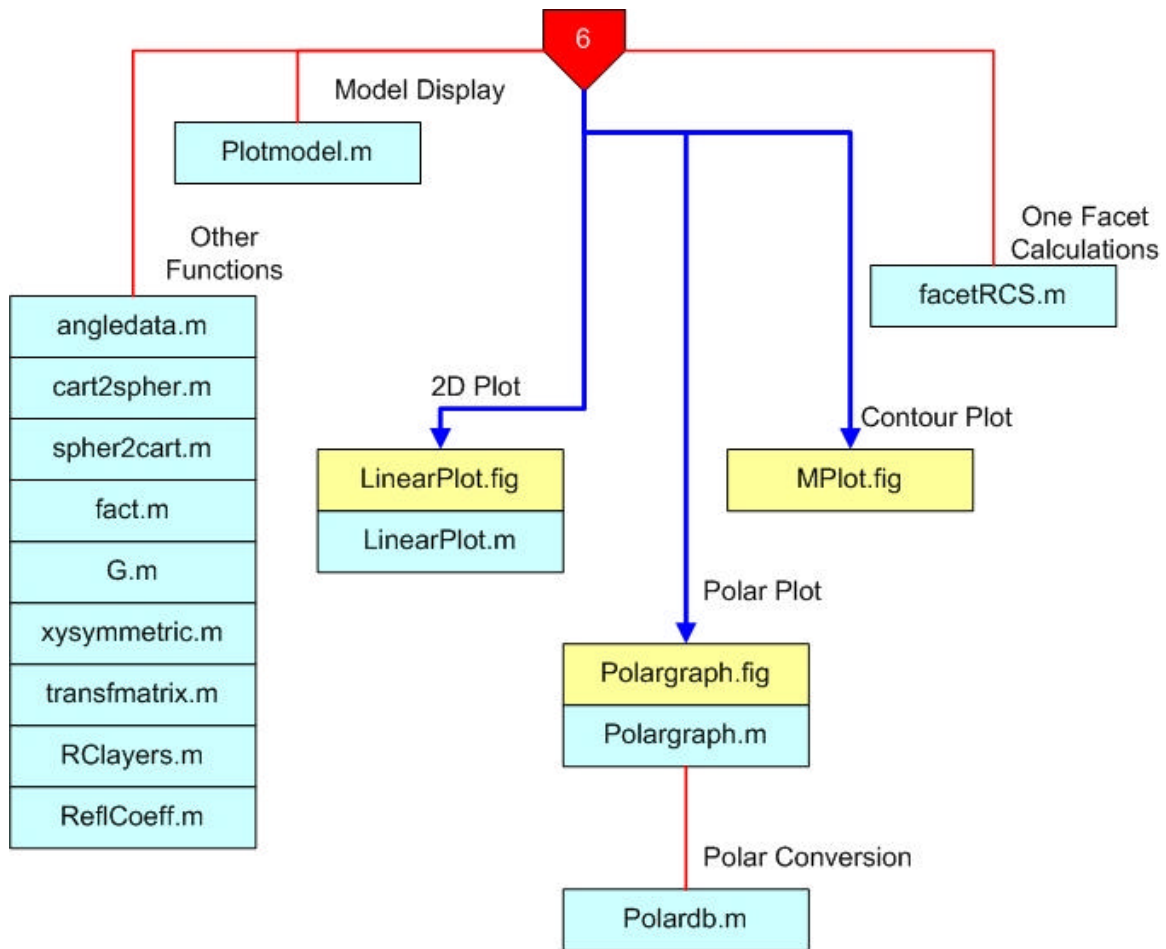


Figure 89. RCS Computation and Display File Framework

B. POFACETS FILE DESCRIPTION

The following list contains all the script and figure files used in the POFACETS 3.0 program. The help files are not included in this list.

about.fig: This file creates the GUI form that presents information about the contributors to the POFACETS program

angledata.m: This function computes the direction cosines of an angle

bistat.m: This program implements the functionalities of the Bistatic RCS Calculation GUI

bistatic.fig: This file creates the Bistatic RCS Calculation GUI

CalcBistat.m: This file computes the bistatic RCS of a target model versus angle

CalcFreq.m: This file computes the monostatic or the bistatic RCS of a target model versus frequency

CalcMono.m: This file computes the monostatic RCS of a target model versus angle

cart2sphere.m: This function converts Cartesian coordinates to spherical coordinates

design.fig & *design.m*: This pair of files creates the Manual Model Design GUI

dsgnFN.m: This file performs data initialization of variables for the manual creation of a new model

facetRCS.m: This function calculates the scattered and diffuse field from a single facet for a given set of incident wave parameters

fact.m: This file implements the factorial function

G.m: This file implements the gamma function described in equations (3.47) and (3.48)

graphworks.fig & *graphworks.m*: This pair of files creates the Graphical Model Design GUI

hlpgui.fig: This file creates the GUI used to present help to the user

LinearPlot.fig & LinearPlot.m: This pair of files creates the GUI used to display two-dimensional RCS graphs and select the dynamic range of these graphs

mainscreen.fig & mainscreen.m: This pair of files creates the GUI activated upon program execution

MaterialDB.fig & MaterialDB.m: This pair of files creates the GUI used to edit the materials database

materials.mat: This file contains the data of the materials database

MaterialSelect.fig & MaterialSelect.m: This pair of files creates the GUI that allows the user to select different materials or layers of materials for the facets of a model

MatList.fig & MatList.m: This pair of files creates the GUI that allows the user to view the materials or layers of materials of a model

mfreq.fig & mfreq.m: This pair of files creates the RCS Calculation versus Frequency GUI for both the monostatic and the bistatic cases

modl.m: This file implements the functionalities of the GUI that displays a model in the manual design case

mono.m: This file implements the functionalities of the Monostatic RCS Calculation GUI

monofreq.m: This file implements the functionalities of the RCS Calculation versus Frequency GUI for both the monostatic and the bistatic cases

monostatic.fig This creates the Monostatic RCS Calculation GUI

Mplot.fig: This file creates the GUI used for contour plots

Plotmodel.m: This file displays a model in either the manual or the graphical design case

poboxes.m: This file creates the model of a box

pocones.m: This file creates the model of a cone

pocylinder.m: This file creates the model of a cylinder

pofacets.m: This file must be executed to run POFACETS. It performs the initialization of variables and activates the program's main screen

pofuselage.m: This file creates the model of a fuselage

Polardb.m: This file converts data so that they can be displayed in polar coordinate form

Polargraph.fig & *Polargraph.m*: This pair of file creates the GUI used to present the RCS plots in polar form

poogive.m: This file creates the model of an ogive

posphere.m: This file creates the model of a sphere or an ellipsoid

potrapezoids.m: This file creates the model of a trapezoid

Rclayers.m: This function calculates the reflection coefficients for layers of materials

ReflCoeff.m: This file creates the reflection coefficients from a surface for a given angle of incidence

showmodel.fig: This file creates the GUI used for model display in the manual design case

spher2cart.m: This function converts spherical coordinates to Cartesian coordinates

spherglobal2local.m: This function converts global spherical coordinates to local facet spherical coordinates

spherlocal2global.m: This function converts local facet spherical coordinates to global spherical coordinates

transfmatrix.m: This function calculates the transformation matrices of a facet

utilities.fig & *utilities.m*: This pair of file creates the Utilities GUI

xysymmetric.m: This function creates an "image" model, which is symmetric to the original model relative to the (x,y) plane

C. POFACETS DATA STRUCTURES DESCRIPTION

POFACETS uses two types of data files: the model files and the material database file described below.

1. Model File Structure

Each model file is comprised of the following data structures.

a. Coord

This is a data array that contains the coordinates of the vertices of the model. Each row corresponds to a vertex. The first field in each row represents the x coordinate of the vertex, the second field represents y and the third represents z .

b. Facet

This is a data array that contains the definition data for the facets of the model. Each row corresponds to a facet. The first three fields in each row represent the facet's vertices. The sequence of the vertices defines the normal to the facet according to the right hand rule. The fourth field in each row indicates whether a facet can only be illuminated from its front side (when it contains a 1) or from both its back and front side (when it contains a 0). The fifth field in each row is the surface resistivity of the facet normalized to the impedance of free space (377 ohms).

c. Scale

This field stores the scale of the model

d. Symplanes

This is a data array that contains the points that form the symmetry planes of the model. If no symmetry planes exist, the array simply holds one row with three fields equal to zero. If symmetry planes exist, each symmetry plane is defined by three points represented by three consecutive rows. Each row contains the coordinates (x, y, z) of each point. The sequence of the points defines the normal to the symmetry plane according to the right hand rule. Up to three symmetry planes (i.e., nine rows) can be stored.

e. Comments

This is a cell array that contains the description of the parts of the model to which the facets belong. Each row contains the parts description for one facet.

f. Matrl

This is a cell array that contains the material of the facets of the model. Each row of the cell array corresponds to one facet. The first cell of the array contains the description of the type of the material used on the facet. The available options here are: “PEC”, “Composite”, “Composite Layer on PEC”, “Multiple Layers”, and “Multiple Layers on PEC”. The second cell is a one-row vector. For each layer of material used, 5 columns are included in the vector. Thus, if three layers are used, the vector will have 15 columns. In each layer, the first column is the relative electric permittivity, the second column is the loss tangent, the third column is the real part of the relative magnetic permeability, the fourth column is the imaginary part of the relative magnetic permeability, and the fifth column is the thickness of the layer in millimeters.

2. Material Database File Structure

The material database file contains a *struct* array called *materials.mat*, which is comprised of the following fields.

a. Name

This field holds the name of the material.

b. er

This field holds the relative electric permittivity of the material.

c. tand

This field holds the loss tangent of the material.

d. mpr

This field holds the real part of the relative magnetic permeability of the material.

e. m2pr

This field holds the imaginary part of the relative magnetic permeability of the material.

THIS PAGE INTENTIONALLY LEFT BLANK

LIST OF REFERENCES

1. Schleher, D. Curtis, *Electronic Warfare in the Information Age*, Artech House, Norwood, Massachusetts, 1999.
2. Jenn, David C., *Radar and Laser Cross Section Engineering*, AIAA Educations Series, Washington D.C., 1995.
3. Garrido, Elmo Jr., *Graphical User Interface for a Physical Optics Radar Cross Section Prediction Code*, Master's Thesis, Naval Postgraduate School, Monterey, California, September 2000.
4. Skolnik, Merrill I., *Introduction to Radar Systems*, 3rd Edition, McGraw Hill, New York, 2001.
5. Jenn, David C., *Microwave Devices and Radar Lecture Notes*, Version 4.7, Volume I (unpublished).
6. Moreira, Fernando J. S., and Prata, Aluizio Jr., "A Self Predictor-Corrector Algorithm for Efficient Evaluation of Reflector Antenna Radiation Integrals," *IEEE Transactions on Antennas and Propagation*, vol. 42, no. 2, pp. 246-254, February 1994.
7. Wadell, J. M., *Scattering From Rough Surfaces*, Master's Thesis, Naval Postgraduate School, Monterey, California, September 1995.
8. Jenn, David C., *Geometrical Optics and the Geometrical Theory of Diffraction Notes*, Version 1.5, 2004 (unpublished).
9. Knott, E., Shaeffer, J., and Tuley, M., *Radar Cross Section*, 2nd Ed., Artech House, Norwood, Massachusetts, 1993.
10. Knott E., Shaeffer, J., and Tuley, M., *Radar Cross Section: Its Prediction, Measurement and Reduction*, Artech House, Norwood, Massachusetts, 1985.
11. Faros, N., *Radar Cross Section Synthesis for Planar Resistive Surfaces*, Master's Thesis, Naval Postgraduate School, Monterey, California, December 1994.
12. Stutzman, W., and Thiele, G., *Antenna Theory and Design*, 2nd Ed., Wiley, Hoboken, New Jersey, 1998.
13. Chapman, Stephen J., *MATLAB Programming for Engineers*, 2nd Ed., Brooks/Cole, Pacific Grove, California, 2002.

THIS PAGE INTENTIONALLY LEFT BLANK

INITIAL DISTRIBUTION LIST

1. Defense Technical Information Center
Ft. Belvoir, Virginia
2. Dudley Knox Library
Naval Postgraduate School
Monterey, California
3. David C. Jenn, Code EC/Jn
Department of Electrical and Computer Engineering
Monterey, California
4. D. Curtis Schleher, Code IS/Sc
Department of Information Sciences
Monterey, California
5. Phillip E. Pace, Code EC/Pc
Department of Electrical and Computer Engineering
Monterey, California
6. Dan C. Boger, Code IS/Bo
Department of Information Sciences
Monterey, California
7. John P. Powers, Code EC/Po
Department of Electrical and Computer Engineering
Monterey, California
8. Filippou Chatzigeorgiadis
Hellenic Air Force
Athens, Greece